DEC 2 9 1995

NAS1.29/3-2:95-11

NASA

Technology Utilization

Electronic Components and Circuits

Electronic Systems

Physical Sciences

Materials

Computer Programs

Mechanics

Machinery

Fabrication Technology

Mathematics and Information Sciences

Life Sciences

95-11

November 1995

for .0830-L-02

96-00942 COMPLETED

Availability of NASA Tech Briefs and TSP's

Distribution of NASA Tech Briefs, a monthly periodical publication, is limited to engineers in U.S. Industry and to other domestic technology transfer agents. Requests for individual Tech Briefs or for Technical Support Packages (TSP's) announced herein should be addressed to

NASA Center for AeroSpace Information
Technology Transfer Office
800 Elkridge Landing Rd.
Linthicum Heights, MD 21090-2934
Telephone No. (301) 621-0245

Please reference the three-letter, five-digit control number located at the end of each Tech Brief. Information on NASA's Technology Utilization Program, its documents, and services is also available at the same facility.

Technology Utilization Officers and Patent Counsels are located at NASA field installations to provide technology-transfer access to industrial users. Inquiries can be made by writing to NASA field installations listed below.

Technology Utilization Officers and Patent Counsels

Ames Research Center
Technology Utilization Officer
Mail Code 223-3
Moffett Field, CA 94035

Patent Counsel
Mail Code 200-11
Moffett Field, CA 94035

Goddard Space Flight Center
Technology Utilization Officer
Mail Code 702-1
Greenbelt, MD 20771

Patent Counsel
Mail Code 204
Greenbelt, MD 20771

Lyndon B. Johnson Space Center
Technology Utilization Officer
Mail Code IC-4
Houston, TX 77058

Patent Counsel
Mail Code AL3
Houston, TX 77058

John F. Kennedy Space Center
Technology Utilization Officer
Mail Stop PT-PMO-A
Kennedy Space Center, FL 32899

Patent Counsel
Mail Code PT-PAT
Kennedy Space Center, FL 32899

Langley Research Center
Technology Utilization Officer
Mail Stop 143
Hampton, VA 23665

Patent Counsel
Mail Code 279
Hampton, VA 23665

Lewis Research Center
Technology Utilization Officer
Mail Stop 7-3
21000 Brookpark Road
Cleveland, OH 44135

Patent Counsel
Mail Code LE-LAW
21000 Brookpark Road
Cleveland, OH 44135

Jet Propulsion Laboratory
Technology Utilization Officer
Mail Stop 156-211
4800 Oak Grove Drive
Pasadena, CA 91109

NASA Resident Office-JPL
Technology Utilization Officer
Mail Stop 180-801
4800 Oak Grove Drive
Pasadena, CA 91109

Patent Counsel
Mail Code 180-801
4800 Oak Grove Drive
Pasadena, CA 91109

George C. Marshall Space Flight Center
Technology Utilization Officer
Code AT01
Marshall Space Flight Center, AL 35812

Patent Counsel
Mail Code CC01
Marshall Space Flight Center, AL 35812

John C. Stennis Space Center
Technology Utilization Officer
Code HA-30
Stennis Space Center, MS 39529

NASA Headquarters
Technology Utilization Officer
Code CU
Washington, DC 20546

Assistant General Counsel for Patent Matters
Code GP
Washington, DC 20546

Dryden Flight Research Center
Technology Utilization Officer
M/S D21-31
Bldg. 4832 Whse 7
Lilly Dr.
Edwards, CA 93523

BEST COPY AVAILABLE

BLANK PAGE

BEST COPY AVAILABLE

NASA

5 Electronic Components and Circuits

21 Electronic Systems

29 Physical Sciences

41 Materials

45 Computer Programs

55 Mechanics

63 Machinery

69 Fabrication Technology

75 Mathematics and Information Sciences

This document was prepared under the sponsorship of the National Aeronautics and Space Administration. Neither the United States Government nor any person acting on behalf of the United States Government assumes any liability resulting from the use of the information contained in this document, or warrants that such use will be free from privately owned rights.

BLANK PAGE

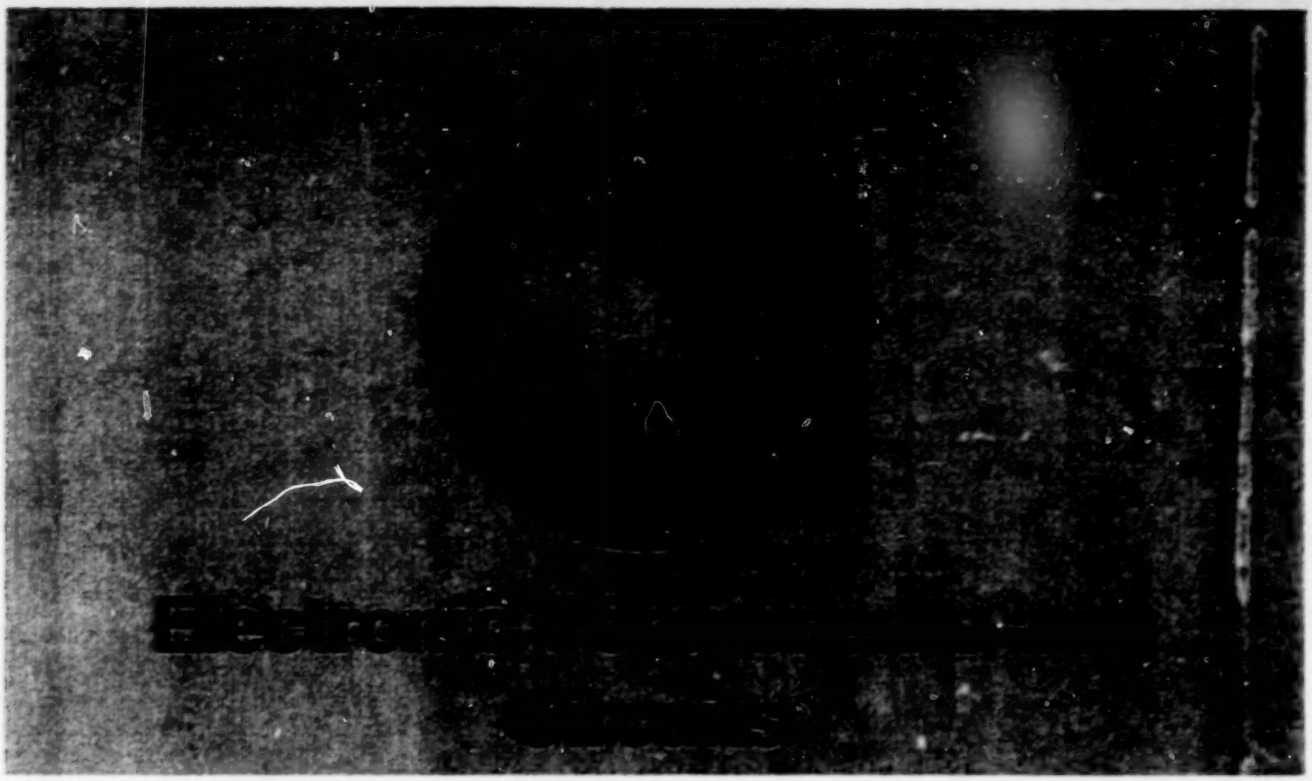

Hardware, Techniques, and Processes

7 Low-Bandgap Thermovoltaic Materials and Devices
8 Digital Frequency-Differencing Circuit
9 Imaging Magnetometer
10 Microbolometers Based on Epitaxial $YBa_2Cu_3O_{7-x}$ Thin Films
11 Garnet Random-Access Memory
11 Fabrication of SNS Weak Links on SOS Substrates
12 High-Voltage MOSFET Switching Circuit
13 Asymmetric Switching for a PWM H-Bridge Power Circuit
14 Better Ohmic Contacts for InP Semiconductor Devices
15 $In_xGa_{1-x}As/GaAs$ Quantum-Well Infrared Photodetectors
16 MQW Optical Feedback Modulators and Phase Shifters
17 Measuring Pixel-Position Errors on CCD Imagers
18 Micromachined, Electrostatically Deformable Reflectors
19 Correcting for Capacitance in Tests of Solar Cells

Books and Reports

19 Effect of Clock Mode on Radiation Hardness of an ADC
20 Data Base on Cables and Connectors

BLANK PAGE

Low-Bandgap Thermovoltaic Materials and Devices

These devices would operate from cooler sources.

NASA's Jet Propulsion Laboratory, Pasadena, California

A proposed class of thermovoltaic devices would be made of semiconductor materials that have relatively low energy gaps between their valence and conduction electron-energy bands ("low bandgaps" for short). These devices would exhibit relatively high energy-conversion efficiencies while receiving energy from sources that are at temperatures lower than those used with older thermovoltaic devices.

A thermovoltaic cell converts thermal energy into electricity. More specifically, it converts a favored spectral subcomponent of the radiant component of thermal energy to electricity, similarly to a photovoltaic device. The relationship between the bandgap, E_g, of the thermovoltaic material and the optimum temperature of the source of energy is straightforward. For most efficient utilization of the incident thermal radiation, E_g should closely match the energy of photons at the peak of the spectrum of the radiation. This is most important if the thermal emitter provides very narrow band output. If the output is relatively broadband, there is somewhat more flexibility in the choice of band gap. For example, the band gap of the cell may lie slightly above the energy of photons at the peak of the spectrum with only a minor reduction of cell efficiency. This would extend the acceptable band gap range slightly upward.

Most of the previous effort to develop thermovoltaic technology has concentrated on photovoltaic cells made of relatively high-bandgap materials like Si (E_g = 1.12 eV) or GaAs (E_g = 1.42 eV). To achieve adequate energy-conversion efficiencies with thermovoltaic cells made of these materials, it is necessary to use energy sources that have temperatures between 2,000 and 2,500 K. However, sources operating at such high temperatures may not always be feasible; they can evaporate and thereby cause contamination. Furthermore, thermal-management considerations may rule out the presence of such high temperatures in some thermovoltaic apparatuses.

The proposed low-bandgap thermovoltaic devices would likely be made of semiconducting compounds from periods III and V of the periodic table of elements (often called "III–V semiconductors" for short). The III–V semiconductors are favored for the development of high-efficiency cells because methods of processing these compounds into electronic devices are reasonably well established and commercialized. Some candidate binary, ternary, and quaternary III–V semiconductors are listed in the table. The bandgaps of most of these compounds are matched to the energies of photons at the peaks of thermal-radiation spectra for temperatures from 866 to 1,255 K. The ternary and quaternary compounds offer more versatility (in terms of degrees of freedom of chemical composition) for such matching.

Material (Note 1)	Lattice Constant, a (Å)	x	y	Substrate	Eg (eV)
InAs	6.0584	-	-	InAs, GaSb	0.36
$Ga_{1-x}In_xAs$	Equation (1)	0.75 to 1	-	InAs, GaSb, InP	0.29 to 0.52
$Al_{1-x}In_xAs$	Equation (2)	0.83 to 1	-	InAs, GaSb	0.36 to 0.52
$InP_{1-x}As_x$		0.82 to 1	-	InAs, GaSb	0.36 to 0.52
$Ga_{1-x}In_xSb$		0.20 to 0.45	-	GaSb, InAs	0.29 to 0.52
$Al_{1-x}In_xSb$		0.81 to 0.93	-	InSb	0.52 to 0.63
$InP_{1-x}Sb_x$		0.47 to 0.85	-	GaSb, InAs	0.29 to 0.52
$Al_xGa_yIn_{1-x-y}As$	2.00 to 0.09	0 to 0.24		InAs, GaSb, InP	0.36 to 0.52
$Ga_xIn_{1-x}As_ySb_{1-y}$ (Note 3)		approx. 0.1 to 0.2	approx. 0.09 to 0.18	GaSb	0.53 eV and up
GaSb (Note 4)	6.0959	-	-	GaSb, InAs	0.72

$a = 6.0584x + 6.1355(1-x)$ (Equation 1)

$a = 6.0584x + 5.6911(1-x)$ (Equation 2)

$Eg = 0.36 + 1.423(1-x) - 0.438x(1-x)$ (Equation 3)

$Eg = 0.36x + 2.95(1-x) - 0.52x(1-x)$ (Equation 4)

Note 1 — There are several other quaternaries which have band gaps in this range (0.29 eV to 0.52 eV) and could be candidates for TPV energy conversion: GaInPAs, GaInPSb, AlGaInSb, AlInPAs, AlInPSb, AlInAsSb and InPAsSb.

Note 2 — The band gap range 0.36 eV to 0.52 eV corresponds to peak photon energies for thermal emitters at temperatures of 866 K to 1255 K. For emitters which are relatively broadband, this range can be extended upward somewhat, perhaps to about 0.8 eV.

Note 3 — This quaternary enters a miscibility gap at band gaps below 0.53 eV.

Note 4 — Although its band gap is too high for use with these thermal emitters, the binary GaSb is included for purposes of comparison.

These III–V Semiconductor Compounds have bandgaps lower than those of materials used previously in thermovoltaic devices.

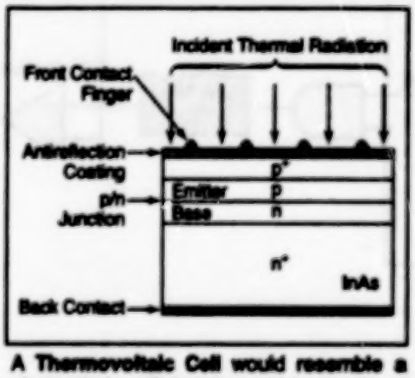

A Thermovoltaic Cell would resemble a photovoltaic cell, but it would be made of low-bandgap semiconductor material to maximize energy-conversion efficiency at appropriate infrared wavelengths.

Of all of these compounds, InAs and $Ga_{1-x}In_xAs$ initially received the most serious consideration. Both materials can be grown readily by the use of various deposition techniques. Three of the most suitable methods for depositing single crystal layers of these III–V compounds on suitable substrates are molecular beam epitaxy (MBE), metalorganic chemical vapor deposition (MOCVD), and liquid phase epitaxy (LPE). The nature of the semiconductor material and the requirements of the device structure both influence the choice of deposition technique. Of these, MBE is considered to be the most straightforward technique for growing heterostructures with monolayer thickness and nearly atomically abrupt junctions. In addition, MBE enables nonuniform doping to achieve tailored novel electronic and/or optical properties. MOCVD offers a faster growth rate, often significantly faster, than MBE. MOCVD is also more readily scaleable to large area deposition, and tends to produce material with very

BEST COPY AVAILABLE

good surface morphology. LPE is the least expensive of these techniques and generally requires the least complex equipment. It permits relatively fast deposition rates and can be scaled up to large areas. It is particularly attractive for devices in which exceedingly sharp interfaces are not required.

The figure shows a conceptual InAs low-bandgap thermovoltaic cell. The p-doped layer would be used as an emitter in order to take advantage of the high electron mobility. The reflection coefficients of the front and back surfaces would typically be made 0.001 and 0.9, respectively, to ensure minimum reflection loss at the front surface and maximum recycling of photons at the back surface. The recombination velocities of the minority electric-charge carriers at the front and back surfaces are assumed to be 10 cm/s; in practice, this could be achieved by use of p^+ and n^+ minority-carrier mirrors.

The performance of the cell was evaluated by computer simulation, using a set of representative dimensions and doping parameters, assuming that the incident black-body radiation was filtered to eliminate photons of energy less than the E_g of InAs (eliminating wavelengths greater than 3.4 μm), and assuming that the cell was maintained at a temperature of 25 °C. The energy-conversion efficiency of the cell was found to increase sharply, as a function of the factor of concentration of the radiation, from an efficiency 12.8 percent at 1 × (natural) concentration to an efficiency 22.8 percent at 32 × concentration, then to decrease gradually after reaching a peak of 23.2 percent near 64 × concentration. It is noteworthy that the computed efficiency is as high as it is at a concentration of 1 ×: this characteristic is as desirable in a thermovoltaic device as it is in a photovoltaic device, because high optical concentration increases cost. Optical concentration may be feasible for certain, although not all, configurations and geometries of the thermal emitter and TPV cells.

This work was by Tiong Ong, Carol Lewis, and Dale Burger of Caltech and Brian Campbell and Paul Baldasaro of Martin Marietta Corp. for NASA's Jet Propulsion Laboratory. Further information is contained in a TSP [see page 1].

NPO-19085

Digital Frequency-Differencing Circuit

This circuit measures both the sign and the magnitude of the difference in frequency.

Langley Research Center, Hampton, Virginia

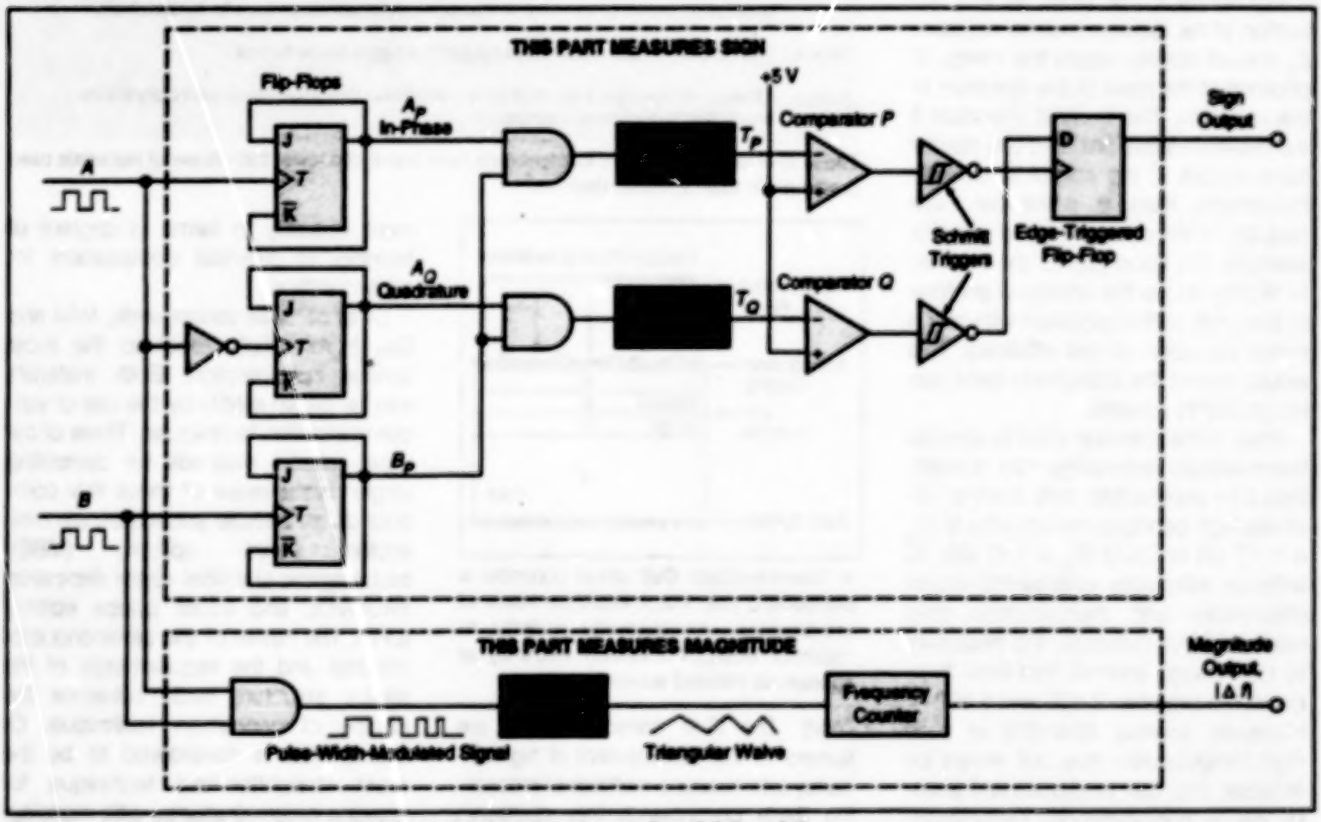

This Circuit Measures $f_A - f_B$, provided that $|\Delta f|$ is less than the smaller of $f_A/2$ or $f_B/2$.

The circuit shown in the figure measures the difference between the frequencies of two square-wave clock signals, *A* and *B* ($\Delta f = f_A - f_B$, where f_A and f_B are the two frequencies). One part of the circuit measures $|\Delta f|$ — the magnitude of the difference — provided that Δf is less than half of either f_A or f_B, whichever is lower. The other part of the circuit measures the sign of Δf.

In the part of the circuit that measures $|\Delta f|$, clock signals *A* and *B* are first multiplied in a two-input AND gate. The output of the AND gate is a pulse-width-modulated signal in which the duration of the pulses oscillates at a frequency of $|\Delta f|$. This signal is low-pass filtered to obtain a triangular waveform of frequency $|\Delta f|$. A counter measures this frequency.

In the part of the circuit that measures the sign of Δf, clock signal *A* is first divid-

BEST COPY AVAILABLE

8

ed, by two flip-flops, into a half-frequency in-phase clock signal A_P and a half-frequency quadrature clock signal A_Q. A third flip-flop divides clock signal B into a half-frequency in-phase clock signal, B_P. A_P and B_P are multiplied in a two-input AND gate and low-pass filtered to produce in-phase triangular wave T_P at frequency $|\Delta f|$. A_Q and B_P are processed similarly to obtain quadrature triangular wave T_Q at frequency $|\Delta f|$.

The sign of Δf can be determined from the phase relationship between T_P and T_Q. If $f_A > f_B$, then T_Q attains its maximum amplitude when T_P is halfway between its minimum and maximum amplitude and is increasing; if $f_A < f_B$, then T_Q attains its minimum amplitude when T_P is halfway between its minimum and maximum amplitude and is increasing.

The remainder of the circuit detects these conditions. The analog comparators detect the half-amplitude-interval levels of both signals. The outputs of the comparators are conditioned by Schmitt triggers and clamped to transistor/transistor-logic voltage levels. Finally, the state of an edge-triggered flip-flop indicates the sign of Δf as follows: Its output is switched to the output level of comparator Q on the low-to-high transition of comparator P. Thus, its output is high if $f_A > f_B$ and low if $f_A < f_B$.

To prevent the state of the edge-triggered flip-flop from changing spuriously during high-to-low transitions of the comparators while T_P is increasing, it is necessary to prevent oscillations in the outputs of the comparators. Such oscillations are prevented by providing 1 percent hysteresis in the comparators and by use of a sharp-cutoff low-pass filter, which limits the amplitudes of the clock-frequency components to within the hysteresis band. If $|\Delta f|$ is close to $f_A/2$ or $f_B/2$, then a filter of high order is needed.

This work was done by John S. Tripp of **Langley Research Center.** *Further information is contained in a TSP [see page 1].*

LAR-14951

Imaging Magnetometer

Images would be formed by magnetic deflection of an electron beam.

NASA's Jet Propulsion Laboratory, Pasadena, California

An imaging magnetometer has been proposed for scientific, industrial, or military use in detecting underground structures that contain magnetic materials (principally, steel) and underground machines that generate and/or alter magnetic fields. The imaging magnetometer would include an electron-beam tube integrated with a phosphor-coated charge-coupled device (CCD). The electron-beam tube would be covered with magnetic shielding material along part of its length, leaving part unshielded at the electron-gun end (see figure).

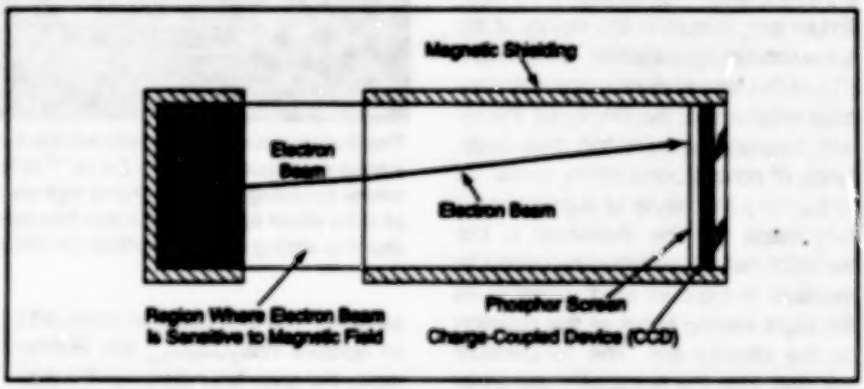

Deflection of an Electron Beam in a long tube would be measured by use of a CCD. The deflection would provide a sensitive indication of the magnetic field perpendicular to the beam.

The electron gun would generate a very fine electron beam, and the beam would be aimed at the phosphor and scanned across the phosphor in a raster or other suitable pattern, as in an ordinary cathode-ray tube. The electron beam in the unshielded portion would be deflected by a perpendicular magnetic field. The resulting distortion of the raster or other scan pattern would be a measure of the magnetic field. Given that typical state-of-the-art CCD pixels are only about 10 μm wide, very small beam displacements could be resolved and thus correspondingly weak magnetic fields could be detected.

A conceptual design of a prototype field model of the imaging spectrometer calls for overall dimensions of about 1.5 × 1.5 × 18 ft (about 0.46 × 0.46 × 5.5 m), an electron-beam tube with an unshielded length of 16 ft. (4.9 m), and a CCD of 1,024 × 1,024 10-μm-square pixels. This prototype should be able to measure a magnetic field smaller than 0.1 nT (smaller than 1/500,000 × the natural magnetic field of the Earth).

Of course, the image produced by the imaging magnetometer would not look like the magnetic object that gave rise to it. Instead, the image would be a transformed image of the magnetic field as generated or altered by the object (e.g., the magnetic field of the Earth as perturbed by the object). In a typical application, the imaging magnetometer would be carried aboard an aircraft flying in a scan pattern over the terrain suspected to contain buried structures or machinery. The CCD readout would be synchronized with the position of the aircraft along its trajectory. Then by use of suitable inversion algorithms, the image data acquired during the flight would be post-processed in correlation with the position data to synthesize a picture of the magnetic field. The locations, magnitudes, and directions of identifiable features of the magnetic field would then be examined to extract data on the locations, sizes, and types of magnetically detected objects.

This work was done by Philip I. Moynihan and Stanley L. Soli of Caltech for **NASA's Jet Propulsion Laboratory.** *Further information is contained in a TSP [see page 1].*

NPO-19268

BEST COPY AVAILABLE

Microbolometers Based on Epitaxial $YBa_2Cu_3O_{7-x}$ Thin Films

These devices exhibit high sensitivity and low noise.

NASA's Jet Propulsion Laboratory, Pasadena, California

Improved microbolometers of the superconducting-transition type are being developed with a view toward the eventual fabrication of staring, infrared-imaging planar arrays of such microbolometers integrated with addressing electronic circuitry. The development of these microbolometers builds upon the prior development of similar microbolometers in which the superconducting thin films that serve as the sensing elements are not epitaxial. The superconducting thin films in the present microbolometers are epitaxial, and this confers an advantage, as explained below.

In a superconducting-transition bolometer, the sensing element is a thin film of superconductive material mounted on a thin substrate maintained at an equilibrium temperature in the vicinity of the superconducting-transition temperature (T_C). In this temperature range, the electrical resistance of the film varies sharply with temperature from the finite resistance of normal conductivity above T_C to the zero resistance of superconductivity below T_C. The sharpness of this transition can be exploited by using it to measure incident infrared radiation via the slight heating effect of this radiation on the sensory film. The temperature rise and thus the bolometric sensitivity can be maximized by thermally isolating the sensing element. Device speed is improved by making the sensing element and substrate thin to minimize thermal mass.

In fabricating a microbolometer of the previous type, a layer of the high-T_C superconductor $YBa_2Cu_3O_{7-x}$ is deposited on a layer of yttria-stabilized zirconia (YSZ) that has previously been deposited on an underlayer of Si_3N_4. The YSZ layer is needed to prevent chemical reactions between the Si_3N_4 and $YBa_2Cu_3O_{7-x}$ layers. Because Si_3N_4 is amorphous in the sense that it lacks crystalline structure, the YSZ and $YBa_2Cu_3O_{7-x}$ layers are polycrystalline or, to state it alternatively, they lack the desired epitaxial single-crystal structure. As a result, the $YBa_2Cu_3O_{7-x}$ film exhibits a relatively broad resistance-vs.-temperature transition instead of the sharp transition that is needed for high sensitivity and that could be achieved in an epitaxial $YBa_2Cu_3O_{7-x}$ film. Furthermore, the grain boundaries of the polycrystalline $YBa_2Cu_3O_{7-x}$ film create excess electrical noise.

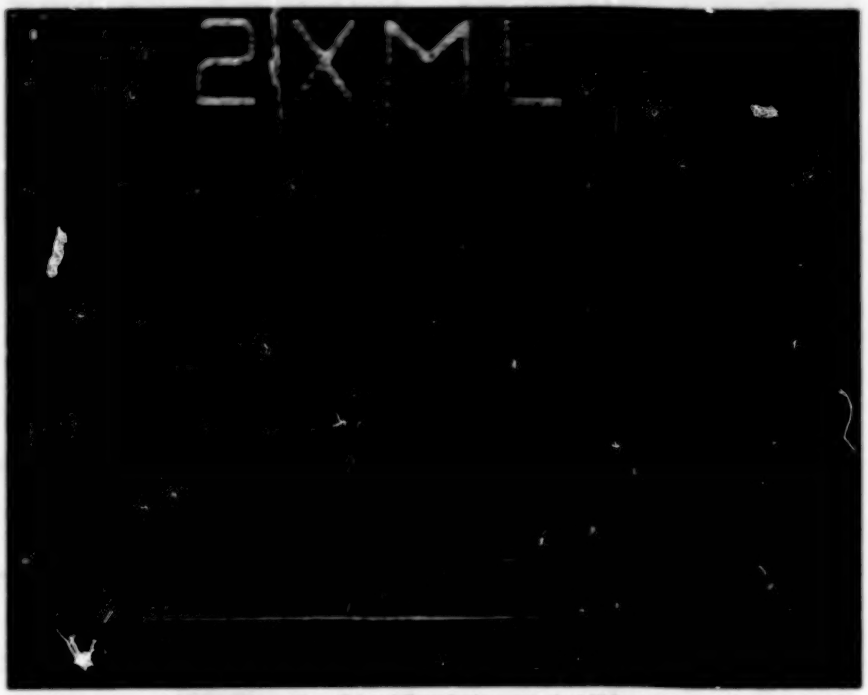

This Superconducting Transition-Edge Microbolometer is 140 by 105 μm in size and has a noise equivalent power of 1.5×10^{-12} W/Hz$^{1/2}$ and a thermal time constant of 105 ms. The central absorbing area and narrow legs are 1-μm thick membranes suspended over an etch pit in the silicon substrate. The dark lines represent via holes cut through the films to allow the chemical etching solution to attack the underlying silicon.

In fabricating a microbolometer of the improved type, an epitaxial $YBa_2Cu_3O_{7-x}$ film is obtained by depositing $YBa_2Cu_3O_{7-x}$ on a YSZ buffer layer that is, in turn, epitaxial with a silicon substrate. The YSZ layer protects the underside of the $YBa_2Cu_3O_{7-x}$ film from a KOH solution that is used subsequently to etch out a volume of silicon from underneath to create a membrane sensor structure and thereafter serves as the lower layer of this membrane.

After deposition of the $YBa_2Cu_3O_{7-x}$ film on the YSZ film on the Si substrate, the $YBa_2Cu_3O_{7-x}$ is ion-milled into a meandering pattern. A cap layer of Si_3N_4 is deposited to form the primary supporting layer of the membrane and to protect the top side of the $YBa_2Cu_3O_{7-x}$ during the final etch. Then, windows are opened through the Si_3N_4 and YSZ to allow the KOH solution to attack the underlying silicon.

A microbolometer (see figure) fabricated from epitaxial $YBa_2Cu_3O_{7-x}$ films has shown a detectivity of $D^* = 8 \times 10^9$ cm·Hz$^{1/2}$/W at 2 Hz and a temperature of 80.7 K. This value of D^* exceeds the highest previously reported D^* for a $YBa_2Cu_3O_{7-x}$ transition-edge bolometer and is comparable to the highest D^* for a thermal detector operating at temperatures of 80 K or higher. Linear arrays of such devices show a uniformity in response of about ±10 percent among working devices, although the current yield is less than 50 percent.

This work was done by Marc C. Foote and Brian D. Hunt of Caltech and Burgess R. Johnson, and Holly A. Marsh of Honeywell, Inc., for **NASA's Jet Propulsion Laboratory.** *Further information is contained in a TSP [see page 1].*

NPO-19251

BEST COPY AVAILABLE

Garnet Random-Access Memory

Magnetic writing and optical readout would be used.

NASA's Jet Propulsion Laboratory, Pasadena, California

Random-access memory (RAM) devices of a proposed type would exploit the magneto-optical properties of magnetic garnets (for example, yttrium iron garnet (YIG)) that exhibit perpendicular anisotropy. These memory devices would provide nonvolatile storage and would resist damage by ionizing radiation. Because of basic architecture and pinout requirements, these RAMs would most likely be useful as small-capacity memory devices.

A RAM of this type would comprise a rectangular array of memory cells containing garnet storage films between column and row conductors (see figure). To store a bit in a cell, current of appropriate magnitude and polarity would be applied to the row and column conductors that intersect at that cell to magnetize the garnet film in either of two binary states (up or down, representing 1 or 0, respectively). The bit state of a cell would change only when the particular cell was selected and the row and column currents exceeded threshold values. The magnetization states of the cells, and thus the data stored in the memory device, would remain when power was turned off; that is, storage would be nonvolatile.

Readout would be accomplished optoelectronically. For example, light from a lamp, array of laser diodes, or another source would be sent through a polarizer, then through the garnet RAM, then through an analyzer (another polarizer), finally impinging on an array of photodetectors, each of which would be positioned to receive the light that passed through one memory. The polarization of the light in each cell would be rotated by an amount dependent on the magnetization state, affecting the intensity of transmitted light and thus the output of the photodetector for that cell.

This work was done by Romney R. Katti of Caltech for **NASA's Jet Propulsion Laboratory.** *Further information is contained in a TSP [see page 1].*

NPO-19342

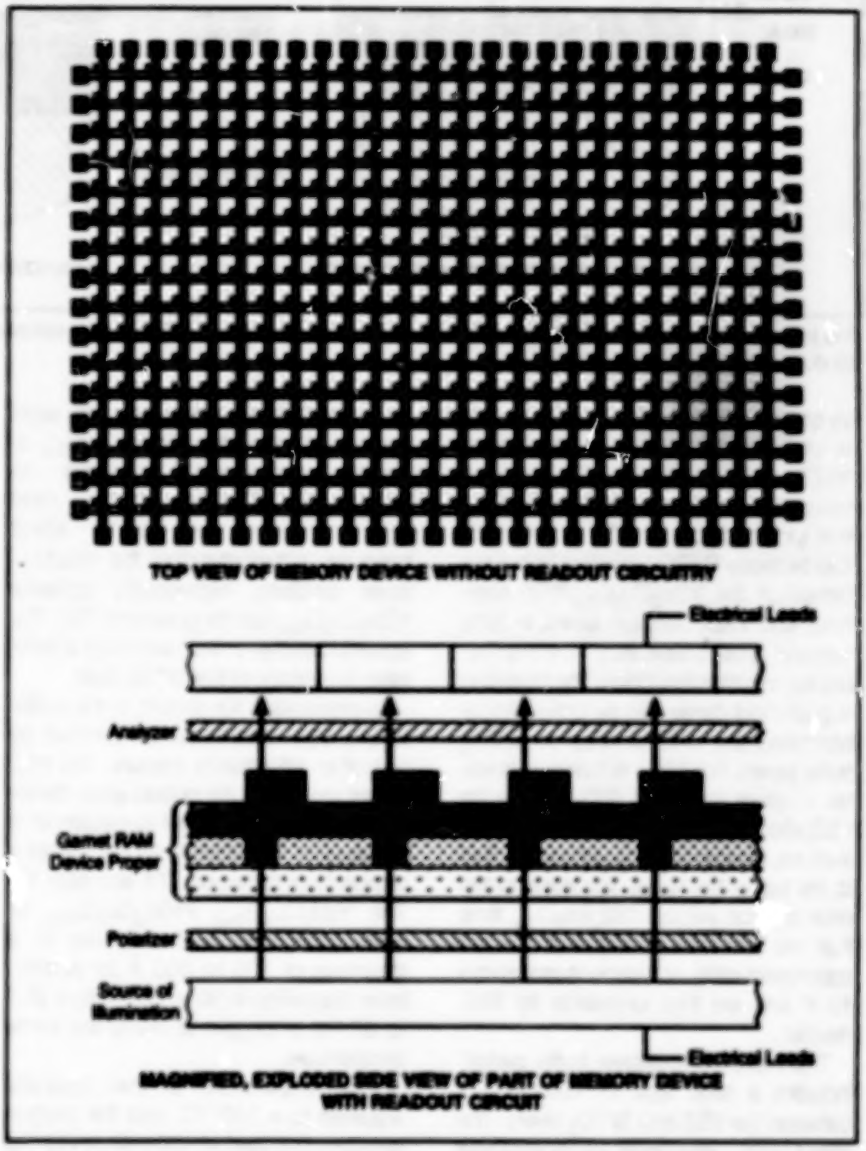
TOP VIEW OF MEMORY DEVICE WITHOUT READOUT CIRCUITRY
Electrical Leads
Analyzer
Garnet RAM Device Proper
Polarizer
Source of Illumination
Electrical Leads
MAGNIFIED, EXPLODED SIDE VIEW OF PART OF MEMORY DEVICE WITH READOUT CIRCUIT

A Garnet RAM Device would feature magnetic writing and magneto-optical readout. Because garnet is an electrical insulator, row and column conductors could be placed directly in contact with the garnet storage films, minimizing switching currents, power dissipation, and memory area. Spacing would be designed to optimize storage density with acceptably low cross-writing. The specific type of garnet would be chosen, according to its properties, to optimize switching characteristics, drive current, and power dissipation.

Fabrication of SNS Weak Links on SOS Substrates

A multilayer buffer system makes it possible to form high-quality epitaxial SNS weak links.

NASA's Jet Propulsion Laboratory, Pasadena, California

High-quality superconductor/normal-conductor/superconductor (SNS) devices ("weak links") that contain epitaxial films of $YBa_2Cu_3O_{7-x}$ and $SrTiO_3$ can be fabricated on silicon-on-sapphire (SOS) substrates with the help of an improved multilayer buffer system. The improved multiple buffer layers overcome major obstacles that have been encountered in previous efforts to fabricate such devices, as explained below.

High-quality epitaxial $YBa_2Cu_3O_{7-x}$ and $SrTiO_3$ films are essential for SNS edge-defined weak links. For reasons that are beyond the scope of this article, it is necessary to deposit these films on buffer lay-

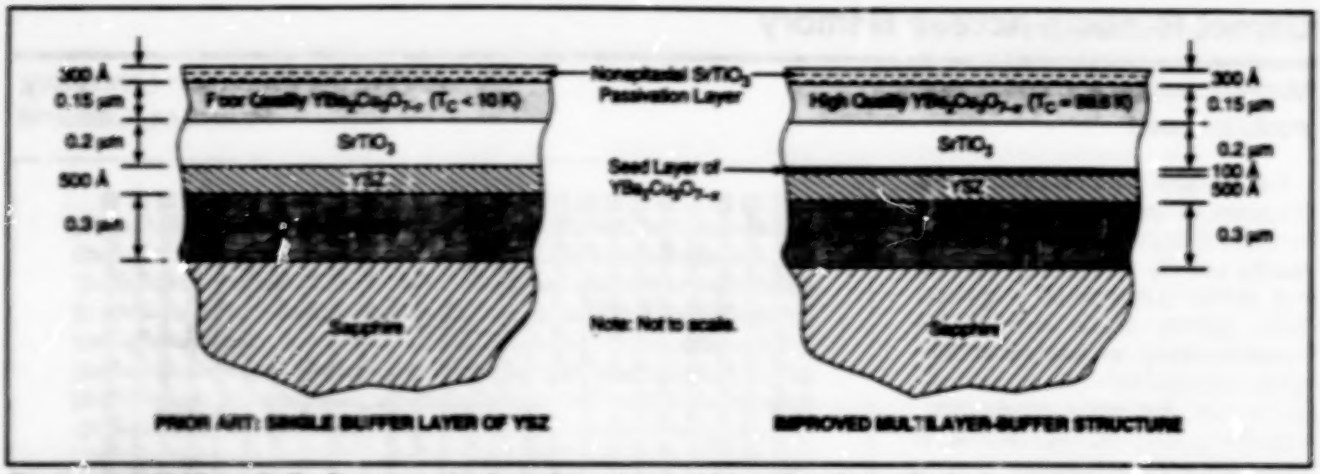

The Improved Multilayer-Buffer Structure makes it possible to deposit a high-quality epitaxial $YBa_2Cu_3O_{7-x}$ layer that exhibits a high superconducting-transition temperature (T_C).

ers of epitaxial cubic zirconia (also known as yttria-stabilized zirconia, abbreviated "YSZ") on SOS substrates. In previous research, it was found that $YBa_2Cu_3O_{7-x}$ films grown directly on YSZ are not suitable because $BaZrO_3$ reaction layers are formed at the $YBa_2Cu_3O_{7-x}$/YSZ interfaces and these reaction layers, in turn, nucleate grain boundaries in the edge-junction counterelectrodes. The formation of grain boundaries can be prevented by fabricating the SNS devices on $SrTiO_3$ buffer layers, but it has not proven possible to grow epitaxial $SrTiO_3$ directly on YSZ, silicon, or SOS substrates. For these reasons, deposition of structures like that at the top of the figure, according to the prior art, has yielded $YBa_2Cu_3O_{7-x}$ films that are nonepitaxial and that are not superconducting at temperatures above 10 K and are thus unsuitable for SNS devices.

The improved multilayer buffer system includes a seed layer of $YBa_2Cu_3O_{7-x}$ between the YSZ and $SrTiO_3$ layers. The $YBa_2Cu_3O_{7-x}$ seed layer greatly improves the epitaxial quality of the $SrTiO_3$ layer and of the main $YBa_2Cu_3O_{7-x}$ layer deposited on top of the $SrTiO_3$ layer. The seed layer was nominally 100 Å thick in the first demonstration of this concept, but could be made thicker. Alternatively, the seed layer could be made of $PrBa_2Cu_3O_{7-x}$ or another compound analogous to $YBa_2Cu_3O_{7-x}$. The $YBa_2Cu_3O_{7-x}$ seed layer produces the desired effect because, notwithstanding the reaction-layer problem, high-quality epitaxial $YBa_2Cu_3O_{7-x}$ can be grown on YSZ. The epitaxial seed layer then serves as a template for epitaxy of the $SrTiO_3$ layer.

In preparation for growth of the buffer layers, SOS substrates are cleaned by use of an HF/ethanol mixture. The YSZ layers are grown by pulsed-laser deposition from a YSZ target in oxygen at a pressure of 1 millitorr (0.13 Pa) and at a temperature between 775 and 825 °C. The $YBa_2Cu_3O_{7-x}$, $PrBa_2Cu_3O_{7-x}$, or other seed layer is then grown to a thickness of 100 to 300 Å by pulsed-laser deposition in 50 to 500 millitorr (6.7 to 67 Pa) of oxygen at nearly the same temperature.

The temperature is then typically adjusted to ≈ 760 °C, and the oxygen pressure changed to 120 millitorr (16 Pa) for pulsed-laser deposition of the thick $SrTiO_3$ layer. Finally, the temperature is returned to a value between 775 and 825 °C, the oxygen pressure is returned to a value between 50 and 500 millitorr, and the main $YBa_2Cu_3O_{7-x}$ layer (possibly doped with La) is grown by pulsed-laser deposition. This $YBa_2Cu_3O_{7-x}$ layer serves as the base electrode for fabrication of the edge-geometry SNS weak link. In some cases, this multilayer structure is capped by a thin nonepitaxial $SrTiO_3$ film, grown near room temperature, which serves as a passivation layer.

The process for fabrication of edge-defined SNS weak links was described in "Edge-Geometry SNS Devices Made of Y/Ba/Cu" (NPO-18552), *NASA Tech Briefs*, Vol. 17, No. 10 (October, 1993), page 50. SNS devices with the improved multilayer buffer structure shown in the lower part of the figure have been fabricated with $PrBa_2Cu_3O_{7-x}$ and, alternatively, with codoped $YBa_2Cu_3O_{7-x}$ as the normally conducting metals. The performances of these devices were found to be superior to those of edge-defined weak links fabricated directly on YSZ buffer layers.

This work was done by Brian D. Hunt of Caltech for **NASA's Jet Propulsion Laboratory**. *Further information is contained in a TSP [see page 1].*

NPO-19306

High-Voltage MOSFET Switching Circuit

This circuit is designed for use in a plasma ion-beam texturing process.

Lewis Research Center, Cleveland, Ohio

The circuit illustrated in the figure reliably switches power at a supply potential of −1,500 V, with controlled frequency and duty cycle. The circuit is used in argon-plasma ion-bombardment equipment for texturing copper electrodes, as described in "Texturing Copper To Reduce Secondary Emission of Electrons" (LEW-15898), page 71. (This circuit is the switching module mentioned in that article.) This circuit can also be adapted to use in powering gaseous flash lamps and stroboscopes.

The circuit includes a pair of series-connected metal oxide/semiconductor field-effect transistors (MOSFETs). A pair of MOSFET-driver integrated circuits (ICs) supply identical signals of +15 V to turn the MOSFETs on and −5 V to turn them off. Two isolated power supplies with a 4,000-V insulation rating ensure isolation of the MOSFET-driver ICs.

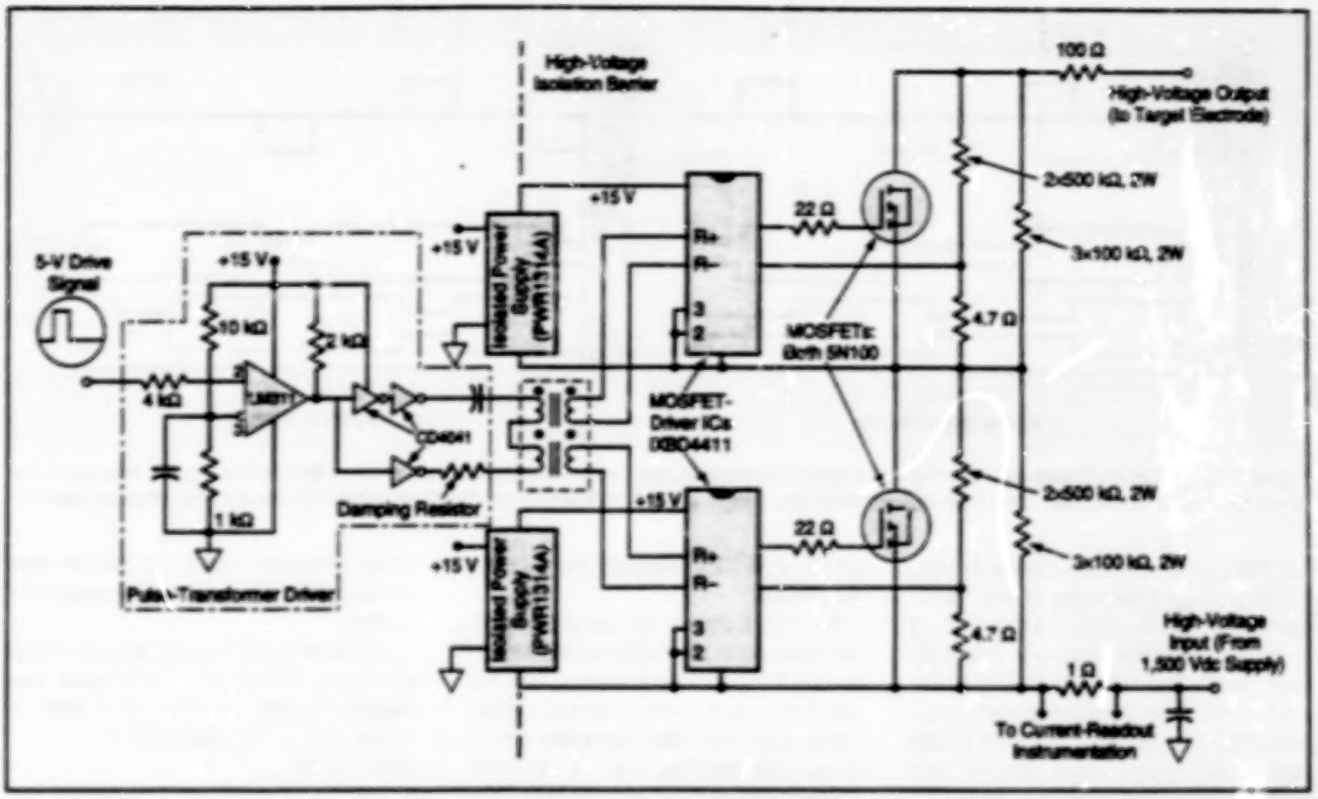

The MOSFETs Are Turned On and Off under control of pulses fed to the MOSFET gates via driver circuits and a pulse transformer. A voltage-divider network of resistors across the series-connected MOSFETs provides both plasma-sustaining (keep-alive) current and voltage protection of the MOSFETs.

The MOSFET-driver ICs are triggered by pulses coupled via pulse transformers. The secondary windings of the transformers are galvanically isolated from the primary windings, which are connected in series. The frequency (typically between 5 and 100 Hz) and duration (typically 20-percent duty cycle) of pulses is that of a 5-V drive signal, which is fed to a pulse-transformer driver circuit. The output of the driver circuit, which has a peak-to-peak amplitude of 1.5 V, is fed to the R+ and R– terminals of the MOSFET-driver ICs.

The load current is typically 100 mA. The MOSFETs chosen for use in this circuit should have current ratings 10 times the anticipated load current; this is desirable to provide margin for arcs and surges that occur when the argon plasma is started. A 100-Ω series resistor in the output lead provides added protection against overcurrent in case of arcing. The circuit has operated reliably in ion-beam texturing of more than 100 copper substrates.

This work was done by Kenneth A. Jansen of **Lewis Research Center.** *Further information is contained in a TSP [see page 1].*
LEW 15986

Asymmetric Switching for a PWM H-Bridge Power Circuit

Only two of the four switches interrupt substantial current.

Lewis Research Center, Cleveland, Ohio

An asymmetric timing scheme improves the design and operation of a pulse-width-modulation (PWM) H-bridge switch-and-transformer circuit like that shown in Figure 1. The circuit could be part of a dc-to-dc converter or a dc-to-ac inverter; in either case, the output current or voltage is regulated by adjusting the times of opening and closing of semiconductor switches 1 through 4 to adjust the durations of current pulses in the primary winding of the transformer.

The asymmetric timing scheme is derived from a symmetric phase-shift-regulator timing scheme (see Figure 2) that provides a local current loop for turn-off snubbing — that is, for dissipat-

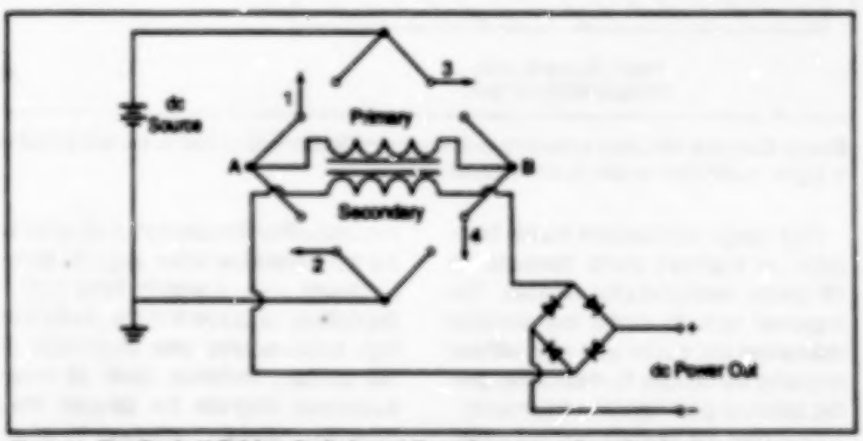

Figure 1. The Basic H-Bridge Switch-and-Transformer configuration is common to numerous dc-to-dc converter and dc-to-ac inverter power-supply circuits.

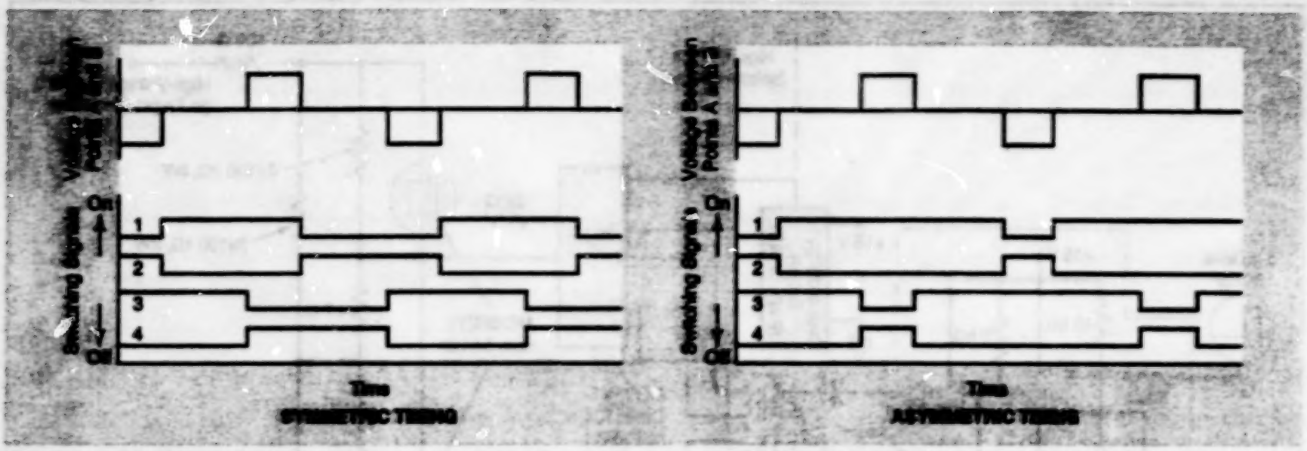

Figure 2. These Timing Diagrams show that in the symmetric scheme, every switch interrupts current at some time during a cycle, whereas in the asymmetric scheme, switches 1 and 3 are opened while they carry no current so that only switches 2 and 4 interrupt current when they are opened.

ing the turn-off-transient current flowing in the leakage inductance of the transformer. This current loop is a short circuit through the primary winding and switches 1 and 3. The main objective in devising the asymmetric timing scheme is to avoid the complication and cost of the high-speed floating drive circuitry that would be needed to open switches 1 and 3 while they were carrying substantial current.

For this purpose, the current-interruption function is distributed asymmetrically among the switches in such a way that switches 1 and 3 are carrying no appreciable current at their respective turn-off times. Only switches 2 and 4, which are referenced to ground and can therefore be turned on and off rapidly with simple drive circuitry, are used to interrupt appreciable current.

This work was done by See-pok Wong of Space Power, Inc., for **Lewis Research Center.** *Further information is contained in a TSP [see page 1].*
LEW-15763

Better Ohmic Contacts for InP Semiconductor Devices

Low-resistance contacts can be fabricated without destructive heat treatments.

Lewis Research Center, Cleveland, Ohio

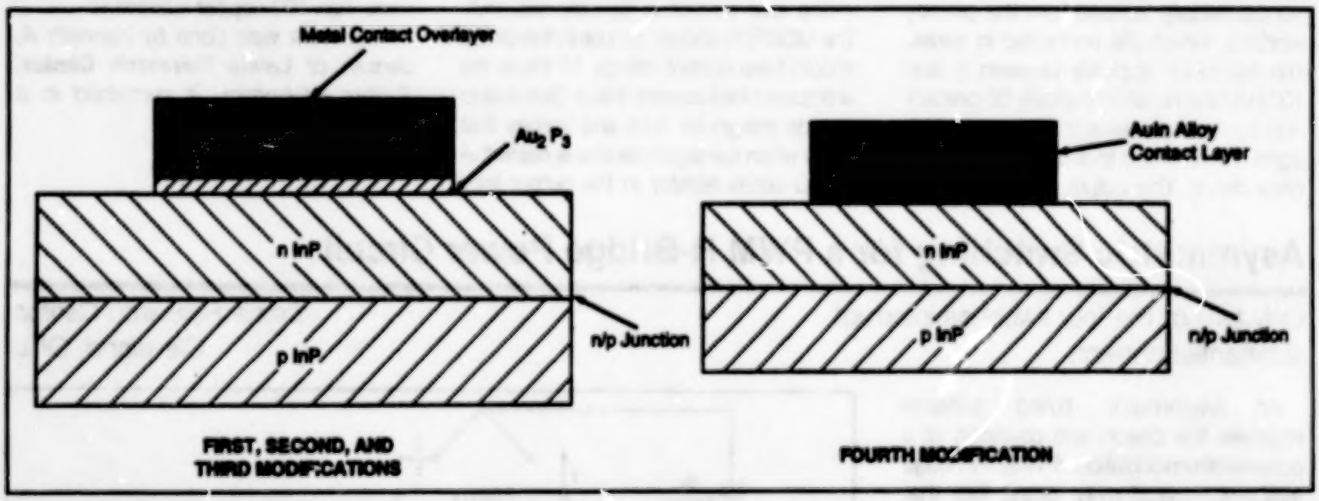

Ohmic Contacts fabricated according to the four modifications described in the text exhibit low contact resistivities, and in some cases, slightly higher resistivities combined with thermal stability.

Four design modifications enable fabrication of improved ohmic contacts on InP-based semiconductor devices. The improved contacts exhibit low electrical resistances and can be fabricated without exposing the devices to destructive predeposition or postdeposition treatments.

Until now, the fabrication of low-resistance contacts on InP devices has involved either the creation of disorder in the InP crystalline lattice (e.g., by bombardment with energetic ions) before deposition, or subjecting the devices to high temperatures after deposition of the contact materials. Both of these treatments degrade the devices; they must be carefully controlled to effect tradeoffs between achieving low contact resistance and inflicting mechanical and electrical damage.

The first modification consists of the insertion of a layer of gold phosphide (Au_2P_3) between n-doped InP and a metal or other overlayer of contact material (see figure). No predeposition bombardment or postdeposition heat treatment is needed, and the resulting

contact resistivity is typically of the order of 10^{-6} Ω·cm^2.

The second modification includes the first modification plus the use of a particular metal overlayer to achieve very low contact resistivities. Specifically, it involves the deposition of an Au_2P_3 interlayer followed by an overlayer of AuGa or AuIn alloy, again without destructive predeposition or postdeposition treatment. It has been found that, depending on the amount of Ga or In in the alloy, the contact overlayer acts synergistically with the Au_2P_3 interlayer to produce contact resistivities as low as 10^{-7} Ω·cm^2.

The third modification also involves the deposition of an Au_2P_3 interlayer; in addition, a refractory metal (W or Ta) is deposited to form the contact overlayer. The contacts thus formed exhibit resistivities of about 10^{-3} to 10^{-4} Ω·cm^2 and can be operated at temperatures of as much as 400 °C for tens of hours without degradation. This modification can be useful in fabricating devices that must withstand deliberate or inadvertent heat treatments during fabrication or that must retain low resistivities when exposed to high operating temperatures.

In the fourth modification, a contact layer of AuIn alloy is deposited directly on the InP. Conventional contact materials are unable to withstand high temperatures for long times without degradation of the p/n junctions in the underlying InP devices. Depending on the relative concentrations of Au and In in this contact alloy, chemical reactions between the metal contact layer and the underlying InP at high temperatures are retarded to varying degrees. In particular, a composition of Au_9In_4 has been found to stop effectively all device-degrading metallurgical reactions at the alloy/InP interface at a temperature of 400 °C: contact resistivities remain of the order of 10^{-4} Ω·cm^2 for many hours, even at this high temperature.

This work was done by Victor G. Weizer of Lewis Research Center and Navid S. Fatemi of Sverdrup Technology, Inc. Further information is contained in a TSP [see page 1].

LEW-15747/497/498

$In_xGa_{1-x}As/GaAs$ Quantum-Well Infrared Photodetectors

Detectivities of experimental devices were found to be comparable to those of $Al_xGa_{1-x}As/GaAs$ devices.

NASA's Jet Propulsion Laboratory, Pasadena, California

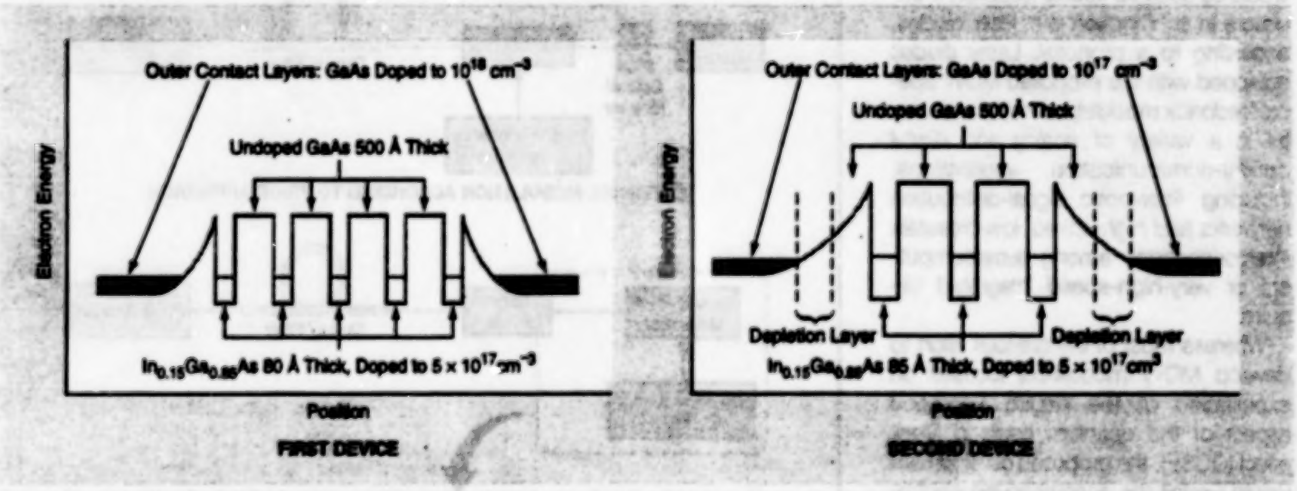
Outer Contact Layers: GaAs Doped to 10^{18} cm^{-3}
Undoped GaAs 500 Å Thick
Electron Energy
$In_{0.15}Ga_{0.85}As$ 80 Å Thick, Doped to 5×10^{17} cm^{-3}
Position
FIRST DEVICE
Outer Contact Layers: GaAs Doped to 10^{17} cm^{-3}
Undoped GaAs 500 Å Thick
Electron Energy
Depletion Layer
Depletion Layer
$In_{0.15}Ga_{0.85}As$ 85 Å Thick, Doped to 5×10^{17} cm^{-3}
Position
SECOND DEVICE

These Conduction-Band Energy-Level Diagrams show the multiple-quantum-well structures of two experimental $In_xGa_{1-x}As/GaAs$ QWIPs. The outer undoped GaAs layers in the second device reduce the dark current.

The first infrared photodetectors that operate at wavelengths as long as 18 μm have been made with multiple-quantum-well structures that consist of quantum-well layers of $In_xGa_{1-x}As$ alternating with non-lattice-matched quantum-barrier layers of GaAs. Heretofore, quantum-well infrared photodetectors (QWIPs) have been made with quantum-well layers of GaAs alternating and lattice-matched, variously, with quantum-barrier layers of $Al_xGa_{1-x}As$, $Ga_{0.5}In_{0.5}P$, or $Al_{0.5}In_{0.5}P$. Note that GaAs is the well material in the older devices and the barrier material in the present devices.

The choice of materials for the present QWIPs was affected principally by two considerations. One was that in comparison with GaAs, $In_xGa_{1-x}As$ is potentially a superior quantum-well material because of its stronger absorption of infrared radiation. The other consideration was that in comparison with $Al_xGa_{1-x}As$, which is the usual barrier material in the older devices, GaAs is potentially a superior barrier material because it exhibits superior transport properties (lower scattering and higher mobility of charge carriers).

The figure illustrates the quantum-well layer configurations of two experimental QWIPs made of $In_{0.15}Ga_{0.85}As/GaAs$. The first device contains five 80-Å-thick $In_{0.15}Ga_{0.85}As$ quantum-well layers doped to 5×10^{17} cm^{-3}, separated by 500-Å-thick quantum-barrier layers of undoped GaAs. The outer contact layers are made of GaAs doped to 10^{18} cm^{-3}; unlike in older QWIPs, the heavily doped contacts are made of the higher-band-gap GaAs semiconductor — in this case, GaAs. This is quite different from the $Al_xGa_{1-x}As/GaAs$ heterosystem, in which the GaAs is the low-band-gap quantum-well and contact material.

This reversal of roles is necessary because a thick contact layer of the strained, non-lattice-matched $In_{0.15}Ga_{0.85}As$ would contain too many defects and threading dislocations. The design of the first device makes use of the strong bending of the energy band in the region between the heavily doped GaAs contact layers and the first and last $In_{0.15}Ga_{0.85}As$ quantum wells. This results in a large quantum-mechanical-tunneling current, which essentially

short-circuits the first and last wells, thus effectively making contact with the low-band-gap material. The active quantum-well structure therefore consists of the middle three quantum wells.

The second device contains three 85-Å-thick $In_{0.15}Ga_{0.85}As$ quantum-well layers doped to 1×10^{17} cm^{-3}, interspersed with four 500-Å-thick quantum-barrier layers of undoped GaAs. The outer contact layers are made of GaAs doped to 1×10^{17} cm^{-3}. It is worth noting that unlike the first device, this device contains undoped GaAs spacer layers between the outermost quantum well and the outer contact layers: as a result, the tunneling injection current from the contacts to the quantum wells should be significantly smaller than it is in the first device. Therefore, the dark current of the second device should be smaller, resulting in higher detectivity.

Experiments have confirmed that the dark current of the second device is much smaller than that of the first device at temperatures below 60 K. The spectral responsivities of the devices were measured at 40 K with a bias of 100 mV. For the first and second devices, the responsivities peak at wavelengths of 15.3 and 18 μm, respectively, while both devices reach their long-wavelength (half-peak) cutoffs at 18.3 μm. The detectivities of both devices increase with decreasing temperature: at 10 K, the detectivities of the first and second devices were found to be 8.0×10^9 $cm\text{-}Hz^{1/2}/W$ and 9.7×10^{10} $cm\text{-}Hz^{1/2}/W$, respectively — comparable to the detectivities of $Al_xGa_{1-x}As/GaAs$ QWIPs.

This work was done by Sarath D. Gunapala, Jin S. Park, True-Lon Lin, and John K. Liu of Caltech for NASA's Jet Propulsion Laboratory. Further information is contained in a TSP [see page 1].
NPO-19323

MQW Optical Feedback Modulators and Phase Shifters

Modulators would consume less drive power and would be compatible with integrated circuits.

NASA's Jet Propulsion Laboratory, Pasadena, California

Multiple-quantum-well (MQW) devices would be used as optical feedback modulators in conjunction with laser diodes, according to a proposal. Laser diodes equipped with the proposed MQW optical feedback modulators may prove useful in a variety of analog and digital optical-communication applications, including fiber-optic signal-distribution networks and high-speed, low-crosstalk interconnections among supercomputers or very-high-speed integrated circuits.

Whereas most of the previous effort to develop MQW modulators focused on exploitation of the electro-absorption aspect of the quantum confined Stark effect (QCSE), the proposed development would exploit the accompanying electro-optical aspect of the QCSE — a variation in the index of refraction with the applied electric field. The proposed development would also exploit the sensitivity of laser diodes to optical feedback. This approach is the reverse of the prior approach, in which optical feedback was regarded as a nuisance because it could cause unstable operation and laser diodes were therefore packaged with optical isolators to suppress optical feedback.

The upper part of the figure illustrates the use of an external modulator, according to the prior approach, to achieve well-behaved modulation of the laser output. Typical radio-frequency and optical insertion losses in this arrangement are about 40 dB. Moreover, because of the low damage-threshold power of the modulator (typically, 10 mW) and optical insertion loss as high as 10 dB in the external modulator, it is often difficult to achieve an acceptably high signal-to-noise ratio at the receiver.

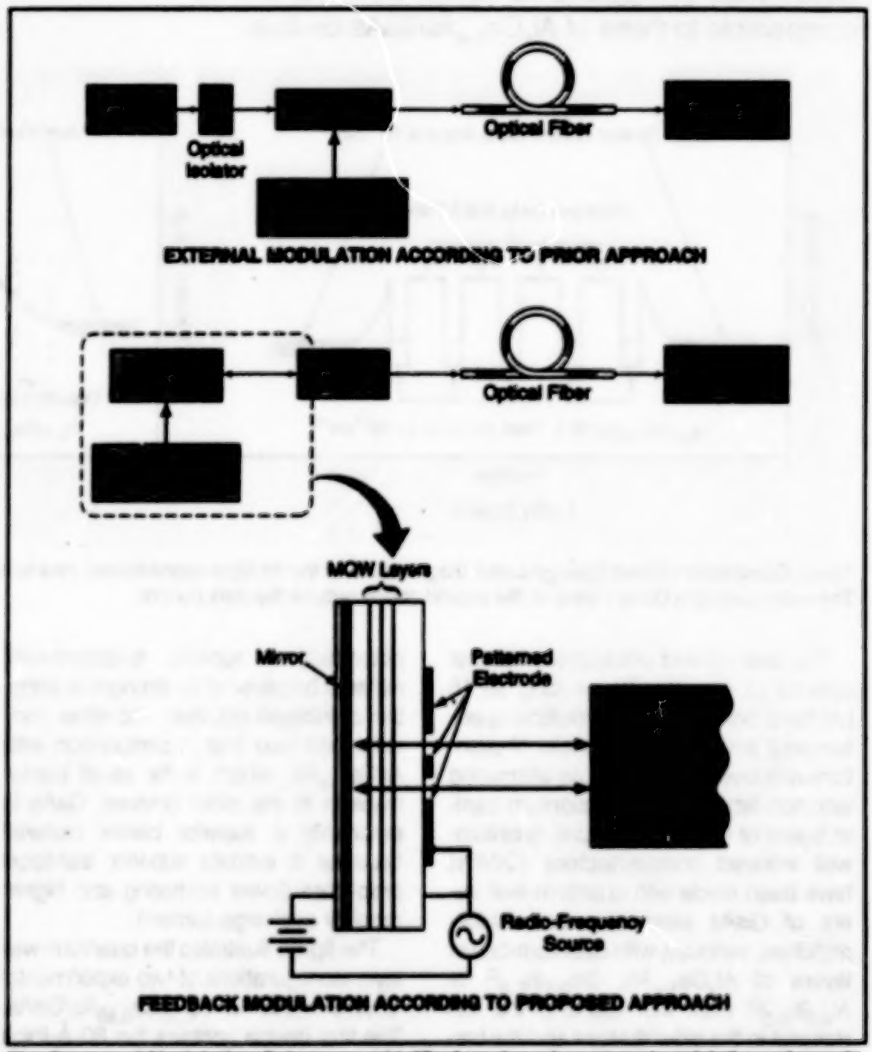

The Proposed Modulation Scheme would differ from the prior external-modulation scheme in that it would exploit feedback, taking advantage of the electro-optical effect in an MQW device.

The lower part of the figure illustrates the use of a proposed MQW optical feedback modulator. Because the sizes and

capacitances of the proposed MQW optical feedback modulators would be smaller than those of typical external modulators used previously, the proposed modulators would require lower drive voltages. Other expected advantages of the proposed modulators include smaller optical insertion losses and compatibility of MQW structures with control electronic circuits of the monolithic microwave integrated-circuit and very-high-speed integrated-circuit types.

To reduce insertion losses and required radio-frequency drive voltages, an MQW modulator according to the proposal would be designed expressly for the purpose, with a novel MQW and electrode structure to achieve feedback modulation through the back side of the laser. Calculations of the electro-optical aspect of the QCSE indicate that optical phase shifts of the order of π radians are potentially achievable with some MQW structures.

An MQW device of the proposed type would include a patterned metal electrode on the surface facing the laser diode. This electrode would be used to bias the device to reflect part of the light incident upon it, shifting the phase of that part of the light by π radians. The part of the light not reflected by this electrode would enter the device, travel back (leftward in the figure) through the MQW layers, be reflected from the rear (leftmost in the figure) mirror, pass through the MQW layers again, then leave the device through the electrode gaps and return to the laser. The phase of this part of the light would depend on the voltage applied to the MQW device. Thus, one could vary the phase of light returned to the diode laser in a spatially complex manner, thereby influencing the spatial pattern of the output laser beam. Because changing the spatial pattern of the laser beam would change the efficiency of coupling of the beam into an optical fiber, the part of the beam that entered the fiber would become correspondingly amplitude-modulated.

This work was done by Deborah J. Jackson of Caltech for NASA's Jet Propulsion Laboratory. Further information is contained in a TSP [see page 1].
NPO-19310

Measuring Pixel-Position Errors on CCD Imagers

Interference fringes are used as a reference pattern.

NASA's Jet Propulsion Laboratory, Pasadena, California

Deviations of the positions of pixels on a charge-coupled-device (CCD) image detector from a nominal rectangular grid pattern can be measured by a method in which coherent-light interference fringes are used as a reference pattern. These deviations are attributed, at least in part, to imperfections in step-and-repeat machinery used to generate the grid patterns in manufacturing. The method was conceived for use in determining pixel-position errors in astrometric cameras to be flown aboard spacecraft. The method can also be applied to the determination of similar errors in (and calibration of) terrestrial CCD cameras used as position sensors; for example, position-measuring cameras that are parts of robotic systems.

Figure 1 illustrates schematically how the interference fringes are formed on the CCD and measured. Light from a helium/neon laser is coupled into a single-mode optical fiber that is split into two single-mode optical fibers at a directional coupler. The other ends of the two fibers are held a few millimeters apart in an aluminum block. The ends of the fibers lie on the surface of the block that faces the CCD, with their optical axes perpendicular to this surface. This surface is polished to make it reflective so that the optical axes can be aligned perpendicular to the face of the CCD by use of an ancillary technique that involves observation of multiple reflections of a laser beam.

The ends of the fibers are held at a distance of about 1 m from the CCD, so that in the case of a CCD of typical dimen-

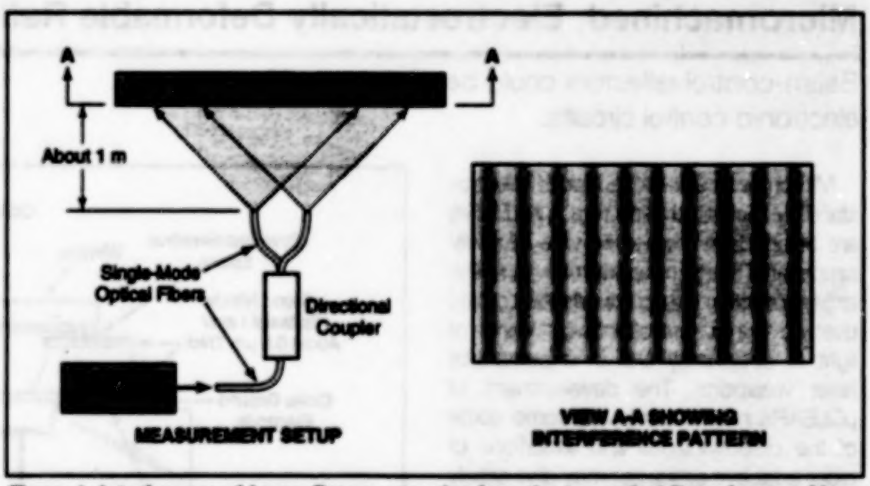

Figure 1. Interference of Laser Beams emerging from the two optical fibers forms a fringe pattern that is used as a reference grid.

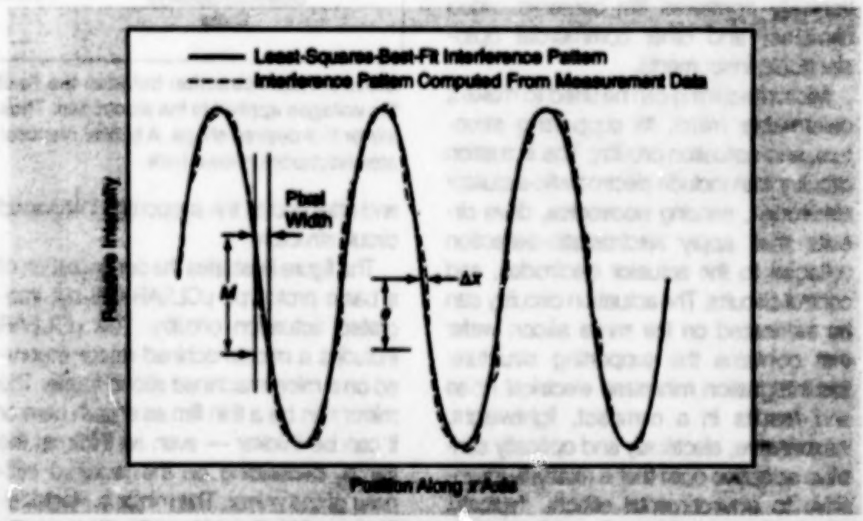

Figure 2. The Error in the Position of a Pixel is estimated from the residual quantity, for that pixel, obtained from the least-squares best fit of the idealized interference pattern.

sions, the spatial interval between successive interference fringes is about 20 pixels. The fringe spacing, the polarization of the laser light, and the orientation of the fringes in the CCD plane are not critical; it is not even necessary to suppress jitter because the effects of fluctuations on the readouts of the pixels are suppressed by integrating the readouts over exposure times of a few seconds. In addition to the exposure taken with interfering light from both fibers, an exposure is taken with light from each fiber alone; these single-fiber exposures provide calibration data that are used to correct for spatial variations of the intensities of the beams from the fibers when analyzing the readouts from the two-fiber exposure by the technique described next.

The time-integrated CCD readouts from the two-fiber exposure are digitized, corrected for beam spatial variations, and compared with the corresponding computer-generated data on ideal interference fringes. The global fringe spacing, orientation, phase, amplitude, and modulation of the actual interference pattern are deemed to be those of whichever computer-generated pattern best fits the measurement data according to the method of least squares.

The residual (error) quantities of the least-squares best fit are due to (1) poor quantum-efficiency calibration, (2) subpixel gradients in illumination and/or sensitivity, and/or (3) the pixel-position errors that one seeks to determine. The effects of quantum-efficiency calibration errors can be suppressed by taking many single-fiber exposures. The effects of intrapixel gradients can be suppressed by making the fringe spacing much larger than a pixel, and preferably at least 10 pixels; this is the reason for the choice of the 20-pixel fringe spacing mentioned above.

The remaining residual quantities can thus be attributed to pixel-position errors; the position error, Δx, for each pixel is estimated from $\Delta x \approx e/M$, where e is the residual quantity for that pixel and M is the gradient (change per unit pixel width) of the idealized interference pattern at the nominal position of the pixel (see Figure 2). The position errors are thus estimated only in the neighborhoods that contain the maximum gradients of the idealized interference pattern; a map of position errors across the entire CCD is obtained by piecing together maps made from fringe patterns with different phases.

This work was done by Stuart B. Shaklan, Mike Shao, Yekta Gursel, and Jeffrey Yu of Caltech for NASA's Jet Propulsion Laboratory. Further information is contained in a TSP [see page 1].
NPO-19419

Micromachined, Electrostatically Deformable Reflectors

Beam-control reflectors could be integrated with electronic control circuits.

NASA's Jet Propulsion Laboratory, Pasadena, California

Micromachined, closed-loop, electrostatically actuated reflectors (μCLEARs) are being developed to provide relatively simple and inexpensive alternatives to the large, complex, expensive adaptive optics used to control wavefronts of beams of light in astronomy and in experimental laser weapons. The development of μCLEARs may not only overcome some of the disadvantages and limitations of older adaptive optics but may also satisfy demands of a potential market for small, inexpensive deformable mirrors in electronically controlled film cameras, video cameras, and other commercial optoelectronic instruments.

Micromachining can be used to make a deformable mirror, its supporting structure, and actuation circuitry. The actuation circuitry can include electrostatic-actuator electrodes, sensing electronics, drive circuits that apply electrostatic-deflection voltages to the actuator electrodes, and control circuits. The actuation circuitry can be fabricated on the same silicon wafer that contains the supporting structure; this integration minimizes electrical noise and results in a compact, lightweight, inexpensive, electrically and optically sensitive adaptive optic that is relatively insensitive to environmental effects. Typically, the deformable mirror is made from a separate piece of silicon or other material and attached to the supporting integrated circuit structure.

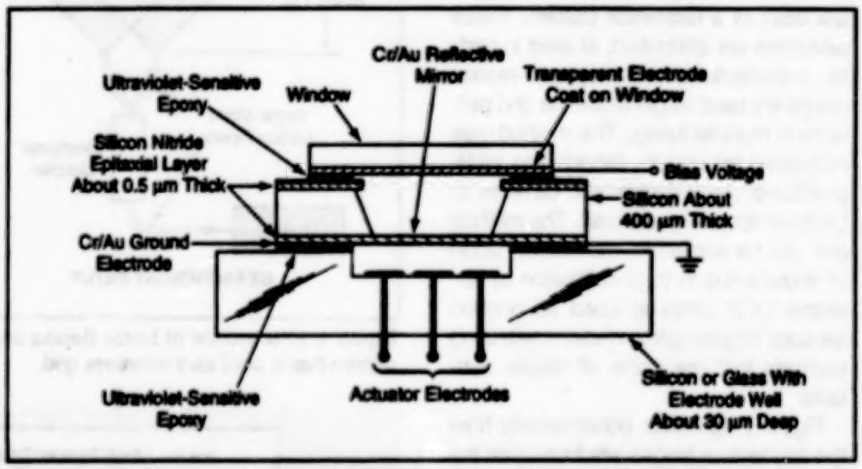

Electrostatic Attraction between the flexible mirror and each of the electrodes varies with the voltages applied to the electrodes. Thus, the applied voltages can be varied to deform the mirror to a desired shape. A typical practical μCLEAR would contain more than the three actuator electrodes shown here.

The figure illustrates the configuration of a basic prototype μCLEAR without integrated actuation circuitry. This μCLEAR includes a micromachined mirror mounted on a micromachined silicon frame. The mirror can be a thin film as shown here or it can be thicker — even as thick as the frame, depending on the required stiffness of the mirror. The mirror is electrically grounded and aligned above a planar array of actuator electrodes, forming an array of parallel-plate capacitors. A window that holds a transparent electrode is mounted in the front of the mirror surface.

A bias voltage applied to the transparent electrode moves the mirror into a preload deformation position away from the array of actuator electrodes. Application of a voltage to an actuator electrode results in electrostatic attraction between that electrode and the mirror, resulting in a deformation, concentrated in the vicinity of that electrode, of the mirror toward that electrode. The capacitances between

actuator electrodes and a mirror can be exploited to obtain capacitive feedback indicative of the distances between the electrodes and the mirror and thus indicative of the state of displacement or deformation of the mirror. The capacitive displacement feedback from each actuator electrode eliminates the need for costly and complex optical deformation feedback, and enables more accurate position control than can be obtained from conventional open-loop systems.

Electrostatic actuation can be achieved at powers and voltages smaller than those of piezoelectrically actuated adaptive optics. The thicknesses of mirrors and structural boundary conditions can be widely varied among μCLEAR designs to obtain deformations in various preferred modes. Actuator electrodes can be laid out in specified patterns to achieve the desired deformations with minimum numbers of electrodes and simplified control algorithms and electronics. Closed-loop electrostatic actuation can be combined with advanced control algorithms that take into account the nonlinear structural behaviors of mirrors. For example, layouts of actuator electrodes, control algorithms, and actuation circuits can be designed to provide control of individual deformation modes (e.g., finite numbers of Zernike modes), with minimal interactions among modes.

This work was done by Randall K. Bartman, Paul K. C. Wang, Linda M. Miller, Thomas W. Kenny, William J. Kaiser, Fred Y. Hadaegh, and Michael L. Agronin of Caltech for **NASA's Jet Propulsion Laboratory.** *Further information is contained in a TSP [see page 1].*
NPO-19154

Correcting for Capacitance in Tests of Solar Cells

Modifications of the test procedure and software yield corrected I-V characteristics.

NASA's Jet Propulsion Laboratory, Pasadena, California

A modified procedure for testing solar photovoltaic cells and modified software for processing the test data provide corrections for the effects of cell capacitance. The modified test procedure and software are needed because (a) some photovoltaic devices (for example, silicon solar cells with a back-surface field region) store minority charge carriers in the cell junction and thus exhibit significant capacitance, (b) capacitance affects current-vs.-voltage (*I-V*) measurements made when a transient load is connected to a cell, and (c) a transient load is used in the unmodified version of the test procedure.

In the modified testing procedure as in the unmodified one, *I* and *V* are measured under various loads when the solar cells are illuminated by a pulsed source of artificial sunlight. The first part of the modified procedure consists of the unmodified procedure, in which *I-V* measurements are taken as the load is swept from short to open circuit during a pulse of artificial sunlight. This procedure yields a complete *I-V* curve, but in the case of high cell capacitance this procedure yields measured values of *V* that are below the true cell voltages for the corresponding measured values of *I*.

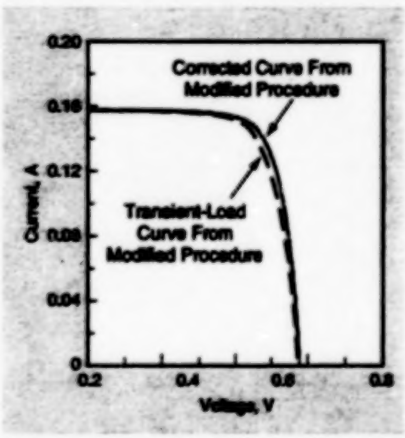

The Corrected *I-V* Curve obtained in a test of a solar cell according to the modified procedure approximates the true cell voltage vs. cell current more closely than does the transient-load *I-V* curve obtained in the unmodified test procedure.

In the modified procedure, *I-V* measurements are also taken under four fixed-load conditions: (1) at a current a few percent below the short-circuit current, (2) at a current near the maximum-power point, (3) at half the short-circuit current, and (4) near the open-circuit voltage, where the current is only a few percent of the short-circuit current.

The modified software uses the fixed-load *I-V* data, which lie on the true *I-V* curve, to produce an interpolated *I-V* curve that closely represents true *I-V* data. This approximation of the true *I-V* curve resembles the transient-load *I-V* curve but is shifted to slightly higher voltage at a given current (see figure).

This work was done by Robert L. Mueller of Caltech for **NASA's Jet Propulsion Laboratory.** *Further information is contained in a TSP [see page 1].*
NPO-19516

Books and Reports

Effect of Clock Mode on Radiation Hardness of an ADC

A report discusses techniques for testing and evaluating the effects of total exposures of ionizing radiation on the performances of high-resolution successive-approximation analog-to-digital converters (ADCs), without having to test each individual bit or transition. The basic thrust of this discussion is to reduce the cost of testing by reducing tests to a few critical parametric measurements, from which one can determine approximate radiation failure levels that will provide good approximations of the responses of the converters for purpose of total-dose-radiation evaluations. The report describes experiments on three ADCs from different manufacturers: a 16-bit complementary metal oxide/semiconductor (CMOS) unit, a 14-bit BICMOS unit, and a 12-bit BICMOS unit. The most significant observation made in the experiments was that the 14-bit unit exhibited an unusual dependence of the failure level on the clock mode: When an external clock was used, this converter failed at a total dose of 4 krad(Si), but when the clock within the converter was used, failure did not occur until a total dose of 40 krad(Si) had been accumulated. This result suggests that the use of the internal clock could increase the radiation failure level in a practical application by an order of magnitude.

This work was done by Choon I. Lee, Bernie G. Rax, and Allan H. Johnston of

Caltech for NASA's Jet Propulsion Laboratory. To obtain a copy of the report, "Hardness Assurance and Testing Techniques for High Resolution (12- to 16-bit) Analog-to-Digital Converters," see TSP's [page 1].
NPO-19697

Data Base on Cables and Connectors

A report describes the Connector Adapter Cable Information Data Base (CONNAID) computer program, which manages a data base containing necessary information concerning electrical connectors, breakout boxes, adapter cables, backshells, and pertinent torque specifications for an engineering project. A connector number can be entered, and the computer will provide compatible and mating connector information and specification references. The correct adapter cable number is presented along with breakout box configuration options, installation instructions, and diagrams.

This work was done by Arlen R. Bowen and John D. Oliver of McDonnell Douglas Corp. for Kennedy Space Center. To obtain a copy of the report, "CONNAID (Connector Adapter Cable Information Data Base)," see TSP's [page 1].

Inquiries concerning rights for the commercial use of this invention should be addressed to the Patent Counsel, Kennedy Space Center [see page 1]. Refer to KSC-11762.

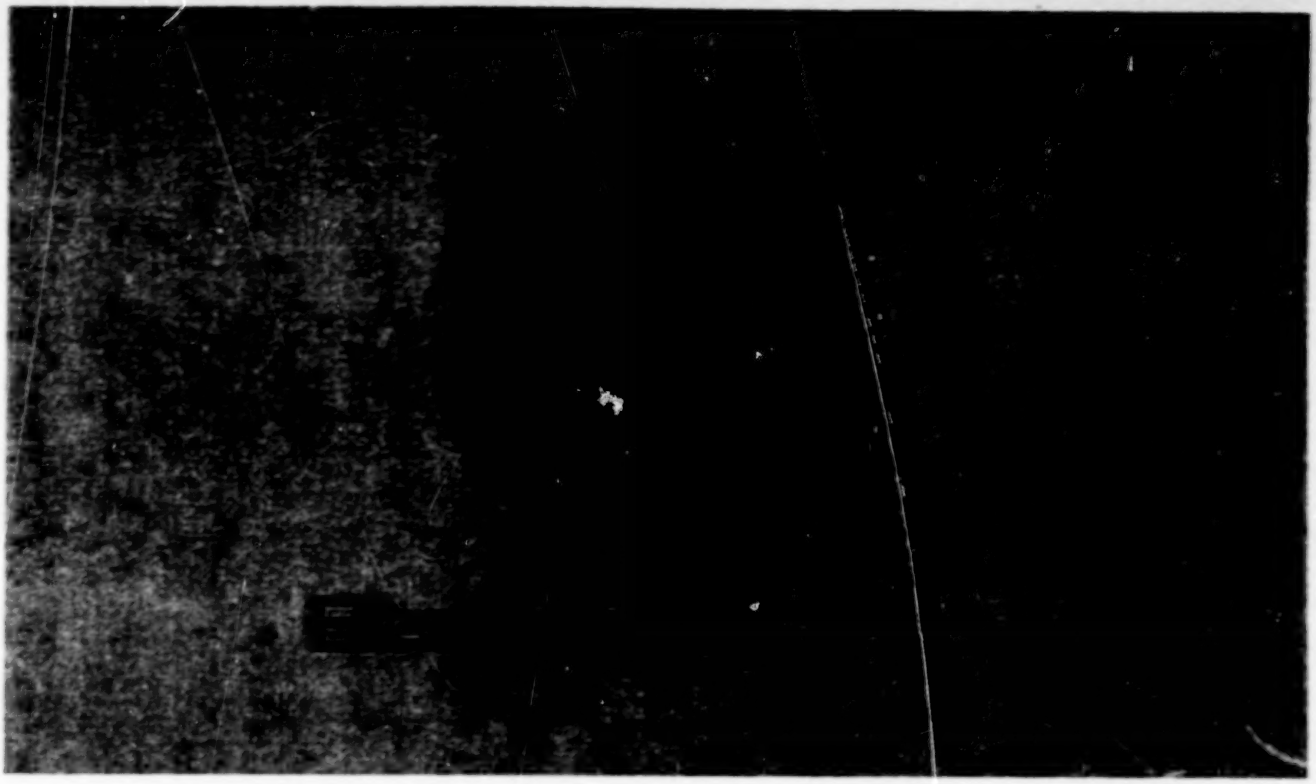

Hardware, Techniques, and Processes

23 Buffered Telemetry Demodulator
24 Computer-Assisted Monitoring of a Complex System
24 Compact Multifunction Inspection Head

Books and Reports

25 Digital Controller for Laser-Beam-Steering Subsystem
25 More About Beam-Steering Subsystem for Laser Communication
26 Digital Controller for Laser-Beam-Steering Subsystem: Part 2
26 Interface Circuit Board for Space-Shuttle Communications
26 Automated Planning of Spacecraft Telecommunications
26 Study of Partial-Band Detection of Frequency-Hopped Signals
27 Neural-Network Controller for Vibration Suppression
27 Artifacts of Spectral Analysis of Instrument Readings

BLANK PAGE

Buffered Telemetry Demodulator

Signals would be processed, recorded, and reprocessed.

NASA's Jet Propulsion Laboratory, Pasadena, California

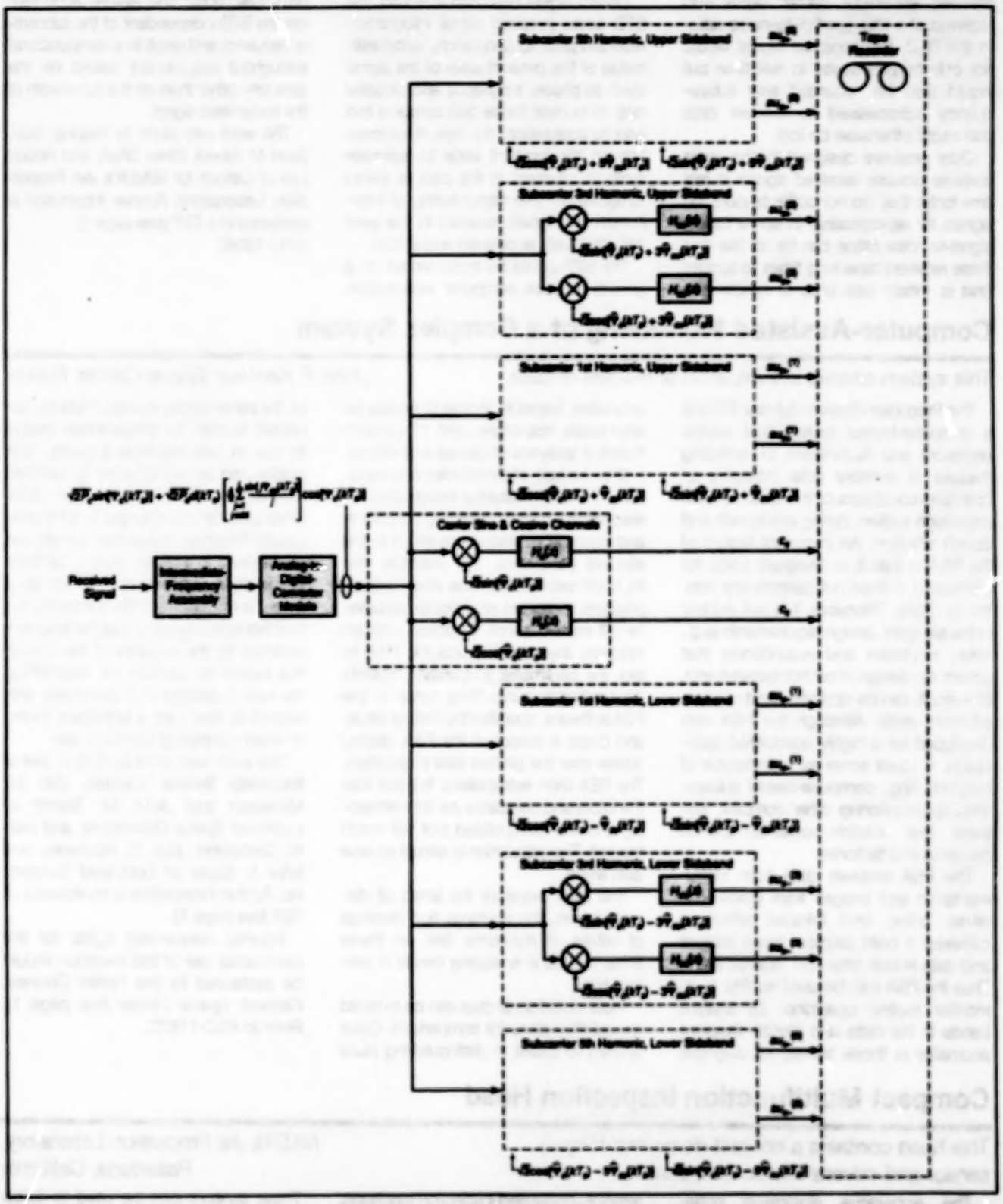
Subcarrier 5th Harmonic, Upper Sideband
Tape Recorder
Subcarrier 3rd Harmonic, Upper Sideband
Subcarrier 1st Harmonic, Upper Sideband
Carrier Sine & Cosine Channels
Received Signal
Intermediate Frequency Assembly
Analog-to-Digital Converter Module
Subcarrier 1st Harmonic, Lower Sideband
Subcarrier 3rd Harmonic, Lower Sideband
Subcarrier 5th Harmonic, Lower Sideband

Signals Would Be Down-Converted to Baseband and recorded on a subcarrier-harmonic basis. This scheme is one of two proposed alternative schemes for down-conversion and recording in the BTD.

The buffered telemetry demodulator (BTD) is a radio receiver designed mainly for recovery of low-rate data binary phase-modulated onto a square-wave subcarrier on a sinusoidal or suppressed sinusoidal carrier signal and received at a low symbol-to-noise ratio. In the BTD, the received signal would not only be processed in real time but would also be recorded and subsequently reprocessed to recover data that might otherwise be lost.

Older receivers designed for the same purpose process received signals in real time (only); they do not buffer or store the signals for reprocessing. In some cases, signal-to-noise ratios can be so low that these receivers take long times to acquire (that is, initially lock onto or synchronize themselves with) the signals and long times to reacquire the signals when they have lost synchronization. Significant loss of data occurs during these long times out of synchronization.

Once a signal has been acquired, the BTD could process signal information recorded prior to acquisition, using estimates of the present state of the signal (such as phase, frequency, and Doppler rate) to recover those data symbols lost prior to acquisition: this use of information on the present state to estimate symbols received in the past is called "smoothing." The reprocessing of information on signals received in the past can effectively accelerate acquisition.

The BTD could be implemented on a general-purpose computer workstation. To reduce the computational requirement, the main processing would take place after the incoming signal had been both open-loop down-converted to baseband and recorded on a subcarrier-harmonic basis (see figure). This feature would render the BTD independent of the subcarrier frequency and result in a computational throughput requirement based on the data rate rather than on the bandwidth of the transmitted signal.

This work was done by Haiping Tsou, Sami M. Hinedi, Biren Shah, and Robert Lee of Caltech for **NASA's Jet Propulsion Laboratory.** *Further information is contained in a TSP [see page 1].*
NPO-19080

Computer-Assisted Monitoring of a Complex System

This system assists in evaluation of masses of data.

John F. Kennedy Space Center, Florida

The Propulsion System Advisor (PSA) is a computer-based system that assists engineers and technicians in analyzing masses of sensory data indicative of operating conditions of the space shuttle propulsion system during pre-launch and launch activities. An important feature of the PSA is that it is designed solely for monitoring; it does not perform any control functions. Therefore, it is not subject to the stringent design requirements (e.g., safety interlocks and redundancy) that govern the design of control systems and, as a result, can be optimized and upgraded more easily. Although the PSA was developed for a highly specialized application, it could serve as a prototype of noncontrolling, computer-based subsystems for monitoring other complex systems like electric-power-distribution networks and factories.

The PSA receives data from instrumentation and images from black-and-white, color, and infrared television cameras. It both displays these images and data in real time and records them. Thus the PSA can be used flexibly, to (a) monitor routine operation, (b) analyze trends in the data and identify incipient anomalies in those trends, (c) diagnose anomalies, hopefully in time to decide on appropriate responses, and (d) perform historical analyses of causes and effects.

With the help of stored rules and equations, the PSA evaluates instrumentation readings to estimate operating conditions and trends in operating conditions in the affected equipment. For example, the PSA can estimate the time when a given pressure, temperature, or other parameter will exceed a limit. To obtain such an estimate, the user instructs the PSA to plot the parameter in question, selects the applicable curve-fitting option in the PSA software, specifies the limiting value, and drags a cursor of the PSA display screen over the plotted data in question. The PSA then extrapolates the plot into the future and calculates the time remaining until the extrapolated plot will reach the limit. The calculation is refined as new data arrive.

The PSA monitors the times of discrete events like openings and closings of valves. It maintains files on these events for use in analyzing trends in performance.

Plots of historical data can be overlaid on real-time plots for comparison. Color is used to assist in distinguishing plots on the same display screen. Plots can be printed in color for presentation and/or for use in near-real-time analysis. Split graphs can be constructed to facilitate comparison of rapidly changing data. Small plots can be enlarged to full screen size for maximum resolution. Labels can be attached to lines on plots to facilitate identification. A mark can be set on a graph, such that the PSA computes the time between the mark and the time represented by the position of the cursor: this feature is valuable for determining the rate of change of a parameter with respect to time near a significant event, or when comparing historical data.

This work was done by Bob J. Bell of **Kennedy Space Center;** *Eric M. Mickelson and John M. Sterritt of Lockheed Space Operations; and Rob W. Costantino, Bob C. Houvener, and Mike A. Super of Lockheed Sanders, Inc. Further information is contained in a TSP [see page 1].*

Inquiries concerning rights for the commercial use of this invention should be addressed to the Patent Counsel, Kennedy Space Center [see page 1]. Refer to KSC-11673.

Compact Multifunction Inspection Head

This head contains a contact (force-and-torque) sensor and several noncontact sensors.

NASA's Jet Propulsion Laboratory, Pasadena, California

The apparatus illustrated schematically in the figure is a multiple-sensor inspection head. It is designed to be mounted at the tip of a robot arm for performing multiple automated and/or remotely controlled inspection functions. The mass of the head is about 3.5 kg.

The inspection head contains two infrared sensors that measure distances up to about 75 cm by triangulation. These sensors can be used to follow and measure surface contours and to prevent collisions as the robot arm moves the head. Along with the proximity sensors, a force-and-torque sensor

with 6 degrees of freedom provides readouts that aid in the control of the robot arm.

An infrared pyrometer in the head is sensitive at wavelengths from 8 to 12 μm; it is used to measure temperatures from 0 to 1,000 °F (-18 to 538 °C). Chemical vapors and other gases are sensed by a metal oxide/semiconductor sensor, the electrical resistance of which changes when it absorbs the gases.

Two color charge-coupled-device video cameras are mounted on the head. Two halogen lamps in the head provide illumination, with intensity controlled by an optical-transistor feedback circuit. This lighting is augmented by two fast-pulse stroboscopic lamps that enable the taking of pictures in single-video-frame bursts (like those of film cameras). The cameras are calibrated for stereoscopic viewing. Because the stroboscopic lamps are mounted on the movable jaws of a parallel-jaw gripper, the angles of flash illumination can be adjusted by movement of the jaws.

This work was done by Richard A. Volpe, Robert Mev, and Timothy Ohm of Caltech for NASA's Jet Propulsion Laboratory. Further information is contained in a TSP [see page 1].
NPO-19368

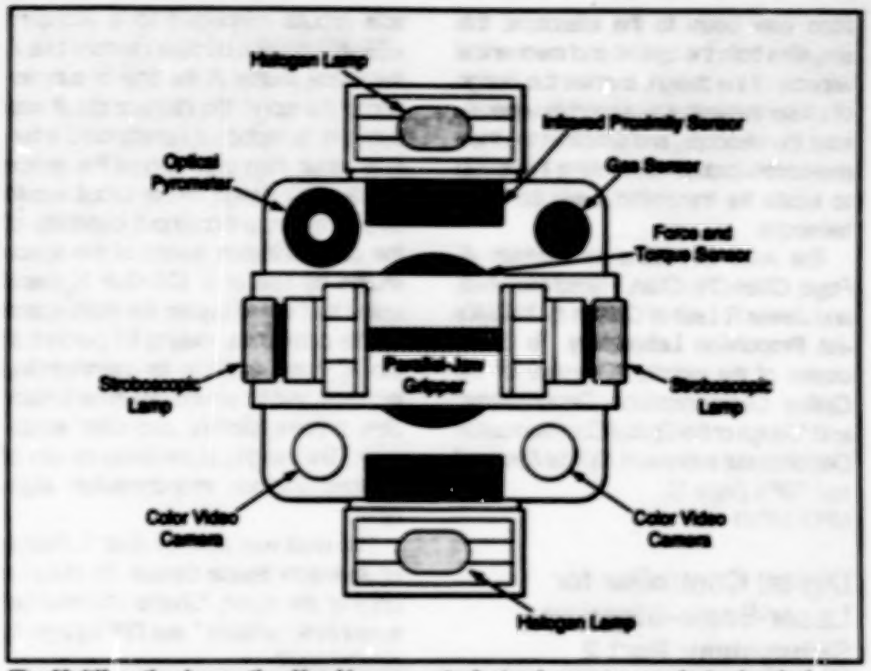

The Multifunction Inspection Head houses optoelectronic sensors, an electrochemical sensor, sources of illumination, and a parallel-jaw gripper.

Books and Reports

Digital Controller for Laser-Beam-Steering Subsystem

Design and performance are described.

A report presents additional information about the proposed apparatus described in "Beam-Steering Subsystem for Laser Communication" (NPO-19089), *NASA Tech Briefs*, Vol. 19, No. 6 (June, 1995), page 32. To recapitulate: Two spots of light would be projected onto a charge-coupled-device imaging array on the focal plane of a telescope, one spot being the projection of a beam of light received from a distant beacon, the other spot being the projection of a transmitted laser beam. The relative angular positions of the two beams would be measured and processed by a digital control subsystem to generate commands to the actuators of a lightweight, relatively inexpensive transmitted-beam-steering mirror to stabilize the relative direction of the two beams at a desired point-ahead angle. The report discusses the design of the digital beam-steering control subsystem and, in particular, that part of the design that pertains to digital compensation for the frequency response of the steering mirror. According to the report, a working prototype of the system was built and was undergoing testing at the time of writing. The prototype control subsystem operates at a digital sampling rate of 2 kHz, which should be more than adequate in view of the 17-Hz resonant frequency of the steering mirror. Preliminary results of computer simulations and experiments suggest that the system will work as expected.

This work was done by Homayoon Ansari of Caltech for NASA's Jet Propulsion Laboratory. To obtain a copy of the report, "Discrete-Time Design of Tracking Control Loop for Optical Communications," see TSP's [page 1].
NPO-19193

More About Beam-Steering Subsystem for Laser Communication

Some details of the optical design are presented.

Two reports present additional information about a developmental beam-steering subsystem of a laser-communication system. Aspects of this subsystem have been described in "Beam-Steering Subsystem for Laser Communication" (NPO-19089), Vol. 19, No. 6 (June, 1995), page 32, and "Digital Controller for Laser-Beam-Steering Subsystem" (NPO-19193), (preceding article). To recapitulate: Two spots of light are projected onto a charge-coupled-device imaging array on the focal plane of a telescope, one spot being the projection of a beam of light received from a distant beacon, the other spot being the projection of an attenuated portion of a transmitted laser beam. The relative angular positions of the two beams on the focal-plane array are measured and processed by a digital control subsystem to generate commands to the actuators of a lightweight, transmitted-beam-steering mirror to stabilize the relative direction of the two beams at a desired point-ahead angle so that the transmitted beam will strike a receiver next to the beacon. The two reports reiterate the basic principles of operation of the beam-steering subsystem and of the laser-communication system as a whole. The reports also present some of the details of the optical and mechanical design of a prototype of the subsystem, called the Optical Communication Demonstrator. One of the notable features of the design is the use of a single-mode optical fiber to deliver the outgoing modu-

lated laser beam to the telescope, this simplifies both the optical and mechanical aspects of the design, enables the design of a laser transmitter as a module separate from the telescope, and simplifies the thermal-control problem by making it possible to locate the transmitter away from the telescope.

This work was done by Norman A. Page, Chien-Chu Chen, Hamid Hemmati, and James R. Lesh of Caltech for **NASA's Jet Propulsion Laboratory.** *To obtain copies of the reports, "Overview of the Optical Communications Demonstrator" and "Design of the Optical Communication Demonstrator Instrument Optical System," see TSP's [page 1].*
NPO-19381

Digital Controller for Laser-Beam-Steering Subsystem: Part 2

Further details of design are described.

A report presents additional information about a laser-beam-steering apparatus described in "Beam-Steering Subsystem for Laser Communication" (NPO-19069), Vol. 19, No. 6 (June, 1995), page 32, and "Digital Controller for Laser-Beam-Steering Subsystem" (NPO-19193), page 25. The report that is the subject of this article reiterates the basic principles of operation of the beam-steering subsystem, with emphasis on the modes of operation, basic design concepts, and initial experiments on a partial prototype of the apparatus. The experiments demonstrated closed-loop control mode in which a transmitted laser beam was made to point at a desired point-ahead angle with respect to a simulated jittering beacon. At the time of the report, experiments to characterize the performance of the control loop were in progress.

This work was done by Homayoon Ansari and LeeAnn Volsinet of Caltech for **NASA's Jet Propulsion Laboratory.** *To obtain a copy of the report, "A CCD-Based Control Loop for Precision Beam Pointing," see TSP's [page 1].*
NPO-19441

Interface Circuit Board for Space-Shuttle Communications

A report describes an interface electronic circuit that was developed to enable ground controllers to send commands and data via K_a-band radio uplink to multiple circuits connected to a standard IEEE-488 general-purpose interface bus in the space shuttle. At the time of submission of the report, this interface circuit was destined to replace a nonstandard interface circuit then used aboard the space shuttle. The design of this circuit would extend the data-throughput capability of the communication system of the space shuttle by use of a 128-Kb/s K_a-band uplink that would bypass the main space shuttle computers, making 90 percent of the K_a band available for commanding payloads and for serving experiment modules, printers, plotters, and other equipment. The integrity is preserved by use of a Reed-Solomon error-correction algorithm.

This work was done by Brett T. Parrish of **Johnson Space Center.** *To obtain a copy of the report, "Shuttle Communications Interface Board," see TSP's [page 1].*
MSC-22367

Automated Planning of Spacecraft Telecommunications

Tedious and error-prone visual and manual analysis procedures are no longer necessary.

A computer program known as SWIT (Software for What-If Telecommunications) is a user-friendly, modular, portable, window-based software tool. SWIT accelerates and automates planning of antenna usage for spacecraft telecommunication systems and enables predictions of the performances of such systems. Previously, in analyzing the performance of a spacecraft telecommunication system, it was necessary to manually annotate and visually analyze printed plots of data points. The "what if" analyses typically performed in planning telecommunications often took days to complete. SWIT eliminates the need for these tedious and error-prone procedures, by providing for the quick plotting of huge amounts of information on graphs and for the performance of the "what if" analyses within minutes. In a typical application, the user selects the mission, Deep Space Network (DSN) station, spacecraft antenna, and radio frequency band from a MOTIF interface display that consists of buttons and menus. The user can specify spacecraft pointing assumptions, DSN configuration assumptions, and station allocation information as part of the telecommunications link definition. The user then enters the desired confidence level in the returned data, selects colors and patterns for as many as nine simultaneous plots, and receives an on-screen color plot and an optional printed copy. The plots provide information on when a given DSN station can be used to support a spacecraft mission to return data, at what data-transmission rate, characterized by a minimal confidence level specified by the user. It has been estimated that the return on investment from the use of SWIT will be tenfold in terms of work years and even greater in terms of dollars.

This work was done by John R. Venegas, Ursula M. Schwuttke, Monica B. Rivera, and Vickere B. Murphy of Caltech for **NASA's Jet Propulsion Laboratory.** *To obtain a copy of the report, "An Automated Approach for Planning Spacecraft Telecommunications," see TSP's [page 1].*
NPO-19476

Study of Partial-Band Detection of Frequency-Hopped Signals

The best detection performance would be achieved by use of a fixed FFT band.

A paper presents a comparative theoretical study of the performances of alternative schemes for partial-band detection of frequency-hopped signals. The basic mathematical model of the study is that of (a) reception of M-ary ($M \geq 2$) frequency-shift-keyed data modulation on a carrier signal that has been hopped to any of G different available frequencies and (b) frequency channelization in the front end of the receiver effected by a fast-Fourier-transform (FFT) preprocessor that, at any given time, can be tuned to one of a number of nonoverlapping frequency subbands, each of which contains $\rho_0 G$ frequency-hop channels (where $\rho_0 < 1$; that is, the FFT frequency band is only a part of the overall frequency-hop band). This model opens up a range of options for partial-band detection: At one extreme, one could keep the receiving band fixed at one of the subbands, with the consequence that, on the average over time, one would intercept only a fraction ρ_0 of all hops; at the other extreme, one could tune the receiver in discrete steps over the entire frequency-hop band, thus intercepting all hops but sampling only ρ_0 of the available signal during each hop. Using routine simplifying assump-

tions and standard detection-performance criteria, the alternative schemes were analyzed as applied to a hypothetical system with specifications similar to those of a U.S. Army transceiver. The numerical results lead to the conclusion that the best detection performance would be achieved by keeping the receiving band fixed, thereby making more reliable decisions within each observed frequency channel during each hop, even though not all hops would be intercepted.

This work was done by Barry K. Levitt, Marvin K. Simon, Andreas Polydoros, and Unjeng Cheng of Caltech for **NASA's Jet Propulsion Laboratory**. *To obtain a copy of the report, "Partial-Band Detection of Frequency-Hopped Signals," see TSP's [page 1].*
NPO-19226

Neural-Network Controller for Vibration Suppression

The controller includes a three-layer feedforward neural network.

A neural-network-based adaptive-control system is proposed for vibration suppression of flexible space structures. The controller features a three-layer neural network and utilizes output feedback. Measurements are generated by the various sensors on the structure. A feed-forward path may also be included to speed up response in the case that the plant exhibits predominantly linear dynamic behavior.

Controller adaptation is accomplished via the real-time (on-line) training of the neural network. Specifically, the neural net synaptic weights are tuned using a modified sequential nonlinear least squares algorithm (NLS), formulated by taking a prediction error approach. The NLS is chosen for this application over back propagation, LMS, and gradient descent algorithms due to its fast convergence that makes it attractive for on-line applications.

The control system described in this report is applicable to single-input single-output systems.

The performance of the adaptive controller is evaluated by numerical simulation for three test cases: (1) a test case in which only the linear feedforward paths of the controller were used; (2) a test case in which all synaptic-connection weights in the neural network were initialized to small nonzero values, allowing for utilization of the complete neural network; and (3) a test case in which the linear feedforward paths were eliminated.

This work was done by Dhemetrios Boussalis and Shyh Jong Wang of Caltech for **NASA's Jet Propulsion Laboratory**. *To obtain a copy of the report, "Neural Network Vibration Control Based on Output Feedback," see TSP's [page 1].*
NPO-19138

Artifacts of Spectral Analysis of Instrument Readings

Topics addressed include 1/f noise and different measures of power spectral density.

A report presents an experimental and theoretical study of some of the artifacts introduced by processing the outputs of two nominally identical low-frequency-reading instruments — in particular, high-sensitivity servo-accelerometers mounted together and operating, in conjunction with signal-conditioning circuits, as seismometers. The processing in question involved analog-to-digital conversion with anti-aliasing filtering, followed by digital processing that included frequency weighting (in effect, frequency filtering) and computation of different measures of power spectral density (PSD). The study began as a comparison of the different measures of PSD, then expanded to include an attempt to understand and reduce that component of noise that has been traditionally characterized by a PSD proportional to $1/f$, where f denotes frequency. The major findings of the study can be summarized as follows: (1) The cross-spectral density (CSD) computed from the outputs of the two accelerometers is more accurate, as a measure of the true PSD of acceleration, than is the coherent-output-power (COP) spectral density. (2) The traditional "1/f noise" is a combination of true 1/f noise plus leakage of dc signal components into side lobes of frequency bins of filters, except, of course, in rare instances in which dc components are exactly zero. (3) Accordingly, weighting functions should be tested to minimize such leakage. (4) The CSD of the accelerometer readings contains lower apparent 1/f noise than do the COP PSDs, but the higher-frequency coherent-signal components of both types of PSDs are essentially the same.

This work was done by James H. Wise of Caltech for **NASA's Jet Propulsion Laboratory**. *To obtain a copy of the report, "Processing Effects on 1/f Noise and Other Data Artifacts," see TSP's [page 1].*
NPO-19499

BLANK PAGE

Hardware, Techniques, and Processes

31 Double-Knudsen-Cell Apparatus Measures Alloy-Component Activities
32 Measuring Traces of Oxygen by Resonant Electron Attachment
33 Calibrating Polarimetric Radar With Only Natural Targets
34 Optical Detection of Fractures in Ceramic Diaphragms
35 Revolving Eddy-Current Probe Detects Cracks Near Rivets
35 Spectroscopic Measurement of Temperature and Pressure of O_2
36 Using Ultrasonic Lamb Waves To Measure Moduli of Composites
37 Apparent Thermal Conductivity of Multilayer Insulation
38 Eddy-Current Detection of Cracks in Reinforced Carbon/Carbon

Books and Reports

38 Pressure and Thermal Modeling of Rocket Launches
38 Field of View of a Spacecraft Antenna: Analysis and Software
38 Microchemical Analysis of Space Operation Debris
38 Determination of LETs of SRAMs by Use of a Laser
39 Experiments on No-Vent Filling of a Tank With Liquid H_2
39 Molecular Beams To Simulate Impinging Rocket Exhaust
39 Predictions of Accretion of Ice on a Commercial Airplane
40 Laser-Based Instrument Measures Propagation of Cracks
40 Temperature and Density Measurements Using O_2 Fluorescence

BLANK PAGE

Double-Knudsen-Cell Apparatus Measures Alloy-Component Activities

Both cells are maintained at the same temperature.

Lewis Research Center, Cleveland, Ohio

A double-Knudsen-cell apparatus has been developed for use in measuring alloy-component activities. Alloy-component activities are important for many aspects of metallurgy. They are used to predict chemical reactions, processing characteristics, and oxidation properties. The most direct indicators of activities are vapor pressures, which can be measured by use of Knudsen cells. In this context, "activity" denotes the ratio between the vapor pressure of a given component material of an alloy and the vapor pressure of that component material in pure form at the same temperature.

The double-Knudsen-cell apparatus operates in conjunction with a mass spectrometer that is used to measure the vapor pressures, as shown schematically in Figure 1. It also includes the pure component, which eliminates the problem posed by variations of calibration parameters when samples are changed in a conventional single-cell apparatus.

The major technical issues associated with this apparatus are the need for uniform heating of the Knudsen cells, translation of the cells, and separation (that is, minimizing mixing) of the molecular beams that emerge from the two cells. Figure 2 shows some aspects of the design of the apparatus that address these issues.

Heating is accomplished by use of a tantalum heating element bent into a serpentine configuration that tends to minimize gradients of temperature. The tantalum heating element is installed adjacent to a tantalum block, which also helps to minimize gradients of temperature. The two Knudsen cells are mounted in this block and are thus assured of being at the same temperature. The temperature of the cell under examination is measured by use of an optical pyrometer aimed into the cell through the cell orifice.

The cell-and-heater assembly is located in an evacuated enclosure (which is not shown in the figures), the vacuum of which communicates with that of the mass spectrometer. The cell-and-heater assembly is translated within this enclosure by a commercial *x-y* motion feedthrough. The assembly is mounted on a stainless-steel cross with ball bearings. This cross is attached to the motion feedthrough via a rigid stainless-steel tube.

The apparatus includes flexible water feedthroughs and copper braid, which, in combination, supply heater power while

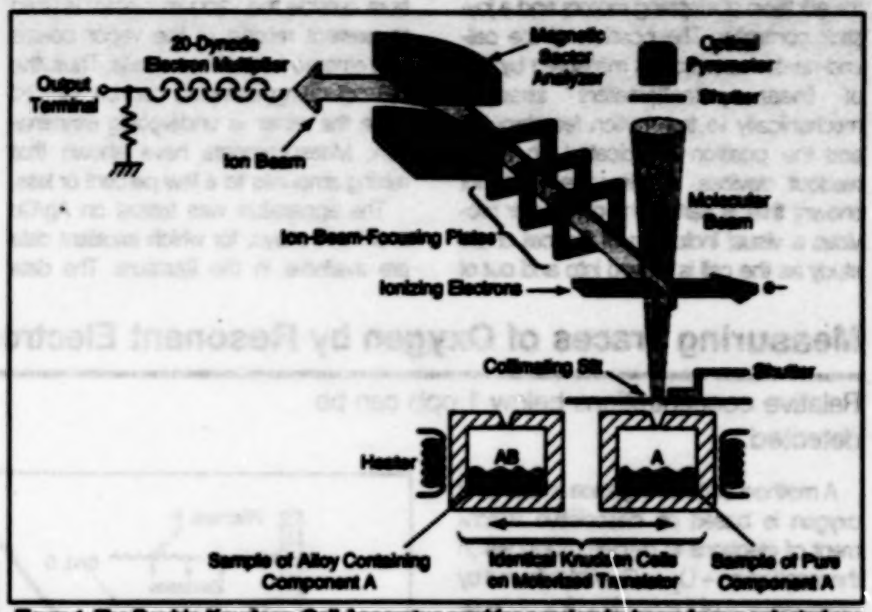

Figure 1. The Double-Knudsen-Cell Apparatus provides a molecular beam from a selected one of two Knudsen cells. The molecular beam is directed into a mass spectrometer for measurement of the vapor pressure of a selected material component — in this case, pure component A.

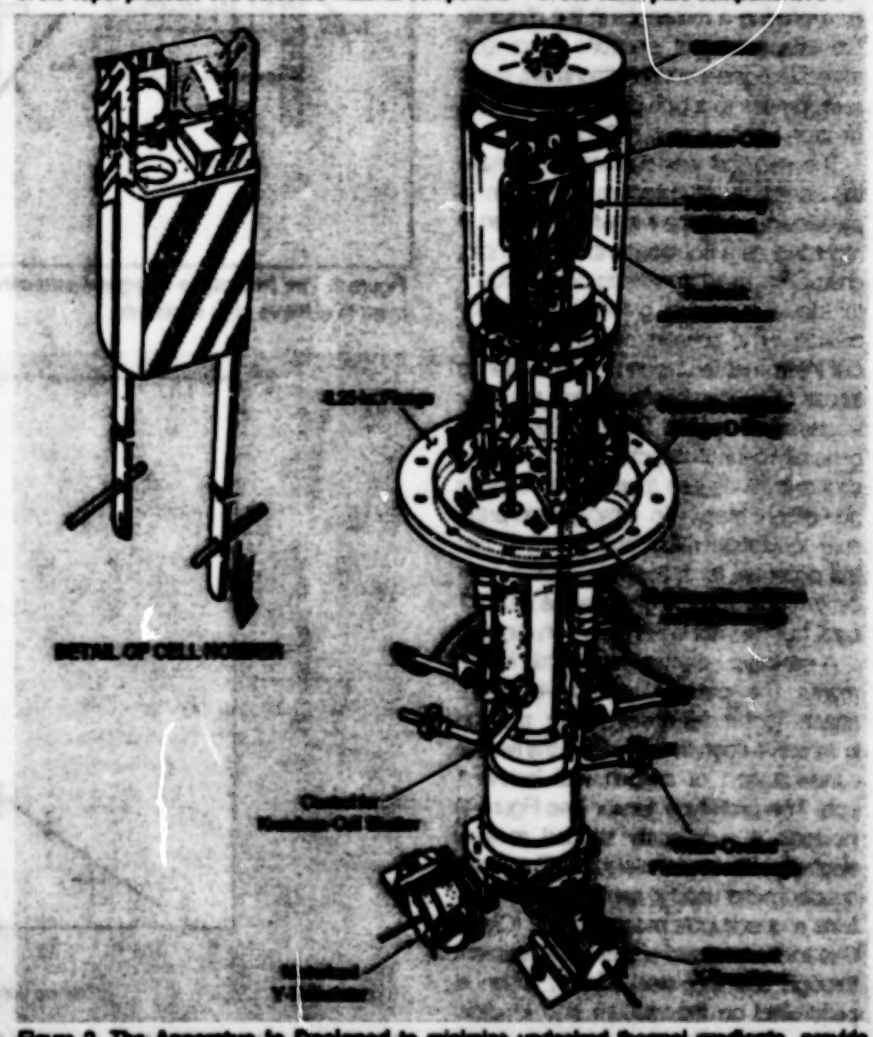

Figure 2. The Apparatus Is Designed to minimize undesired thermal gradients, provide appropriate translation to place the selected cell in position for sampling, and minimize mixing of the molecular beams from the cells.

providing water cooling of translatable heater-contact blocks. The commercial motion feedthrough has been modified by the addition of stepping motors and a joystick controller. The position of the cell-and-heater assembly is measured by use of linear potentiometers attached mechanically to the motion feedthrough, and the position is indicated on digital readout devices. A telescope (also not shown) that is part of the pyrometer provides a visual indication of the cell under study as the cell is moved into and out of the vapor-pressure-measurement position.

A novel system of shutters controlled from outside the vacuum system is used to prevent mixing of the vapor beams that emerge from the two cells. Thus, the cell not being sampled can be shut off while the other is undergoing examination. Measurements have shown that mixing amounts to a few percent or less.

The apparatus was tested on Ag/Cu and Fe/Al alloys, for which excellent data are available in the literature. The data obtained in the tests were in very good agreement with those in the literature. In addition, a partial molar heat of vaporization of Al in an alloy of 0.526Fe/0.474 Al was calculated by plotting the logarithm of the activity of aluminum vs. the reciprocal of the absolute temperature, and the results agreed with data in the literature.

This work was done by Nathan S. Jacobson and Warren A. Moore of Lewis Research Center. Further information is contained in a TSP [see page 1].
LEW-16075

Measuring Traces of Oxygen by Resonant Electron Attachment

Relative concentrations below 1 ppb can be detected.

NASA's Jet Propulsion Laboratory, Pasadena, California

A method of detecting trace amounts of oxygen is based on dissociative attachment of electrons to oxygen molecules (in the reaction $e^- + O_2 \rightarrow O + O^-$) followed by measurement of the resulting flux of negative oxygen ions in a mass spectrometer. High sensitivity is achieved in this method by exploiting a resonance in the dissociative attachment of electrons to oxygen molecules: the electron-attachment cross section rises to a high peak at an incident electron kinetic energy of 6.2 eV.

The method was devised to increase the sensitivity of detection of oxygen in processing chambers in which oxygen is regarded as a contaminant; for example, chambers used in making semiconductor devices and in growing high-purity crystals. The sensors of most commercial instruments designed for measuring traces of oxygen contamination are electrochemical cells. These instruments generally cannot detect oxygen at relative concentrations less than about 50 parts per billion (ppb). An atmospheric-pressure ionization mass spectrometer has the potential for measuring relative concentrations of some gas species below 1 ppb, but has not been tested on oxygen.

A prototype oxygen sensor that implements the present resonant-electron-attachment/mass-spectrometry method is sensitive enough to measure the relative concentration of oxygen well below 1 ppb. The prototype sensor (see Figure 1) includes a cylindrically shaped reversal electron-attachment detector. The mass spectrometer used to sample the O^- contains a quadrupole mass analyzer (QMA). Gas to be analyzed enters the instrument through a stainless-steel tube T, which is perforated on the vacuum side to allow gas to effuse. Electrons are produced at filament F.

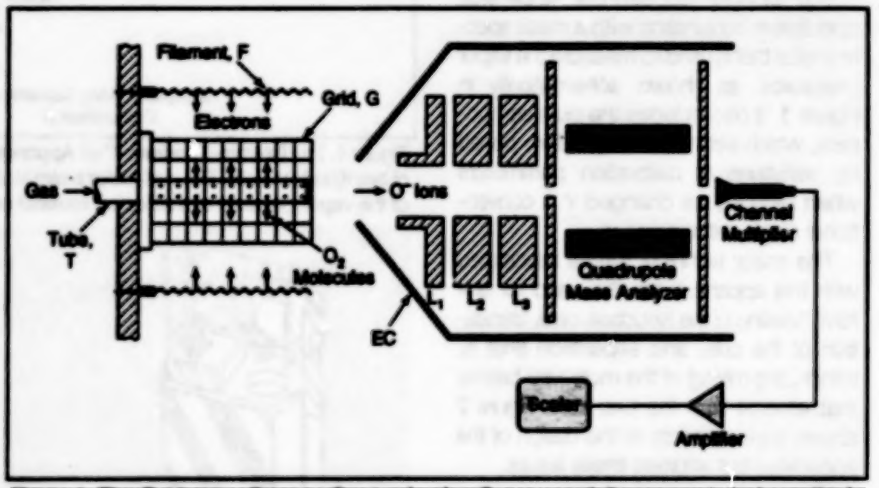

Figure 1. The Prototype Oxygen-Contamination Sensor exploits resonant electron attachment to achieve high sensitivity.

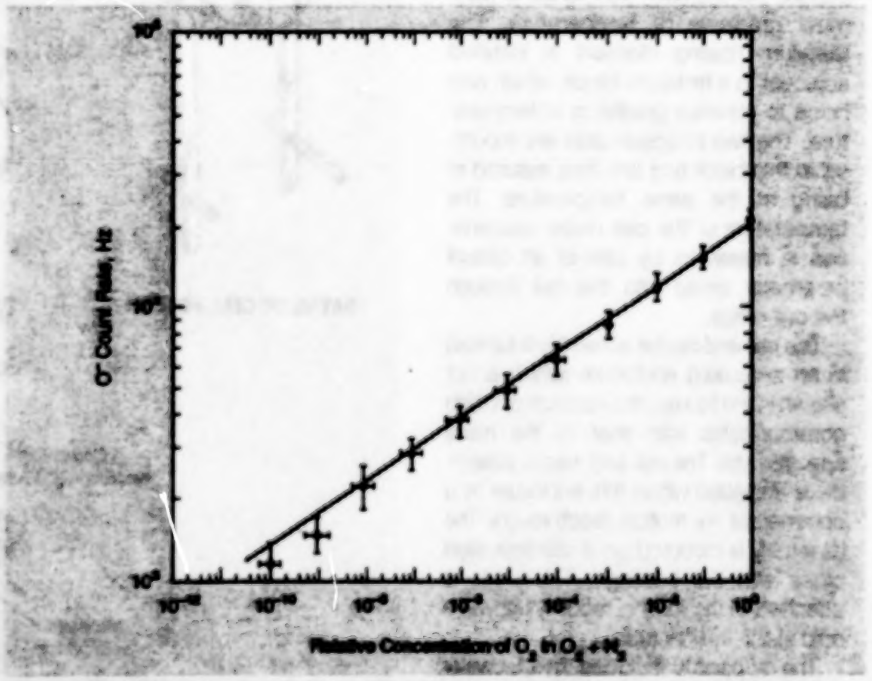

Figure 2. The Response of the Prototype Sensor demonstrates sub-ppb sensitivity at relative concentrations below 10^{-10}.

Electric potentials are applied to T and F and to cylindrical grid G between them in periodic pulses in coordination with the potentials applied to the electrodes of the QMA. During the "electrons on" portion of the operating cycle, the potentials on F, G, and T are chosen so that the electrons from F are accelerated through G, then decelerated and reflected near the surface of T. In the reflection (reversal) region, the electrons have a range of kinetic energies from 0 to several eV, depending on the applied potentials. Those that have kinetic energies around 6.2 eV produce many O^- ions from the O_2 effusing through the T.

During the "electrons on and ions off" period, the EC and L_1 electrodes are held at ground potential so as not to generate an electric field that could interfere with the electric field in the interaction region. During the second half of the cycle, "electrons off and ions on," the potentials are chosen so that electrons are not accelerated toward T and the electric field from the EC, L_1, L_2, and L_3 electrodes extracts the O^- ions from the interaction region. The extracted ions are focused into the QMA and detected in a channel multiplier. The output of the channel multiplier is amplified, then counted by a single-channel scaler with a variable dwell time.

Figure 2 shows results of a test of the prototype apparatus on mixtures of known small concentrations of O_2 in N_2. These results clearly demonstrate that high sensitivity can be achieved. Even higher sensitivity could be achieved by use of increased electron current, improved ion-extraction optics, and a more sensitive mass spectrometer.

This work was done by Kin Fung Man, Said Bouneallak, and Ara Chutjian of Caltech for NASA's Jet Propulsion Laboratory. Further information is contained in a TSP [see page 1].

This invention is owned by NASA, and a patent application has been filed. Inquiries concerning nonexclusive or exclusive license for its commercial development should be addressed to the Patent Counsel, NASA Resident Office-JPL [see page 1]. Refer to NPO-19098.

Calibrating Polarimetric Radar With Only Natural Targets

The calibration algorithm is based on known scattering properties.

NASA's Jet Propulsion Laboratory, Pasadena, California

A method of calibrating polarimetric radar images involves the use of natural, distributed targets only; that is, there is no need to place artificial point calibration targets like corner-cube reflectors in the target scene. The method is based on a few simplifying mathematical assumptions that are, in turn, based on known electromagnetic-scattering characteristics of natural targets.

Accurate calibration is essential for the use of polarimetric radar data gathered in remote sensing of terrain. Heretofore, artificial point targets have been used; typically, this has involved great difficulty, especially when it has been necessary to place such targets in harsh environments. In addition, the iterative computations of older methods of calibration based on distributed targets have frequently failed to converge or have taken excessive time. Some older methods of calibration are based partly on the assumption that crosstalk parameters are small. The present method does not depend on this assumption, is computationally efficient, and always yields convergence.

The method provides a step-by-step procedure for the determination of six unknown complex calibration parameters. The basic equations of the method are derived in a matrix formulation that provides a compact representation of the electromagnetic-scattering characteristics of the target and the gain, crosstalk, and other parameters of the radar equipment. The assumption that the target is reciprocal (with respect to electromagnetic scattering) is incorporated into this formulation. On the basis of this reciprocity, the measured scattering matrix is symmetrized and the number of unknowns is reduced to three. These unknowns are two crosstalk parameters and one channel-imbalance parameter.

It is further assumed that the natural distributed target exhibits reflection symmetry with respect to the incidence plane, which contains the radar wave incidence direction and the normal direction of surface above distributed targets. For natural targets, which are reflection-symmetric to the incidence plane, the statistical distribution of position, shape, and orientation of scatterers constituting the target is symmetric with respect to this plane. This assumption is valid for most natural distributed targets. The method incorporates a novel algorithm that estimates the crosstalk parameters

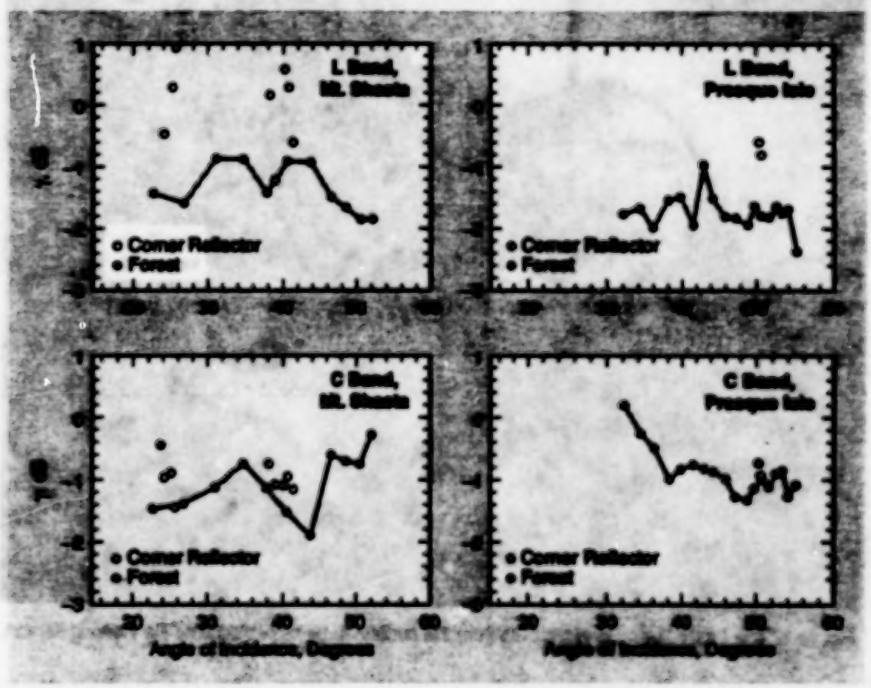

These Plots of Copolarization Ratio, γ, of forests and corner-cube reflectors contain data used in amplitude calibration. The data show that, among other things, amplitude imbalance between the horizontal and vertical polarization channels can be corrected to less than 0.5 dB if forests are used to estimate this imbalance.

BEST COPY AVAILABLE

by use of equations that exploit reflection symmetry. The effect of crosstalk can then be removed from the radar image. The foregoing symmetrization of data and removal of crosstalk can be performed on almost any set of polarimetric radar image data.

Next, the phase and amplitude of the channel imbalance are determined by use of distributed targets that exhibit rotation symmetry or by use of volume and surface targets that provide known phase and amplitude relations between the radar responses obtained while using (1) horizontal polarization in both transmission and reception and (2) vertical polarization in both transmission and reception.

This method has been applied to synthetic-aperture radar images of ice on the Beaufort sea (no corner-cube reflectors in the scene), forest near Mt. Shasta in northern California (with corner-cube reflectors) and forest on Presque Isle in Maine (with corner-cube reflectors). In the two scenes in which corner-cube reflectors were available, their radar signatures were analyzed to verify the calibration by this method (see figure). When the method was applied to the sea-ice images, the extracted crosstalk parameters were found to agree very well with those obtained from the forest images, indicating that both sea ice and forests are good candidates for polarimetric calibration.

This work was done by Simon H. Yueh, Son V. Nghiem, and Ronald Kwok of Caltech for NASA's Jet Propulsion Laboratory. Further information is contained in a TSP [see page 1].
NPO-19192

Optical Detection of Fractures in Ceramic Diaphragms

A fracture causes reflection of a laser beam into multiple speckled spots.

NASA's Jet Propulsion Laboratory, Pasadena, California

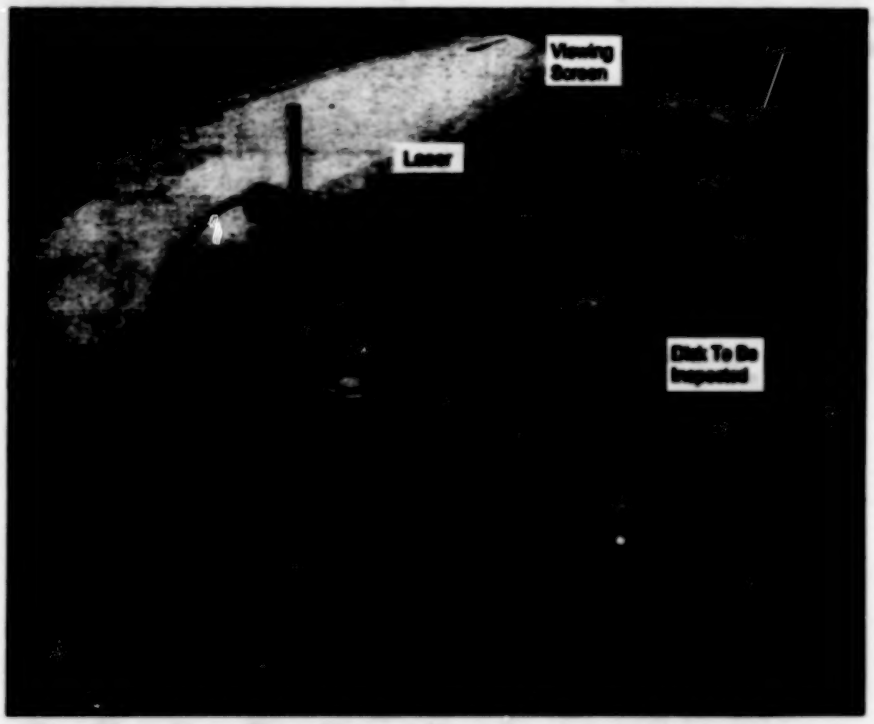

Figure 1. The Laser Beam Is Reflected from the surface to be inspected onto the viewing screen.

A simple optical technique enables quick, nondestructive inspection of surfaces of ceramic diaphragms and disks for fractures and discontinuities. The technique involves reflecting a beam of light from a laser at a glancing angle of about 20° to 25° off the surface to be inspected and examining the pattern of reflected light on a suitable viewing surface as the beam is swept across the surface (see Figure 1). When a fracture is present, the reflection pattern separates into two or more speckled spots (see Figure 2).

The technique has been applied in the inspection of ceramic diaphragms bearing electronic circuits. Detection of fractures is especially important where the circuits carry high voltages because fractures can cause high-voltage breakdown with failure of associated equipment. The technique may also be useful in detection of fatigue cracks on aircraft (but has not yet been tested in this application).

This work was done by Eric G. Laue of Caltech for NASA's Jet Propulsion Laboratory. No further documentation is available.
NPO-19131

REFLECTION FROM INTACT SURFACE

REFLECTION FROM FRACTURED SURFACE

Figure 2. Reflection Patterns on the viewing screen Illustrate the utility of the technique in revealing fractures.

BEST COPY AVAILABLE

Revolving Eddy-Current Probe Detects Cracks Near Rivets

A circular scanning pattern reduces the interfering effects of the rivets themselves.

Langley Research Center, Hampton, Virginia

Scanning an eddy-current probe in a circular pattern has been found to increase the sensitivity with which the probe indicates fatigue cracks and other defects in metal surfaces in the vicinity of rivets. The technique was devised to facilitate the inspection of riveted joints in aircraft.

The eddy-current probe in question (see Figure 1) was described in "Electromagnetic Flaw Detector Is Easier To Use" (LAR-15046), *NASA Tech Briefs*, Vol. 18, No. 7 (July, 1994), page 36. In operation, the magnetizing coil is excited with a sinusoidal waveform and the probe is laid flat on the surface of the metal plate or sheet to be inspected. As explained in more detail in that article, the voltage induced in the pickup coil is close to zero when the probe is placed on or sufficiently close to a metal plate or sheet that contains no defects, but rises from zero when a defect in the vicinity of the probe interrupts the electrical continuity of the plate or sheet and thereby diverts some of the eddy current into the area under the pickup coil. Thus, the probe is self-nulling and provides a simple, easy-to-interpret output indicative of defects.

Previously, it was observed that when the probe is scanned over a riveted joint, the discontinuity of the rivet itself causes some of the eddy current to flow under the pickup coil, giving rise to an output voltage that does not signify a defect but is large enough to mask the signal from a small defect located close to the shank of the rivet. The circular-scan technique was developed to reduce the interfering effect of the rivet. The technique is based on the observation that when the probe is held flat against the surface and moved around the rivet at a constant radius, the component of the output signal attributable to the rivet remains more nearly constant than it otherwise would as the angular position of the probe varies. Thus, any further increase in the output signal as a function of angular position is more likely to signify a defect (see Figure 2).

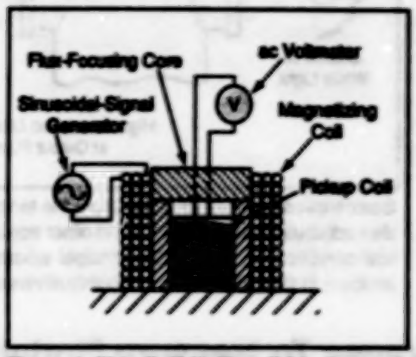

Figure 1. This Self-Nulling Eddy-Current Probe is used to detect subsurface flaws in riveted joints.

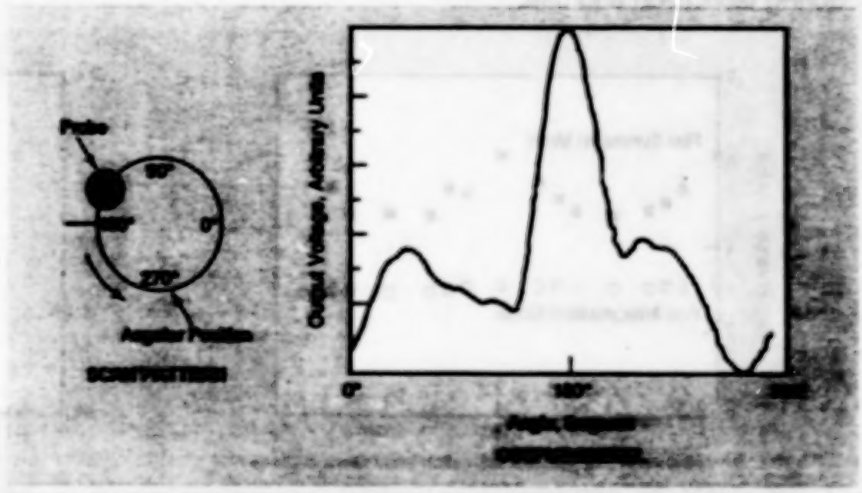

Figure 2. The Output Voltage of the probe, measured as a function of angular position during a circular scan around a riveted joint, includes a component contributed by a notch introduced at the 180° position to simulate a defect. The notch, made by electrical-discharge machining, extended out to 0.3 mm beyond a rivet head 8 mm in diameter.

This work was done by Min Namkung of Langley Research Center, Buzz Winchenbach, James P. Fulton, and Shridhar Nath of Analytical Services and Materials, Inc.; and John Simpson of Lockheed Engineering and Sciences Co. Further information is contained in a TSP [see page 1].

This invention is owned by NASA, and a patent application has been filed. Inquiries concerning nonexclusive or exclusive license for its commercial development should be addressed to the Patent Counsel, Langley Research Center [see page 1]. Refer to LAR-15231.

Spectroscopic Measurement of Temperature and Pressure of O_2

Measurements can be taken nonintrusively during pneumatic impact.

Lyndon B. Johnson Space Center, Houston, Texas

A spectroscopic technique (see figure) has been found to be useful in measuring the temperature and pressure of oxygen in laboratory experiments that involve high temperatures and/or high pressures. This technique was devised especially for use in experiments in which oxygen or a gas that contains oxygen is subjected to sudden adiabatic compression, as in a shock tube. This technique might also be useful in combustion experiments and other experiments in which gaseous oxygen plays a role.

This spectroscopic technique exploits temperature and pressure dependences of the absorption spectrum of the oxygen-complex molecules that form during adiabatic compression. The intensities of the double electronic absorption spectral peaks are approximately proportional to the square of the pressure, and these peaks are broadened to approximately Gaussian shapes that can be evaluated in terms of the temperature dependence of

Doppler broadening. Furthermore, collisionally induced electronic transitions to normally spin-forbidden states have been observed, and the profiles of the P and R branches exhibit a temperature dependence consistent with a Boltzmann population distribution.

This work was done by Ralph M. Tapphorn, Dwight D. Janoff, and Norman J. Armendariz of Lockheed Engineering & Sciences Co. for Johnson Space Center. Further information is contained in a TSP [see page 1].
MSC-21908

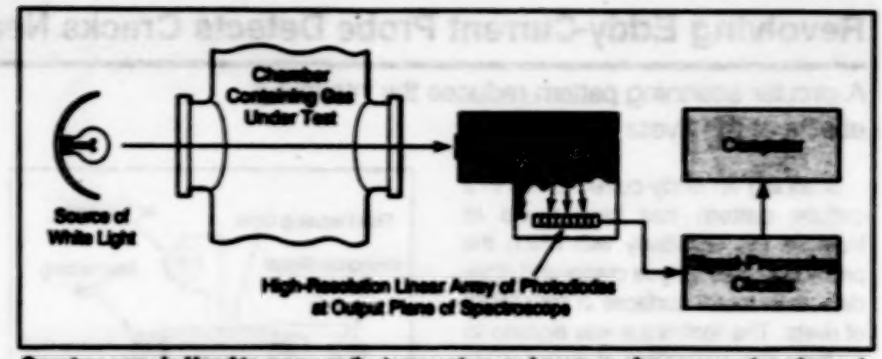
Chamber Containing Gas Under Test
Source of White Light
Computer
High-Resolution Linear Array of Photodiodes at Output Plane of Spectroscope

Spectroscopy Is Used to measure the temperature and pressure of oxygen undergoing sudden adiabatic compression. As in other applications of spectroscopy to measurement of physical conditions in gases, the principal advantage of the use of spectroscopy (instead of solid probes) in this application is nonintrusiveness.

Using Ultrasonic Lamb Waves To Measure Moduli of Composites

Specimens can be characterized nondestructively during fabrication and use.

Lewis Research Center, Cleveland, Ohio

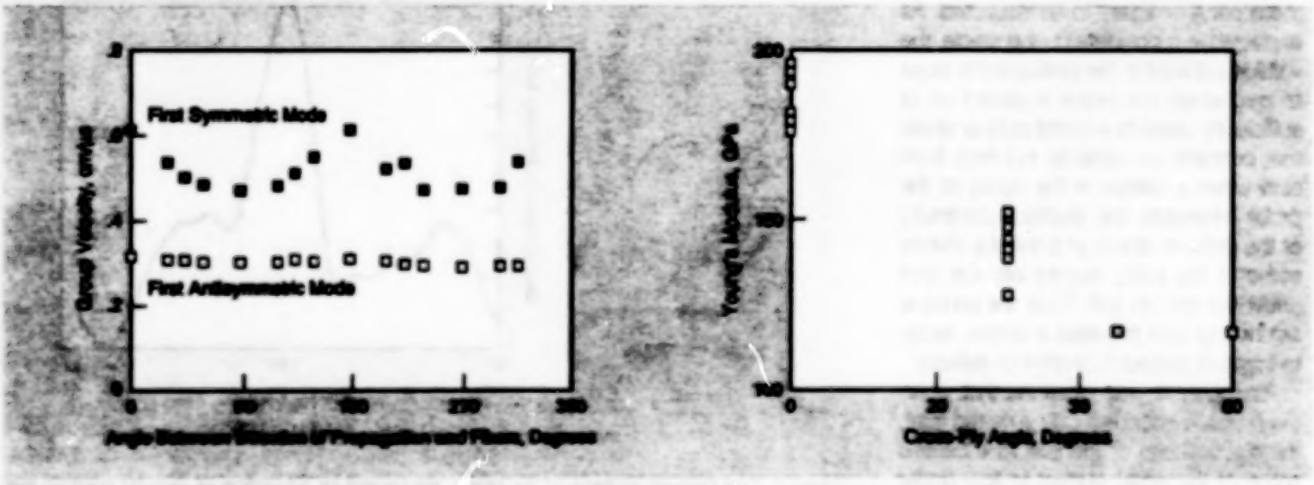

Figure 1. The Group Velocity of the first symmetric mode in a panel specimen of a composite of unidirectional SiC fibers in a Ti-15-3 matrix was found to vary with the direction of propagation. This variation is consistent with the Young's moduli of symmetric cross-ply specimens of the same composite with various cross-ply angles.

Measurements of broad-band ultrasonic Lamb waves in plate specimens of ceramic-matrix/fiber and metal-matrix/fiber composite materials can be used to determine the moduli of elasticity of the materials. In one class of potential applications of this concept, Lamb-wave responses of specimens would be measured and analyzed at various stages of thermal and/or mechanical processing to determine the effects of the processing, without having to dissect the specimens. In another class of potential applications, structural components that have shapes that support the propagation of Lamb waves would be monitored ultrasonically to identify signs of deterioration and impending failure.

In the present Lamb-wave analysis method, pulsed acoustic excitation is applied by a first broad-band ultrasonic

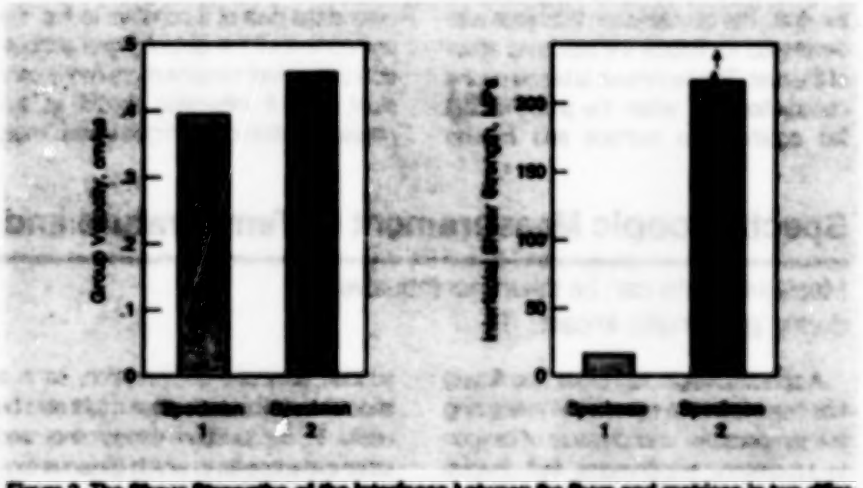

Figure 2. The Shear Strengths of the Interfaces between the fibers and matrices in two different composites of silicon carbide fibers in reaction-bonded silicon nitride matrices, as measured by the fiber-push-out method, were found to be semiquantitatively related to each other in the same way as were the group velocities of the first antisymmetric mode in those composites.

transducer in contact with one face of a specimen. The acoustic response is measured by use of a second broad-band ultrasonic transducer in contact with the same face of the specimen at a known distance and direction from the first transducer. The measurements yield data on the dispersion of Lamb waves; that is, on the speeds of sound in various acoustic modes that propagate along the surface. The speeds of sound, in turn, can be used to calculate the moduli.

The two most useful Lamb wave modes are the first symmetric and first antisymmetric modes. The speed of sound in the first symmetric mode is a measure of the Young's modulus in the direction of propagation (see Figure 1). Thus, the Young's modulus determined by use of the first symmetric mode depends on the relative positions of the transducers. For example, one could determine the Young's modulus of a tensile specimen along the load-bearing direction, without having to stress the specimen. One could use the first symmetric mode to construct an initial Young's-modulus map of a plate before cutting the plate into specimens. One could also use it to monitor the effects of fatigue on the Young's moduli of platelike structural components in aircraft, for example.

The first antisymmetric mode provides data on variations in the shear modulus, or, under some conditions, the flexural modulus with respect to the direction of propagation. Similarly to the case of the first symmetric mode, one could use the first antisymmetric mode to construct a shear- or flexural-modulus map of a plate or to monitor the effects of fatigue on shear or flexural moduli. In addition, experiments have shown that the speed of sound in the first antisymmetric mode in ceramic-matrix composite materials is sensitive to the shear strengths of the interfaces between the matrices and the fibers (see Figure 2).

The Lamb modes are best characterized by constructing dispersion curves. For this purpose, it is necessary to determine the phase velocity for each mode of interest. Previously, this was done by collecting data from a tone-burst measurement at each frequency of interest. However, collecting data separately at each frequency is a time-consuming task. The advantage of the present broad-band pulse measurement concept is that each pulse contains a range of frequencies, so that each measurement can contain data on all frequencies of interest. To extract these data, the acoustic response signals are processed by software that separates the frequencies, determines the velocities, and plots the dispersion curves. The software provides the speed and automation necessary for application to research on materials and to monitoring of components during service or processing.

This work was done by Harold E. Kautz of Lewis Research Center. Further information is contained in a TSP [see page 1].
LEW-15907

Apparent Thermal Conductivity of Multilayer Insulation

A mathematical model offers potential for optimization of design.

Lewis Research Center, Cleveland, Ohio

A mathematical model of the apparent or effective thermal conductivity between two successive layers of multilayer thermal insulation (MLI) offers potential for optimizing the performance of the insulation. Heretofore, efforts to design MLI blankets were focused on overall results, without detailed examination of the physical mechanisms by which heat is transferred across the gaps between layers. By using the present mathematical model in layer-by-layer calculations, one can gain an understanding of how each physical mechanism contributes to the overall flow of heat through an MLI blanket. With the help of the model, one can analyze engineering tradeoffs among such parameters as the number of layers, thicknesses of gaps between layers, types of spacers placed in the gaps, weight, overall thickness, and the effects of the foregoing on the apparent thermal conductivity through the blanket.

The mathematical model accounts for radiation across a gap, conduction through the gas in the gap, and conduction through solid separators that maintain the gap at a specified thickness. One version of the model comprises the following equation:

$$k = \underbrace{\sigma(\varepsilon/(2-\varepsilon))\left(T_w^2 + T_c^2\right)\left(T_w + T_c\right) - 4\sigma T_m^3 L_f/N\alpha^2)}_{\text{(radiation)}} + \underbrace{0.007505P\left[1 - 0.2\left(T_w - 78\right)\right]}_{\text{(conduction in gas)}} + \underbrace{\left(0.01/\Delta X\right)\left[0.017 + 7\times10^{-6}\left(800 - T_w\right) + 0.0228\ln\left(T_w\right)\right]}_{\text{(conduction in separators)}}$$

where k = apparent thermal conductivity across the gap;
ε = emissivity of insulating layer;
σ = the Stefan-Boltzmann constant, 5.675 $Wm^{-2}K^{-4}$;
f = fraction of volume of the gap occupied by separator material;
T_w = temperature of the warmer layer of insulation, K;
T_c = temperature of the colder layer of insulation, K;
$T_m = (T_w + T_c)/2$;
N = number of layers per unit thickness of blanket, m^{-1};
α = radiation absorptivity of the separator material;
P = pressure of gas in the gap, Pa;
ΔX = thickness of gap; and
L_f = apparent or effective size of separator pores.

The numerical values in the gas-conduction term are for nitrogen gas, while those in the separator-conduction term are from a curve fit to data on the thermal conduction of Dacron (or equivalent) polyethylene terephthalate. Typically, the separators consist of solid, round fibers laid parallel to each other in the gap, in which case L_f = (diameter of fiber) × [$(\pi/4) - 1$]. Alternatively, separators could be made in parallel strips, each covering about 10 percent of the total blanket area; multiple interlayers of this type could be laid out with strips crossed, so that only 1 percent of the total blanket area is available for conduction through the separator material.

The software to solve the equation layer by layer was undergoing refinement when the information for this article was submitted, and the coefficients may yet have to be adjusted somewhat to make the numerical results fit empirical data. Even so, the model has already yielded numerical results that suggest improvements in MLI design. In particular, the results have shown that to optimize overall performance, it is necessary

to optimize local performance by varying the density of layers with depth within the blanket: the density of layers should be smallest near the colder side (where conduction through the separator material tends to predominate) and largest near the warmer side, where radiation tends to predominate.

This work was done by Glen E. McIntosh of Cryogenic Technical Services, Inc., for Lewis Research Center. Further information is contained in a TSP [see page 1].
LEW-15594

Eddy-Current Detection of Cracks in Reinforced Carbon/Carbon

Invisible cracks can be detected nondestructively. *Lyndon B. Johnson Space Center, Houston, Texas*

Investigations of failures of components made of reinforced carbon/carbon have shown that eddy-current flaw-detection techniques are applicable to these components. The investigation focused on space shuttle parts, but the findings should be applicable to other parts made of carbon/carbon materials. Indeed, eddy-current techniques are already used commercially to determine thicknesses of coating materials and to detect discontinuities.

More specifically, the investigation showed that eddy-current techniques can reveal cracks, too small to be detected visually, in carbon/carbon matrix substrates and in silicon carbide coats on the substrates. Eddy-current techniques can also reveal delaminations in carbon/carbon matrices. Eddy-current techniques can also be used to characterize the extents and locations of discontinuities in substrates in situations in which ultrasonic techniques and destructive techniques are not practical.

This work was done by Scott V. Christensen and Ajay M. Koshti of Rockwell International Corp. for Johnson Space Center. No further documentation is available.
MSC-22479

Books and Reports

Pressure and Thermal Modeling of Rocket Launches

A report presents a mathematical model for use in designing a rocket-launching stand. The model predicts the pressure and thermal environment, as well as thermal responses of structures to impinging rocket-exhaust plumes. The model enables a relatively inexperienced analyst to determine the time-varying distributions and absolute levels of pressure and heat loads on the structures. A submodel of particle/shock-interaction provides a large improvement for solid rocket motors in that arbitrary accommodation coefficients are no longer required to specify the amounts of particulate mass and energy flux that are transferred to a surface of an object; this submodel accounts for the size and orientation of the object, the properties of the shock flow field upstream of the object, and subsequent effects on the particles. A submodel of radiant heating has been incorporated to determine the radiant heat loads to the structure due to the high-temperature shock layer upstream of each surface in question.

This work was done by Sheldon D. Smith, Brian L. Myruski, Richard C. Farmer, and Jon A. Freeman of SECA, Inc., for Marshall Space Flight Center. To obtain a copy of the report, "Model Development for Exhaust Plume Effects on Launch Stand Design - PLIMP/LSD," see TSP's [page 1].
MFS-26283

Field of View of a Spacecraft Antenna: Analysis and Software

A report summarizes a computational analysis of the field of view of a rotating elliptical-cross-section parabolic-reflector antenna for the SeaWinds spacecraft. Issues considered in the analysis include blockage and diffraction by other objects near the antenna, related concerns about electromagnetic interference and electromagnetic compatibility, and how far and in what configuration other objects should be positioned with respect to the antenna to achieve the required performance. The analysis was conducted by use of a modified version of a computer code called "Apatch," and ancillary software, with all of which the reader is apparently assumed to be familiar. The modifications were necessary to enable Apatch to handle the elliptical cross section. The report describes the modifications in some detail, describes several aspects of mathematical modeling with the modified software, and discusses results of computations of performance by the modified software. Portions of the modified software pertaining to modeling the curved reflector surface by use of facets are included in an appendix. A second appendix contains sample Apatch input files.

This work was done by Te-Kao Wu of Caltech and R. Kipp and S. W. Lee of DEMACO for NASA's Jet Propulsion Laboratory. To obtain a copy of the report, "Spacecraft Antenna Field of View Analysis and Computer Code," see TSP's [page 1].
NPO-19549

Microchemical Analysis of Space Operation Debris

A report discusses techniques used in analyzing debris relative to space shuttle operations. The debris are collected from the space shuttle, expendable launch vehicles, payloads carried by the space shuttle, and payloads carried by the expendable launch vehicles. The debris samples are often small and contaminated by oil or organic components. Optical microscopy, scanning electron microscopy with energy-dispersive spectrometry, [illegible]tical electron microscopy with wavelength-dispersive spectrometry, and X-ray diffraction have all been chosen as techniques to be used in examining samples of debris. A combination of all these techniques has proven most effective in qualitative and quantitative characterization of debris samples.

This work was done by Virginia J. Cummings and Hae Soo Kim of Kennedy Space Center. To obtain a copy of the report, "Procedures for Analysis of Debris Relative to Space Shuttle Systems," see TSP's [page 1].
KSC-11695

Determination of LETs of SRAMs by Use of a Laser

A report describes an experimental study of the use of the microelectronic advanced laser scanner (MEALS) to cause single-event upsets (SEUs) in integrated logic circuits. [The basic concepts of SEU testing by use of the MEALS were described in several previous articles in

NASA Tech Briefs; namely, "Laser Scanner Tests for Single-Event Upsets" (NPO-18218), Vol. 16, No. 2 (February, 1992), page 38; "Single-Event-Upset Laser Scanner With Optical Bias" (NPO-18217), Vol. 16, No. 2 (February, 1992), page 36; and "More About Laser Scanner Tests for Single-Event Upsets" (NPO-18494), Vol. 17, No. 1 (January, 1993), page 58.] The MEALS includes a pulsed dye laser, the output of which is focused onto the device under test. This study is part of a continuing effort to study the SEU effects of ionizing radiation on such circuits and to use the MEALS as a relatively inexpensive SEU-prescreening laboratory apparatus that would serve as an alternative to a heavy-ion accelerator. In this study, the lowest linear energy thresholds (LETs) at 125 °C for SEU in a 64K static random-access memory (SRAM) were found to be 27 MeV-cm^2/mg and 24 MeV-cm^2/mg, as measured by use of a heavy-ion accelerator and the MEALS, respectively. In the case of a radiation-hardened SRAM, no SEUs were observed even at the maximum LET (79 MeV-cm^2/mg) of the heavy-ion test beam, while MEALS tests indicated an SEU LET of 90 MeV-cm^2/mg. These results suggest that the MEALS can be used as an SEU-prescreening laboratory apparatus in certain cases.

This work was done by Quisup Kim, Kenneth P. McCarty, Charles E. Barnes, Harvey R. Schwartz, and James R. Coss of Caltech for **NASA's Jet Propulsion Laboratory.** *To obtain a copy of the report, "Single Event Effects and Laser Simulation Studies," see TSP's [page 1].*
NPO-19315

Experiments on No-Vent Filling of a Tank With Liquid H_2

The technique works in a gravitational setting.

A report describes experiments on no-vent filling of an insulated, vacuum-jacketed tank with liquid hydrogen. The experiments, conducted in a laboratory in normal Earth gravity, were conducted to ascertain the feasibility of no-vent filling of tanks with cryogenic liquids in zero gravity, where filling with venting as in normal gravity could cause substantial loss of the liquids. The no-vent-filling process begins with a preparatory phase in which the cryogenic liquid is sprayed onto the walls of the tank to cool them, then the resultant vapor is vented. Thereafter, there is no further venting, and the liquid is sprayed into the tank to mix it with the ullage vapor. By filling the tank in this manner, the vapor is kept cool enough so that the pressure in the tank does not rise to a level at which it would prevent filling of most of the tank with liquid. The tank used in the experiments had a volume of 71 ft^3 (2 m^3); the experiments were conducted at inlet saturation pressures of 5, 15, and 25 psia (34, 103, and 172 kPa, respectively), at transfer pressures of 20, 30, and 45 psia (138, 207, and 310 kPa, respectively), and at various starting wall temperatures. Two spray systems were used. One was a series of small holes along a length of pipe. The other was a single orifice at the bottom of the tank. Although pretest analysis predicted superior performance for the series of holes, both systems proved effective in filling the tank. In all of the experiments except the one at the highest starting wall temperature [238 R (132 K)], it was possible to fill at least 90 percent of the volume of the tank with liquid hydrogen. The overall results of the test agree fairly well with a mathematical model based on equilibrium thermodynamics.

This work was done by D. J. Chato of **Lewis Research Center.** *To obtain a copy of the report, "Ground Testing for the No-Vent Fill of Cryogenic Tanks: Results of Tests for a 71 Cubic Foot Tank," see TSP's [page 1].*
LEW-16161

Molecular Beams To Simulate Impinging Rocket Exhaust

Beams of the required molecular species are produced at the required velocities and fluxes.

A report discusses the development of a small-scale apparatus to generate molecular beams for use in simulating the impingement of rocket-engine exhaust on nearby spacecraft surfaces. To create the simulated exhaust, gases of interest are made to flow into a conical expansion nozzle, where irradiation by a pulsed laser beam heats the gases, accelerating the gas molecules to high speeds. The use of a pulsed (instead of a continuous) source eliminates the need for heavy vacuum pumping. The use of laser (instead of combustion) heating enables the selection of both molecular species and velocities. The apparatus has generated pulsed beams of N_2, CO_2, and H_2O with speeds of 3 to 3.6 km/s, and is expected to be capable of generating similar beams of CO. (These molecular species are the major components of exhaust from the space shuttle bi-propellant engines.) The N_2 and CO_2 beams have been shown to be more than 90 percent molecular. The H_2O beams are only 75 percent molecular H_2O, but optimization should be possible. Furthermore, the results of several measurements with gas mixtures are sufficiently promising to suggest that it is possible to simulate exhaust plumes realistically.

This work was done by George E. Caledonia, Robert H. Krech, and Bernard L. Upschulte of Physical Sciences, Inc., for **Marshall Space Flight Center.** *To obtain a copy of the report, "Plume Impingement Effects," see TSP's [page 1].*

Inquiries concerning rights for the commercial use of this invention should be addressed to the Patent Counsel, Marshall Space Flight Center [see page 1]. Refer to MFS-26292.

Predictions of Accretion of Ice on a Commercial Airplane

Calculated ice shapes looked reasonable and appeared representative of rime and a mixed ice.

A report presents a computational study of the accretion of ice on the wings and on the horizontal tail surfaces of a simplified version of the Boeing 737 airplane. The calculations were performed by use of the LEWICE3D computer code, which incorporates a panel-method mathematical model of three-dimensional potential flow and mathematical models of trajectories of drops of water entrained in the flow, impingement of drops on surfaces, and transfer of heat. The calculations were performed for airspeeds and airfoil configurations typical of a 30-minute hold condition (cited as a crucial design condition for ice protection systems). Calculations were performed for two types of flow models: a model of flow around the whole airplane, and a simplified model in which the wing and horizontal tail surfaces were treated as though each moved through the air in isolation from the rest of the airplane; this was done to assess the validity of using such simplified models. In general, the calculated ice shapes looked reasonable and appeared representative of rime and a mixed ice. With respect to the wing, the simplified model gave results consistent with those of the full-aircraft model, except at the wing root, where it overpredicted the amount of accreted ice relative to the

full-aircraft model. For the tail, the sizes and amounts of ice computed with both models were comparable, but the accretions were located more toward the upper surface for the full model than they were for the simplified model; the difference was attributed to downwash from the main wing, with a resultant lower effective angle of attack of the tail in the full model relative to that of the simplified model.

This work was done by C. S. Bidwell of **Lewis Research Center**. *To obtain a copy of the report, "Ice Accretion Prediction for a Typical Commercial Transport Aircraft," see TSP's [page 1].*
LEW-15975

Laser-Based Instrument Measures Propagation of Cracks

A report describes the use of a commercial laser displacement meter to measure the propagation of cracks in stainless-steel specimens in stress tests in a corrosive (salt-spray) environment. The measurements were directed toward determining the time from the beginning of each test until the onset of propagation of the crack. Displacements measured were of the order of microns.

This work was done by Rupert U. Lee of **Kennedy Space Center** *and Robert B. Cox, Robert C. Youngquist, John T. Sentz, and Kenneth A. Rose of I-Net. To obtain a copy of the report, "Crack Initiation Sensor," see TSP's [page 1].*

Inquiries concerning rights for the commercial use of this invention should be addressed to the Patent Counsel, Kennedy Space Center [see page 1]. Refer to KSC-11697.

Temperature and Density Measurements Using O_2 Fluorescence

A report presents a theoretical and experimental study of the use of laser-induced fluorescence in oxygen to measure temperatures and densities in air flowing in a hypersonic wind tunnel. In this application, oxygen is excited by narrowband, tunable radiation from a pulsed ArF excimer laser. It was found that for temperatures of 60 K and densities above 0.01 amagat, the temperature and density measurements can be accurate to within 2 percent if signal uncertainties are dominated by photon-statistical noise. The measurements are unaffected by collisional atomic quenching.

This work was done by Robert L. McKenzie and Douglas G. Fletcher of **Ames Research Center** *and Gabriel Laufer of Analatom, Inc. To obtain a copy of the report, "A Method for Measuring Temperatures and Densities in Hypersonic Wind Tunnel Air Flows Using Laser-Induced O_2 Fluorescence," see TSP's [page 1].*

Inquiries concerning rights for the commercial use of this invention should be addressed to the Patent Counsel, Ames Research Center [see page 1]. Refer to ARC-12856.

Hardware, Techniques, and Processes

43 Device for Sampling Surface Contamination
43 Optimizing Misch-Metal Compositions in Metal Hydride Anodes

Books and Reports

44 Improved Silicon Nitride for Advanced Heat Engines
44 Study of Rocket-Engine Joints Bonded by Ni/Cu/NARloy-Z
44 Hazardous Fluids Compatibility Test Apparatus

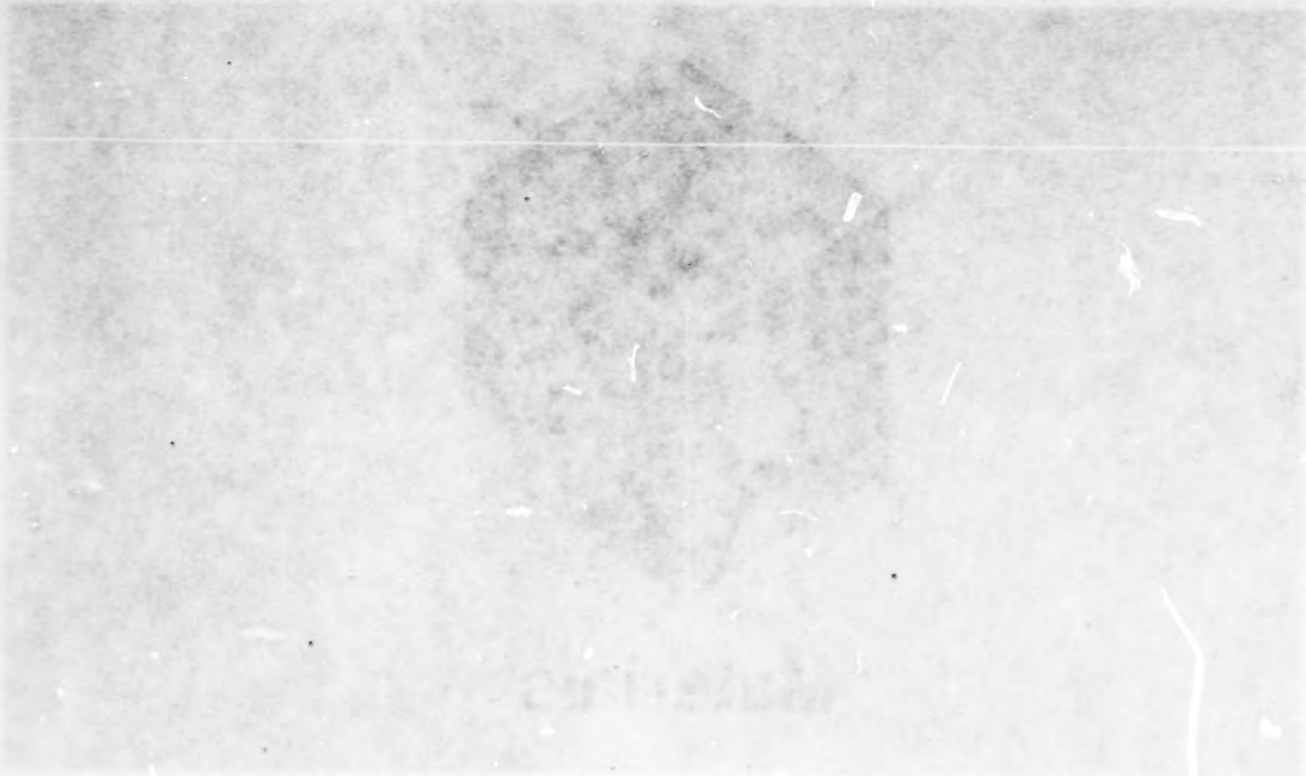

BLANK PAGE

Device for Sampling Surface Contamination

A specially designed cotton swab is suitable for use in a clean room.

Marshall Space Flight Center, Alabama

The figure illustrates an easy-to-use contamination-sampling device in the form of a specially designed cotton swab. Unlike ordinary cotton swabs on wooden applicator tips, this device does not shed cotton and wood fibers, which would (if shed) further contaminate the inspected surface. The device satisfies clean-room standards.

The device includes a nylon-covered cotton tip on a wooden applicator dowel 6 in. (15 cm) long. Most of the dowel and part of the cotton tip are covered with a shrink-fit plastic tube, which holds the nylon in place, retains wood fibers, and increases the diameter for a better grip. The tube has a nonslip finish. The tube-covered dowel is flexible and strong enough to withstand bending associated with sampling in relatively inaccessible recesses. The nylon fabric covering the cotton tip (to retain cotton fibers) is held in place with another shorter piece of shrink-fit tubing. No glue (which could add contamination) is used in fabricating the device.

In the next-to-last stage of fabrication, the device is cleaned to remove hydrocarbons, which could contaminate the surface to be inspected and/or contribute spurious contamination readings. The cleaned device is then packaged in aluminum foil for storage until use. Before using the device, the foil package is removed but saved. The cotton tip is used to wipe the surface to be inspected, then the device is rewrapped in the foil package for transport to a laboratory for analysis of the contaminants picked up by the cotton tip. Typically, the contaminants are extracted from the cotton tip by use of a solvent.

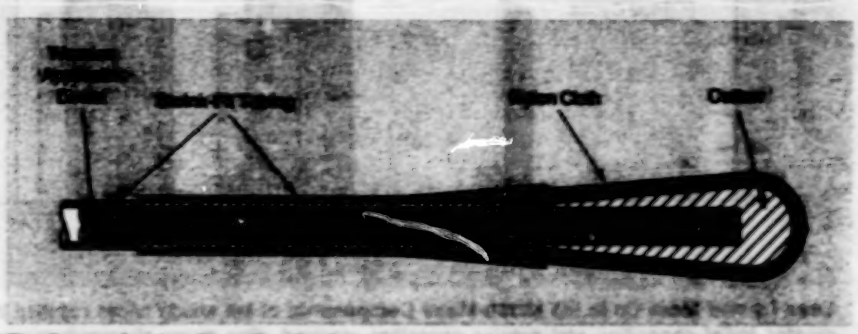

The Contamination-Sampling Device is an improved version of the basic cotton-tipped wooden applicator, designed for extreme cleanliness and to enhance utility for sampling according to exacting specifications.

This work was done by Felix A. Delgado and Susan M. Stern of Rockwell International Corp. for Marshall Space Flight Center. Further information is contained in a TSP [see page 1].

Inquiries concerning rights for the commercial use of this invention should be addressed to the Patent Counsel, Marshall Space Flight Center [see page 1]. Refer to MFS-30096.

Optimizing Misch-Metal Compositions in Metal Hydride Anodes

Optimization of compositions promotes retention of charge and discharge capacities.

NASA's Jet Propulsion Laboratory, Pasadena, California

Electrochemical cells based on metal hydride anodes have been investigated experimentally in an effort to find anode compositions that maximize charge/discharge-cycle performances. More specifically, the experimental anodes contained misch metal (a naturally occurring alloy of La, Ce, Nd, and Pr) alloyed with various proportions of Ni, Co, Mn, and Al, and the experiments were directed toward optimization of the composition of the misch metal (see table).

In preparation for fabrication of the experimental anodes, the alloys as received from the manufacturer were pulverized by ball milling, sifted, and preactivated by a few gas-phase hydrogen-absorption/desorption cycles. Carbonyl Ni powder in the proportion of 20 percent was mixed into each alloy powder as a conductive diluent. Then 5 percent of polytetrafluoroethylene powder was added to each powder mixture, and the anodes were fabricated by hot-pressing the mixtures.

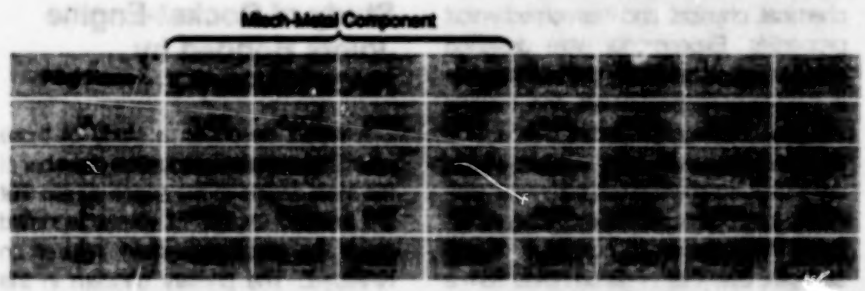

The anodes were evaluated experimentally by charging and discharging them in all-glass prismatic cells with 31-percent-KOH electrolyte and Hg/HgO reference electrode. An important consideration in any such evaluation is that if a metal hydride cell is to operate at ambient atmospheric pressure, then the equilibrium pressure at which the metal alloy can absorb hydrogen should not exceed the ambient pressure. Accordingly, in the experiments, the anodes were charged at pressures close to ambient, and alloys for which the equilibrium pressures are higher (e.g., $LaNi_5$) were expected to exhibit low capacities.

As shown in the figure, the initial measured capacities were smaller for anodes in which the La contents of the misch-metal components were relatively high and greater for anodes in which the La contents were smaller. This trend can be explained in terms of a decrease in equilibrium pressure upon the substitution of Ce for La.

The capacities were then measured in charge/discharge cycles at a 5-hour rate between –600 mV vs. Hg/HgO (considered to represent full discharge) and

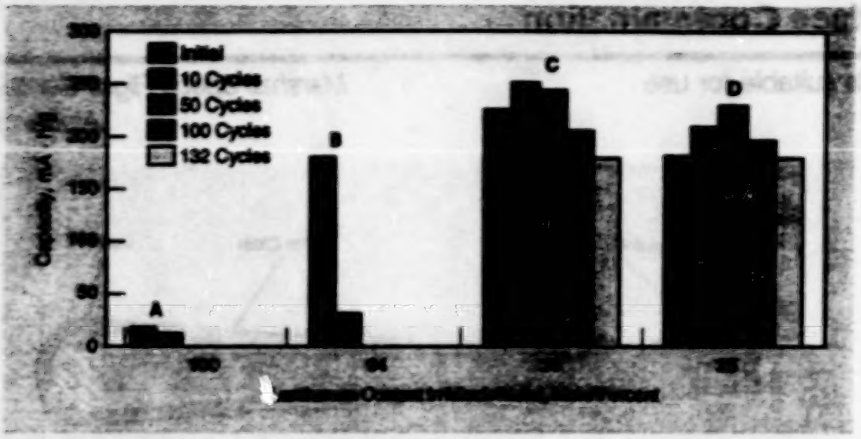

Less La and More Ce in the Mlech-Metal Components of the anode alloys resulted in greater initial capacities and greater capacities retained after many charge/discharge cycles.

–1,200 mV vs. Hg/HgO (considered to represent full charge) with a charge return of 120 percent. The figure shows that the retention of capacity after numerous charge/discharge cycles was greater for the anodes with smaller La (larger Ce) contents. The optimum composition of the misch-metal component appears to lie in the range of 25 to 30 mole percent of La and 50 to 55 mole percent of Ce, the balance being Nd (13 mole percent) and to some extent Pr (7 mole percent).

This work was done by Ratnakumar V. Bugga and Gerald Halpert of Caltech for NASA's Jet Propulsion Laboratory. Further information is contained in a TSP [see page 1].
NPO-19325

Books and Reports

Improved Silicon Nitride for Advanced Heat Engines

Experimental studies guided the development of improved formulations and processes.

A report summarizes the results of four years of research directed toward increasing the strength and reliability of injection-molded silicon nitride parts for advanced heat engines. The research involved extensive experimental studies of formulations, additives, processes, and the resultant chemical, physical, and thermomechanical properties. Experiments were designed and performed to identify and optimize critical processing parameters and material variables. Physical properties over a wide temperature range and microstructures were used to characterize parameter variables. Improvements in processing resulted in increases of 20 percent in flexural strength, over that of silicon nitride from a baseline formulation and process, at room temperature and at a temperature of 2,000 °F (1,102 °C). Screening of alternative sintering aids led to the development of a new composition and process. The new composition, called GN-10, has high flexural strength at high temperature, characterized by a modulus of rupture of 84.3 kpsi (581.2 MPa) at a temperature of 2,550 °F (1,399 °C). This strength was achieved by encapsulated hot isostatic pressing of the material. A composite of GN-10 matrix reinforced by silicon carbide whiskers exhibited a room temperature toughness of 6.3 kpsi-in.$^{1/2}$ (6.9 MPa-m$^{1/2}$) as measured by the Chevron-notched-bar technique. Exploratory experiments on injection molding of turbocharger rotors were conducted, and these results showed promise of processing improvements.

This work was done by Harry C. Yeh and Ho T. Fang of Allied-Signal Aerospace Co. for Lewis Research Center. For further information, see TSP's [page 1].
LEW-15843

Study of Rocket-Engine Joints Bonded by Ni/Cu/NARloy-Z

A report describes a study of those joints in the main combustion chamber of the main engine of the space shuttle that are bonded by use of electrodeposited nickel on electrodeposited copper on NARloy-Z. The primary concern in this study was to understand interrelationships among stresses in the joints, the strengths of the joints, and variations of parameters of the joints, with a view toward developing process controls to ensure strong joints free of defects. These relationships were evaluated via finite-element computations of stresses, with emphasis on the regions closest to the bond terminations and interfaces, where failures are generally thought to occur. The results of the study appear to be applicable to any similarly bonded joints that can be characterized by the parameters used and assumptions made in this study.

This work was done by J. B. Min and K. L. Spanyer of Marshall Space Flight Center. To obtain a copy of the report, "A Study on Strength Evaluations of EDNi/EDCu/NARloy-Z Bonded Joints," see TSP's [page 1].
MFS-28957

Hazardous Fluids Compatibility Test Apparatus

A document describes a test apparatus designed to hold test tubes containing hazardous fluids such as hydrazine, nitrogen tetroxide, or ammonia. The test tube can be suspended over a water bath or other solution or mixture. Control of the test sample can be performed by one-hand operation within a fume hood or glove box. The system is adaptable for automated control of the lowering and raising of the test samples.

This work was done by Frank Flores and James Daniel of Lockheed Engineering and Sciences Co. for Johnson Space Center. To obtain a copy of the report, "Hazardous Fluids Compatibility Test Apparatus," see TSP's [page 1].
MSC-21826

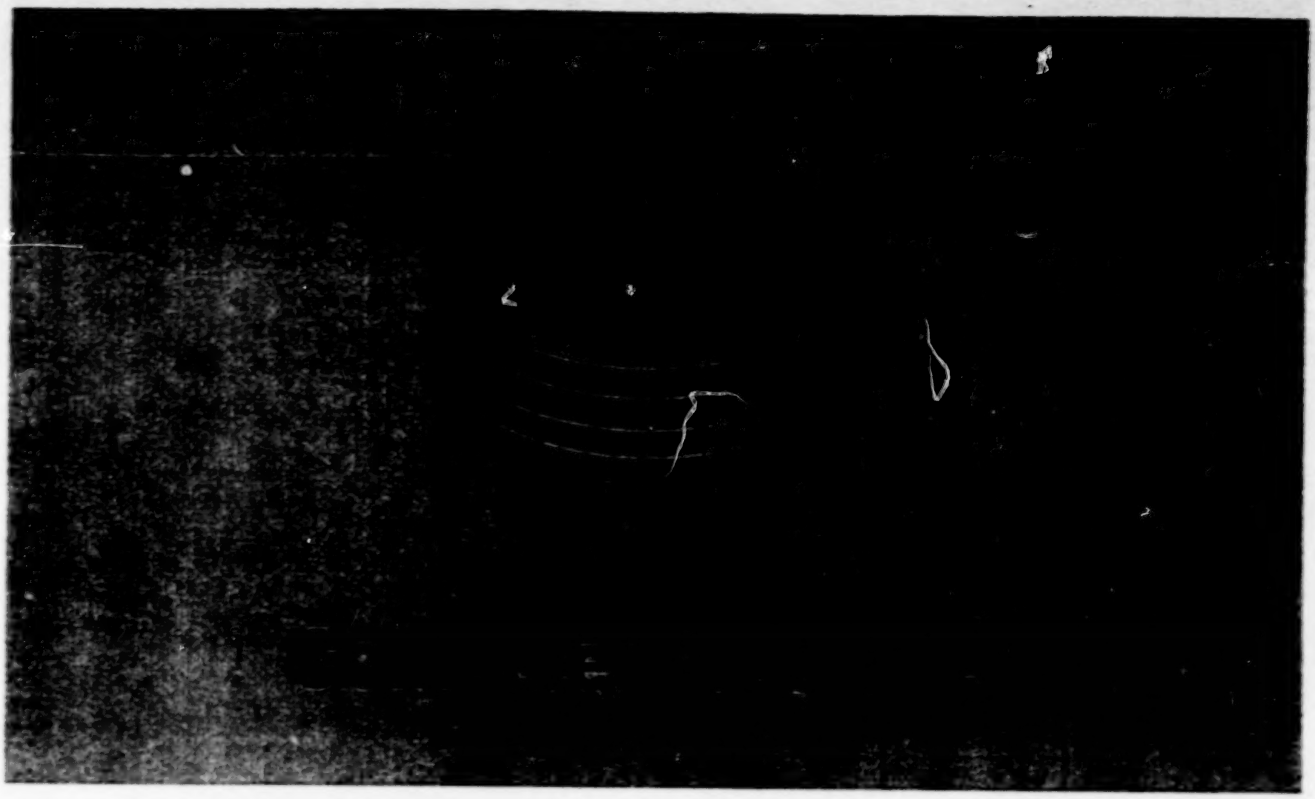

Electronic Components and Circuits

47 Computing Efficiency of Transfer of Microwave Power
47 Program Calculates Power Demands of Electronic Designs
47 Cost-Estimation Program
48 Program Estimates Areas Required by Electronic Designs

Physical Sciences

48 Computing Equilibrium Chemical Compositions
49 Program Processes Thermocouple Readings

Materials

49 iCAN — Second-Generation Integrated Composite Analyzer
50 Integrated Composite Analyzer with Damping Capabilities

Mechanics

50 Probabilistic Failure Assessment for Fatigue
51 Probabilistic Fatigue and Flaw-Propagation Analysis

Machinery

51 Program To Balance Mapped Turbopump Assemblies

Mathematics and Information Sciences

52 BiblioTech
52 Subband/Transform MATLAB Functions for Processing Images
53 Windows Program for Driving the TDU-850 Printer

BLANK PAGE

Computer Programs

These programs may be obtained from COSMIC. Please contact

COSMIC®
Computer Services Annex
University of Georgia
Athens, GA 30602
Telephone No. (404) 542-3265.

Electronic Components and Circuits

Computing Efficiency of Transfer of Microwave Power

This program calculates electromagnetic fields in and between two apertures.

The BEAM computer program enables the user to calculate the microwave power-transfer efficiency between two circular apertures in an arbitrary range. The power-transfer efficiency is obtained numerically. The two apertures can have generally different sizes and arbitrary taper illuminations. BEAM can also analyze the effect of distance and taper illumination on the transmission efficiency for two apertures of equal size.

BEAM simulates the transmitting tangential aperture field with a tapered aperture field distribution. A numerical evaluation of the Kirchhoff and Helmholtz vector diffraction solution is used to calculate the distributions of the electric and magnetic fields at arbitrary observation distances. To obtain the transmission efficiency, the power transmitted is compared to the power intercepted by a receiving aperture antenna located at an arbitrary distance from the transmitting antenna.

BEAM is written in FORTRAN and was originally developed for Amdahl computers running VM/CMS. This version has been successfully compiled and implemented on an IBM 3080 computer running VM/CMS, a Sun4-series computer running SunOS, a DECstation 3100-series computer running DEC RISC ULTRIX, an HP9000 series-700 computer running HP-UX, an IBM PC-compatible computer running MS-DOS, and a DEC VAX-series computer running VMS. BEAM requires 1MB of random-access memory (RAM) and 3MB of virtual memory for execution on an IBM 3080 mainframe computer. It requires 238K of RAM for execution in a VMS environment, and approximately 408K of RAM for execution in UNIX and DOS environments. The standard distribution medium for this program is a 3.5-in. (8.89-cm), 1.44MB, MS-DOS-format diskette. Alternate distribution media and formats are available upon request. No sample executable code is provided. BEAM was developed in 1989 and was released to COSMIC in 1993.

This program was written by L. R. Pinero and R. Acosta of Lewis Research Center. Further information is contained in a TSP [see page 1].
LEW-15853

Program Calculates Power Demands of Electronic Designs

Overall currents and power levels are estimated from component current demands.

The CURRENT computer program calculates power requirements of electronic designs. For a given design, CURRENT reads in the applicable parts-list file and a file that contains the current required for each part. The program also calculates the power required for the circuit at supply potentials of 5.5, 5.0, and 4.5 volts.

The user invokes CURRENT with the input parts list, the current-requirements list, and the name of the output file. Any parts not in the current-requirement list are reported, and the current-requirement list can be modified for particular needs.

CURRENT is written by use of the AWK utility for Sun4-series computers running SunOS 4.x and IBM PC-series and compatible computers running MS-DOS. The program was written to be used with the OrCad Schematic Capture Program, but also can be used with a list of parts in ASCII format. The UNIX "nawk" utility is used to run the Sun version of CURRENT. The Sun version of the program (NPO-19590) has been successfully implemented on a Sun4-series computer running SunOS 4.1.3. The PC version of the program (NPO-19111) has been successfully implemented on a DECpc 486-series computer running MS-DOS v6.2. A sample executable file is provided for the PC version of CURRENT. The standard distribution medium for the Sun version of CURRENT is a 3.5-in. (8.89-cm), 1.44MB diskette in UNIX tar format. The standard distribution medium for the PC version of CURRENT is one 3.5-in. (8.89-cm), 1.44MB, MS-DOS-format diskette. An electronic copy of the documentation in Microsoft Word v2.0 for MS-DOS format is included on all distribution media. CURRENT was released in 1995 and is a copyrighted work with all copyright vested in NASA.

This program was written by Brian Cox of Caltech for NASA's Jet Propulsion Laboratory.

For further information on NPO-19590, see TSP's [page 1].

For further information on NPO-19111, see TSP's [page 1]
NPO-19590/NPO-19111

Cost-Estimation Program

Costs of designs are estimated from design parts lists and files of unit costs.

The COSTIT computer program estimates the cost of an electronic design by reading an item-list file and a file that contains the cost for each item. The accuracy of the cost estimate is based on the accuracy of the cost-list file.

The user invokes COSTIT with the item-list file, the cost-list file, and the name of the output file. Any parts not in the cost list are reported, and the cost list can be modified for particular needs.

COSTIT is written by use of the AWK utility for Sun4-series computers running SunOS 4.x and IBM PC-series and compatible computers running MS-DOS. The program was written to be used with the OrCad Schematic Capture Program, but also can be used with a list of parts in ASCII format. The UNIX "nawk" utility is used to run the Sun version of COSTIT. The Sun version of the program (NPO-19587) has been successfully implemented on a Sun4-series computer running SunOS 4.1.3. The PC version of the program (NPO-19157) has been successfully implemented on a DECpc 486-series computer running MS-DOS v6.2. A sample executable file is provided for the PC version of COSTIT. The standard distribution medium for the Sun version of COSTIT is a 3.5-in. (8.89-cm), 1.44MB

diskette in UNIX tar format. The standard distribution medium for the PC version of COSTIT is one 3.5-in. (8.89-cm), 1.44MB, MS-DOS-format diskette. An electronic copy of the documentation in Microsoft Word v2.0 for MS-DOS format is included on all distribution media. COSTIT was released in 1995 and is a copyrighted work with all copyright vested in NASA.

This program was written by Brian Cox of Caltech for **NASA's Jet Propulsion Laboratory.**

For further information on NPO-19587, see TSP's [page 1]

For further information on NPO-19157, see TSP's [page 1]

NPO-19587/NPO-19157

Program Estimates Areas Required by Electronic Designs

Both unit areas of components and inherent additional space requirements are taken into account.

The PSIZE computer program calculates the space required for an electronic design. PSIZE reads in a parts-list file and a file that contains the required area for each type of part. A "reality factor" is applied to the calculated amount to account for the inherent additional space required by any layout.

The user invokes PSIZE with the input parts list, the component-size list, and the name of the output file. Any parts not in the component-size list are reported, and the component-size list can be modified for particular needs.

PSIZE is written by use of the AWK utility for Sun4-series computers running SunOS 4.x and IBM PC-series and compatible computers running MS-DOS. The program was written to be used with the OrCad Schematic Capture Program, but also can be used with a list of parts in ASCII format. The UNIX "nawk" utility is used to run the Sun version of PSIZE. The Sun version of the program (NPO-19589) has been successfully implemented on a Sun4-series computer running SunOS 4.1.3. The PC version of the program (NPO-19065) has been successfully implemented on a DECpc 486-series computer running MS-DOS v6.2. A sample executable file is provided for the PC version of PSIZE. The standard distribution medium for the Sun version of PSIZE is a 3.5-in. (8.89-cm), 1.44MB diskette in UNIX tar format. The standard distribution medium for the PC version of PSIZE is one 3.5-in. (8.89-cm), 1.44MB, MS-DOS-format diskette. An electronic copy of the documentation in Microsoft Word v2.0 for MS-DOS format is included on all distribution media. PSIZE was released in 1995 and is a copyrighted work with all copyright vested in NASA.

This program was written by Brian Cox of Caltech for **NASA's Jet Propulsion Laboratory.**

For further information on NPO-19589, see TSP's [page 1]

For further information on NPO-19065, see TSP's [page 1]

NPO-19589/NPO-19065

Physical Sciences

Computing Equilibrium Chemical Compositions

This program aids calculation of thermodynamic properties of chemical systems.

The Chemical Equilibrium With Transport Properties, 1993 (CET93) computer program provides data on chemical-equilibrium compositions. Scientists and engineers need such data to calculate the theoretical thermodynamic properties of chemical systems. This information is essential in the design and analysis of such equipment as compressors, turbines, nozzles, engines, shock tubes, heat exchangers, and chemical-processing equipment.

For more than 40 years, the NASA Lewis Research Center has been involved in developing methods and computer programs for calculating complex chemical-equilibrium compositions and calculating thermodynamic and transport properties of the equilibrium mixtures, and for applying these properties to a number of problems. CET93 is the latest of these computer programs. CET93/PC is a version of CET93 specifically designed to run within the 640K memory limit of the MS-DOS operating system.

CET93 is a general program that calculates chemical-equilibrium compositions and properties of mixtures for any chemical system for which thermodynamic data are available. Generally, mixtures may include condensed and gaseous products. CET93/PC performs the following operations:

1. It obtains chemical equilibrium compositions for assigned thermodynamic states.
2. It calculates dilute-gas transport properties of complex chemical mixtures.
3. It obtains Chapman-Jouguet detonation properties for gaseous species.
4. It calculates incident- and reflected-shock properties in terms of assigned velocities or mach numbers.
5. It calculates theoretical performances of rockets for both equilibrium and frozen compositions during expansion. The rocket-performance part of the program includes the option of assuming either a finite- or an infinite-area combustor.

CET93/PC includes a file of thermodynamic data for over 1,100 gaseous and condensed species and a file of data on thermal-transport properties of 155 gaseous species. These data are in the form of least-squares coefficients in binary form. Through use of a new "ONLY" option, the users can instruct CET93/PC to consider only particular species as possible products for a given equilibrium composition calculation. Relative to CET93, CET93/PC imposes a few limitations on the sizes of arrays so that it can run within the basic 640K of random-access memory (RAM) available under MS-DOS. The maximum number of possible reaction species accommodated for any chemical system was reduced from 600 to 300, and the maximum number of condensed reaction species was reduced from 300 to 200. Experience has shown, however, that even in the presence of these limits, CET93/PC is sufficient for most practical chemical systems.

CET93/PC is written in FORTRAN and is available only as executable code for use on IBM PC-series and compatible computers running MS-DOS. The executable code was created by use of Microsoft FORTRAN 5.1 on a 386SX PC without a math coprocessor; however, the executable code takes advantage of a math coprocessor when one is present. At least 400K of RAM must be available for this executable code to run properly. The distribution medium for CET93/PC includes input and output files for the example problems and two files that describe how to use the program. The paper documentation for CET93/PC consists of a copy of these instructions plus NASA Technical Memorandum 4557, which includes a list of the names of chemical species of possible products. The standard medium for distribution of

CET93/PC is a 3.5-in. (8.89-cm), 1.44MB, MS-DOS-format diskette. CET93/PC was developed in 1993.

This program was written by Bonnie J. McBride of Lewis Research Center, Sanford Gordon of Sanford Gordon and Associates, and Martin A. Reno of Heidelberg College. Further information is contained in a TSP [see page 1].
LEW-16017

Program Processes Thermocouple Readings

Voltages are converted to temperatures.

The Digital Signal Processor for Thermocouples (DART) computer program implements a precise and fast method of converting voltage to temperature for large-temperature-range thermocouple applications. The conventional method of generating precise measurements requires multiple high-order equations that are difficult to solve in real time.

DART was written using LabVIEW software. Virtual instruments (VIs) were created by use of National Institute of Standards and Technology (NIST) tables, the precision of which is limited to 0.01 mV. Interpolation is used to generate more precise values. At NASA/Stennis Space Center, instrumentation in the field transmits information to a control room, where LabVIEW VIs display the data on computer monitors.

DART is available only as object code for use on Macintosh II FX or higher-series computers running System 7.0 or later and IBM PC-series and compatible computers running Microsoft Windows 3.1. The Macintosh version of DART (SSC-00032) requires LabVIEW 2.2.1 or 3.0 for execution. The IBM PC version (SSC-00031) requires LabVIEW 3.0 for Windows 3.1. LabVIEW requires a minimum of 5MB of random-access memory (RAM) on a Macintosh computer and 8MB of RAM on a PC. The LabVIEW software is a product of National Instruments (Austin, TX, 800-433-3488), and is not included with this program. The standard distribution medium for the Macintosh version of DART is a 3.5-in. (8.89-cm), 1.44MB diskette in Macintosh format. The standard distribution medium for the PC version of DART is a set of two 3.5-in. (8.89-cm), 1.44MB diskettes in MS-DOS format. DART was developed in 1994.

This program was written by Christine A. Quave and William "Bud" Nail II of Stennis Space Center.

For further information on SSC-00031, see TSP's [page 1]

For further information on SSC-00032, see TSP's [page 1]

Inquiries concerning rights for the commercial use of this invention should be addressed to the Patent Counsel, Stennis Space Center [see page 1]. Refer to SSC-00031/32.

Materials

ICAN — Second-Generation Integrated Composite Analyzer

This program computes stresses and strains in multilayer composites.

The Integrated Composite Analyzer (ICAN) computer program provides for comprehensive linear analyses of multilayered matrix/fiber composite materials. The analyses include the features that are essential for effective design of structural components made of such materials. ICAN includes micromechanical design features to predict ply-level hygral, thermal, and mechanical properties. Laminate-analysis features are included to account for interply layer effects. ICAN integrates these with additional features to provide a capability for comprehensive analyses of composite structures.

ICAN also includes the following features: (1) ply stress-vs.-strain influence coefficients; (2) microstresses and microstrain influence coefficients; (3) concentration factors around a circular hole; (4) calculation of probable delamination locations around a circular hole; (5) Poisson's-ratio mismatch details near a straight edge; (6) free-edge stresses; (7) material card input for finite-element analysis by use of NASTRAN (also available from COSMIC) or MARC; (8) failure loads based on a maximum-stress criterion; (9) laminate failure stresses based on first-ply failures and fiber-breakage criteria; (10) transverse shear, normal, and interlaminar stresses; and (11) durability/fatigue-type analyses for thermal as well as mechanical cyclic loads. The code can assess degradation due to mechanical and thermal cyclic loads with or without a defect. A modified version of ICAN that includes prediction of damping in polymer-matrix composites, ICAN/DAMP (LEW-15986, LEW-16073), is also available from COSMIC.

ICAN includes a dedicated data bank of constituent material properties that enables the user to build a data base of material properties of commonly used fibers and matrices. The user need only specify code names for constituents. Input to ICAN includes properties of constituent materials (or code names), factors that reflect the fabrication process, and geometry of the composite to be analyzed. Output includes the various properties of the plies and of the composite, the structural response of the composite, and the results of stress analysis of the composite with details of failure.

Two machine versions of ICAN are available: the Amdahl version and the PC version. The Amdahl version (LEW-15832) is written in FORTRAN 77 for Amdahl-series computers running VM. The Amdahl version has also been successfully ported to a variety of mainframes operating under different operating systems: VAX/VMS, CRAY/UNICOS, and ALLIANT. The most common difficulty experienced in converting this code to other systems is attributed to the different conventions followed in allocating the various OPEN statements (input/output units) under individual operating systems. The Amdahl version requires 3.5MB of memory for execution. No sample executable code is provided.

The IBM PC version (LEW-15592) is written in FORTRAN 77 for use on the IBM PC-series computers running MS-DOS. Microsoft FORTRAN v5.1 is required to recompile the source code. For the IBM PC version, a sample executable code along with sample input and output is included on the distribution medium. Although the included executable code requires a math coprocessor, the ICAN source code can be compiled into an executable code that does not require a math coprocessor. The standard distribution medium for either version of ICAN is a 3.5-in. (8.89-cm), 1.44MB, MS-DOS-format diskette. ICAN was originally developed in 1986. The IBM PC version was released in 1992, and the Amdahl version was released in 1993.

This program was written by P. L. N. Murthy of Lewis Research Center and S. K. Mital of the University of Toledo. Further information is contained in a TSP [see page 1].
LEW-15832

Integrated Composite Analyzer with Damping Capabilities

Damping properties are computed from equations of micromechanics.

The Integrated Composite Analyzer with Damping Capabilities (ICAN/DAMP) computer program combines the comprehensive linear analysis of a multilayered fiber composite material in ICAN (COSMIC programs LEW-15832, LEW-15592) with the prediction of damping in a polymer-matrix composite. As in ICAN, the analysis contains the essential features needed for effective design of structural components made from fiber composites, including micromechanical design features to predict ply-level hygral, thermal, and mechanical properties, and laminate-analysis features to account for interply layer effects. ICAN/DAMP incorporates a new module for synthesizing the material damping from micromechanics to the laminate level.

In ICAN/DAMP, explicit equations of micromechanics based on hysteretic damping are programmed to relate the on-axis damping capacities to the fiber and matrix properties and fiber volume ratio. The damping capacities of unidirectional composites subjected to off-axis loading are synthesized from on-axis damping values. The hygrothermal effects (that is, the effects of variations in temperature and moisture) on the damping performances of unidirectional composites are modeled along with the damping contributions from interfacial friction between broken fibers and matrices. The temperature rises in continuously vibrating composite plies and composite laminates are also estimated.

ICAN/DAMP is written in FORTRAN 77 for DEC VAX-series computers running VMS and Amdahl 5870-series computers running the VM/SP operating system. Sample input and output are provided. The standard distribution medium for the VAX version is a 1,600-bit/in. (630-bit/cm), 9-track magnetic tape in DEC VAX BACKUP format. It is also available on a TK50 tape cartridge in DEC VAX BACKUP format. The standard distribution medium for the Amdahl version is a 3.5-in. (8.89-cm), 1.44MB, MS-DOS-format diskette. ICAN was developed in 1986 and ICAN/DAMP was released in 1994.

This program was written by J. G. Santiago, and C. C. Chamis of Lewis Research Center and D.A. Saravanos of Ohio Aerospace Institute. Further information is contained in a TSP [see page 1].
LEW-15966

Mechanics

Probabilistic Failure Assessment for Fatigue

This program contains nine subprograms that effect various components of fatigue analysis.

Probabilistic Failure Assessment for Fatigue (PFAFAT) is a package of software that utilizes the probabilistic failure-assessment (PFA) methodology to model high- and low-cycle-fatigue modes of failure of structural components. PFAFAT consists of nine programs. Three of the programs perform probabilistic fatigue analysis by means of Monte Carlo simulation. The other six programs are used for generating random processes, characterizing fatigue-life data pertaining to materials, and processing the outputs of computational simulations.

PFAFAT includes routines for the simulation of both high-cycle and low-cycle-fatigue cases. The example applications for the high-cycle-fatigue-analysis software include the following components of the main engine of the space shuttle: the main discharge duct of the high-pressure oxidizer turbopump (HPOTP), the main drive duct of the low-pressure fuel turbopump (LPFTP), and the heat-exchanger coil of the HPOTP. The PFAFAT software package includes programs to analyze elbow ducts with welds and straight ducts with welds and large differences in temperature across the duct walls. The example application for the low-cycle-fatigue-analysis software is the turbine disk of a high-pressure fuel turbopump.

The PFAFAT software package includes other programs for fatigue analysis. MATCHR is a program for simulating the cyclic fatigue behavior of a material, using fatigue-test data. This program contains both the stress and strain formulations of the materials-characterization model in a stand-alone form. PFAFAT also includes a set of programs that compute the prior failure-distribution parameters and perform assurance calculations. Routines to implement the Bayesian statistical procedure are supplied. This procedure is used to combine operating experience with the prior failure distribution obtained from the probabilistic failure modeling. A number of random number generators are provided, including uniform, normal, gamma, beta, and Weibull distributions.

The probabilistic failure-assessment (PFA) methodology utilized by PFAFAT is an advanced approach for evaluating the risk of failure, assessing service life, and establishing design parameters for structures subject to fatigue failure. This approach combines engineering analysis with experience from tests and service to quantify the risk of failure. The PFA methodology is particularly valuable when information on which to base design analysis or prediction of failure is sparse, uncertain, or approximate and is expensive or difficult to acquire.

The PFA methodology is a prescribed statistical structure in which engineering analysis models that characterize failure phenomena are used in conjunction with uncertainties about analysis parameters and/or modeling accuracy to establish failure-probability distributions for specific failure modes. These distributions can then be modified by means of statistical procedures of the PFA methodology to reflect test or service experience.

The PFA methodology is applicable to failure modes of structures that can be analytically or empirically modeled. Engineering analysis models employed for design or prediction of failure due to specific failure modes are used in PFA. PFA can be applied at any time in the design, development, or operational phases of a program, using the information available. Sensitivity analyses conducted as a part of PFA can be used to evaluate alternative measures to control risks, thereby enabling the more effective allocation of limited program resources. Such alternative measures can include changes in designs, testing, or inspections.

PFAFAT is written in FORTRAN 77 to be machine-independent. With minor modifications, it has been successfully implemented on a Sun4-series computer running SunOS, an HP9000-series 700 computer running HP-UX, an IBM PC-compatible computer running MS-DOS, a DEC VAX-series computer running VMS, and CRAY XMP-series computers running COS and UNICOS. It may be necessary to adjust the sizes of arrays, depending on the specific application; however, 5MB of main memory and 10MB of hard-disk space should be sufficient for most

applications. The IMSL Libraries are necessary for compiling ABTRT, one of the statistical-analysis programs. The standard distribution medium for PFAFAT is a 3.5-in. (8.89-cm), 1.44MB, MS-DOS diskette. Alternate distribution media and formats are available upon request. PFAFAT was under development from 1987 through 1992 and is a copyrighted work with all copyright vested in NASA.

This program was written by Nicholas Moore, Donald Ebbeler, Laura Newlin, Sravan Sutharshana, and Matthew Creager of Caltech for NASA's Jet Propulsion Laboratory. Further information is contained in a TSP [see page 1].
NPO-18965

Probabilistic Fatigue and Flaw-Propagation Analysis

This program is an extension of the PFAFAT software.

Probabilistic Failure Assessment for Fatigue and Flaw Propagation (PFAFAT II) is a package of software that utilizes the probabilistic failure-assessment (PFA) methodology to model flaw-propagation and low-cycle-fatigue modes of failure of structural components. PFAFAT II comprises one program for performing probabilistic crack-growth analysis and two programs for performing probabilistic low-cycle-fatigue analysis. These programs perform probabilistic fatigue and crack-propagation analysis by means of Monte Carlo simulation.

PFAFAT II is an extension of, rather than a replacement for, the PFAFAT software. The probabilistic fatigue- and flaw-propagation-analysis methodology implemented in PFAFAT II, plus the PFAFAT II software itself, are thoroughly documented. The statistical methodology is explained in the PFAFAT documentation. Programs from PFAFAT are required for generating random processes, characterizing fatigue-life data pertaining to materials, and processing the outputs of computational simulations.

The crack-growth-analysis program in this software package can be used to probabilistically predict the crack-growth lives of structural components. Example applications include a Heat-Exchange (HEX) Coil and a plate Heat Exchanger (EXHEX). This code is very modular and hence can be easily modified for crack-growth analyses of various components. Different modules are provided for stress analysis and stress-intensity-factor calculations for the HEX and EXHEX analyses.

The low-cycle-fatigue (LCF) failure model calculates the crack-initiation life of a structure subjected to a small number of high-amplitude load cycles. Values of such drivers as environmental parameters, loads, material properties, structural parameters, and uncertainties in driver values and engineering-model accuracy are used by the LCF failure model. The LCF-model example application is a program to analyze a turbopump turbine blade. There are two versions of the LCF model in PFAFAT II: One version follows a parametric approach to characterization of material fatigue data, while the other version follows a nonparametric or "bootstrapping" approach to characterization of fatigue-life data.

The probabilistic failure-assessment (PFA) methodology, which is utilized by PFAFAT and PFAFAT II, is an advanced approach for evaluating the risk of failure, assessing service life, and establishing design parameters for structures subject to fatigue failure. This approach combines engineering analysis with experience from tests and service to quantify the risk of failure. The PFA methodology is particularly valuable when information on which to base design analysis or prediction of failure is sparse, uncertain, or approximate and is expensive or difficult to acquire.

The PFA methodology is applicable to failure modes of structures that can be analytically or empirically modeled. Engineering analysis models employed for design or prediction of failure due to specific failure modes are used in PFA. PFA can be applied at any time in the design, development, or operational phases of a program, using the information available. Sensitivity analyses conducted as a part of PFA can be used to evaluate alternative measures to control risks, thereby enabling the more effective allocation of limited program resources. Such alternative measures can include changes in designs, testing, or inspections.

PFAFAT II is written in FORTRAN 77 to be machine-independent. It has been successfully implemented on a Sun4-series computer running SunOS, an HP 9000-series 720 computer running HP-UX, a CRAY Y-MP-series computer running UNICOS, a DECstation 3100-series computer running RISC ULTRIX, an IBM PC-compatible computer running DOS, an Intel Touchstone Delta-series computer running iPSC/860, and a DEC VAX-series computer running VMS. It may be necessary to adjust the sizes of arrays, depending on the specific application; however 5MB of random-access memory and 10MB of hard-disk space should be sufficient for most applications. The standard distribution medium for PFAFAT II is a 3.5-in. (8.89-cm), 1.44MB, MS-DOS-format diskette. Alternate distribution media and formats are available upon request. PFAFAT II was under development from 1988 through 1992 and was released in 1993. This program is a copyrighted work with all copyright vested in NASA.

This program was written by Nicholas Moore, Laura Newlin, Donald Ebbeler, Sravan Sutharshana, and Matthew Creager of Caltech for NASA's Jet Propulsion Laboratory. Further information is contained in a TSP [see page 1].
NPO-19319

Machinery

Program To Balance Mapped Turbopump Assemblies

TPA computes outlet conditions and work from inlet conditions and performance maps.

Accurate computational simulation of nuclear thermal propulsion systems will enable reductions in testing and, thus, the time and cost of making these advanced systems ready for use in flight. An accurate simulation must maintain a "balance-of-plant" in which the required pump work equals the supplied turbine work. This turbopump-assembly balancing must be integrated into the overall system-analysis models. The TPA computer program was developed to balance turbine and pump work using performance maps. TPA requires input data on the inlet properties, performance maps, and shaft speed. TPA then computes the exit conditions and work terms. The work terms can then be balanced by varying the input shaft speed.

The objective of the pump analysis is to determine (1) the state properties of the propellant at the exit from the pump and (2) the work done by the pump. The pump-analysis algorithm for liquid flow is based partly on the assumption that the shaft speed, the state properties of the propellant at the entrance to the pump, the rate of flow of propellant, the entrance and exit areas of the pump, and the

pump-performance curves are all known. The analysis also requires both the pressure rise in the pump and the pump efficiency curves.

The objective of the turbine analysis is to determine (1) the propellant-state properties at the exit from the turbine and (2) the work done by the turbine. The turbine-analysis algorithm is based partly on the assumption that the shaft speed, the propellant-state properties at the entrance to the turbine, the rate of flow of the propellant, the root-mean-square diameter of the turbine blades, the entrance and exit areas of the turbine, and the turbine-performance curves are all known. The analysis also requires the turbine flow-parameter curve and the turbine total-efficiency curve.

TPA is written in FORTRAN 77 to be machine-independent. The TPA package includes the NBS+_PH2 code, which is also available separately (LEW-15505). TPA has been successfully implemented on a DEC VAX-series computer running VMS, a Sun4-series computer running SunOS, and an IBM PC-compatible computer running MS-DOS. Lahey F77L3 EM/32 v. 5.01 or higher is required for compilation on an IBM PC-compatible computer; however, a PC executable code is included on the distribution diskette. The standard distribution medium for this program is one 5.25-in. (13.34-cm), 360K, MS-DOS-format diskette. The contents of the diskette have been compressed by use of the PKWARE archiving software tools. The utility software to unarchive the file, PKUNZIP.EXE, is included. Alternate distribution media and formats are available upon request. TPA was developed in 1993.

This program was written by J. T. Walton of Lewis Research Center. Further information is contained in a TSP (see page 1).
LEW-15712

Mathematics and Information Sciences

BiblioTech

This program helps to retrieve and use data on diverse technological developments.

The BiblioTech computer program was originally developed to capture information about continuing advanced technological developments in fields applicable to spacecraft systems and subsystems in data-base files called "libraries." There is, however, no element of the design that restricts BiblioTech from addressing other technological fields beyond the specialized area of spacecraft technology. A BiblioTech data base can be used to determine what technologies are being developed by government institutions, laboratories, and private companies under government contract relating to spacecraft systems and subsystems. A data base also contains contact information to enable the user to gain more information about technologies in the library. The BiblioTech application program and the information contained in the BiblioTech libraries are dependent upon design and content inputs, which were provided by a variety of participating government agencies.

The BiblioTech system is composed of two interrelated elements. The first is the BiblioTech application program, which is a relational data-base-management system based upon the 4th DIMENSION environment. BiblioTech comprises data-base structure and code that implements functional capability for input, display, output, query and report generation, analysis, and maintenance. The second element consists of one or more populated libraries. These are data files, with spacecraft-subsystem-technology entries, supplied by a variety of developing agencies.

A library can refer to several different technology application areas, or different application areas can be maintained in separate libraries, using the same BiblioTech application program to manage their content and use. The overall organization of the library for local use depends upon the manner in which an organization intends to use it to support its technology-development programs.

The content and functions of BiblioTech specifically provide for the following: (1) determining the identity, status, and goals of technological items within the community of organizations that supply input to the library; (2) capturing information on programs being planned or developed at the local user organization; (3) developing material for periodic program-status reviews; (4) assessing the ability of proposed programs to supplement or augment development by other organizations, while avoiding conflict or duplication of effort; and (5) creating and maintaining a definitive list of organizational contacts for each item in the library.

BiblioTech is a data-base program and is available only as executable code for use with 4th DIMENSION Runtime on Macintosh computers running System 6.0.7 or later. This program requires at least a Macintosh SE computer with 4MB of random-access memory and 8MB of hard-disk memory space; however, it is recommended that BiblioTech be installed on Macintosh II or better to improve execution speed. There are three modules of BiblioTech for which licenses are required: 4D Runtime 2.2.3, 4D CALC 1.1, and 4D Communications Kit 1.0. These modules provide the basic data-base engine, spreadsheet, and communications capabilities required to operate BiblioTech. The data-base and communications modules are included on the BiblioTech distribution medium but will be operable only after the user obtains licenses for them. The spreadsheet module, 4D CALC, will be provided by the licensor and placed into the BiblioTech application program during the licensing procedure. Licenses for 4D CALC 1.1 and 4D Runtime 2.2.3 are available from ACI US, Inc. (Cupertino, CA, 408-252-4444). The license for 4D Communications Kit 1.0 is available from Full Moon Software (San Jose, CA, 408-253-7199).

BiblioTech also requires installation of Apple's Macintosh Communications Toolbox and Macintosh Basic Connectivity Set. In addition, an AppleTalk-compatible network and a modem will be necessary if the ability to communicate with other BiblioTech sites is desired. The Communications Toolbox is distributed as part of Apple's Macintosh System 7. The Communications Toolbox, Basic Connectivity Set, and MacTCP 1.1.1 are also available from Apple Computer, Inc. (Cupertino, CA, 408-996-1010). The standard distribution medium for this package of software is a set of five 3.5-in. (8.89-cm), 800K, Macintosh-format diskettes. BiblioTech was developed in 1993 and is a copyrighted work with all copyright vested in NASA.

This program was written by David S. Mittman and Phillip R. Turner of Caltech for NASA's Jet Propulsion Laboratory. Further information is contained in a TSP (see page 1).
NPO-19112

Subband/Transform MATLAB Functions for Processing Images

For example, the transforms can be used to prepare data for lossy compression.

The SUBTRANS software is a package of routines that implement image-data-processing functions for use with MATLAB* software. These functions provide the capability to transform image data with block transforms (such as the Walsh-Hadamard) and to produce spatial-frequency subbands of the transformed data. Block transforms are equivalent to simple subband systems. Subband coding is a data-processing technique in which an original signal is transformed into several frequency bands. The classic method involves the use of a bank of digital filters to provide the frequency decomposition followed by decimators to reduce the total number of samples in all bands to the same (or nearly the same) number as the number of samples of the original signal. The low-frequency subband contains a low-resolution version of the original image, while the higher-frequency subbands contain information on edges.

The SUBTRANS functions can be cascaded to provide further decomposition into more subbands. If the cascade is applied to all four of the first-stage subbands (in the case of a four-band decomposition), a uniform structure of sixteen bands is obtained. If the cascade is applied to the low-frequency subband only, an octave structure of seven bands results. SUBTRANS also contains routines for the inverses of the transforms.

SUBTRANS functions can be used in image-data-compression systems. The transforms do not compress data, but they prepare the data for lossy compression by use of quantizer and statistical coders. Sample quantization functions for subbands are included in the software package. In a typical approach to compression of image data, one first transforms the data into subbands, then quantizes the data, then uses statistical coding (e.g., run-length coding followed by Huffman coding) for compression.

The SUBTRANS functions were written for use in the MATLAB mathematical-analysis environment. (MATLAB is available from The MathWorks, Inc.) This software package is compatible with MATLAB 386 running on IBM PC-series and compatible computers; it also works under the UNIX version of MATLAB. An electronic copy of the documentation is provided in WordPerfect 5.1 format. The medium for distribution of this program is a 3.5-in. (8.89-cm), 1.44MB, MS-DOS-format diskette. The contents of the diskette have been compressed by use of the PKWARE archiving software tools. The utility software to unarchive the files, PKUNZIP.EXE v2.04g, is included. This software package was developed in 1992.

* MATLAB is a trademark of The MathWorks, Inc.

This program was written by D. Glover of Lewis Research Center. Further information is contained in a TSP [see page 1].
LEW-15891

Windows Program for Driving the TDU-850 Printer

This program provides WYSIWYG compatibility between the video display and the printout.

PDW is a Microsoft Windows printer-driver computer program for use with the Raytheon TDU-850 printer. PDW provides a previously unavailable linkage between this printer and IBM PC-compatible computers running Microsoft Windows. The PDW enhances the capabilities of the Raytheon TDU-850 hardcopier by emulating all of the textual and graphical features normally supported by laser/ink-jet printers and thereby making this printer compatible with any Microsoft Windows application. The PDW also provides capabilities not found in laser/ink-jet printer drivers by providing certain Windows applications with the ability to render high-quality, true gray-scale photographic hardcopy on the TDU-850.

The user can be assured of a true WYSIWYG ("What you see is what you get") compatibility between the on-screen display of high-end application programs and the final printed images. PDW can be called upon by the Windows Graphical Device Interface (GDI) software to draw graphical objects (circles, lines, etc.) directly via the printer or to render graphical objects via shared memory so that the objects can then be copied to the video screen by screen-driver software. This enables Microsoft Windows, in conjunction with the screen-driver software, to provide maximum WYSIWYG fidelity while a document is being composed whenever PDW is selected.

PDW can reside simultaneously on as many as three separate personal computers attached to a single Raytheon printer by use of the standard IEEE-488 general-purpose interface bus (GPIB) of the printer. PDW contains special software to determine whether other computers are contending for the bus before attempting to gain access to the printer.

PDW is written in C language for IBM PC-series and compatible computers running MS-DOS v4.0 or later and Microsoft Windows v3.0 or later. PDW also requires a National Instruments PC-compatible GPIB board and cable and a Raytheon TDU-850 printer. If it becomes necessary to modify the source code, then a Microsoft Quick C for Windows (or compatible) compiler must be used. The Microsoft UniTool may also be needed if the source code is being completely rewritten for another printer. An electronic copy of the documentation is available on the distribution medium in Microsoft Word for Windows format. The standard medium for distribution of PDW is a set of two 5.25-in. (13.335-cm), 360K MS-DOS-format diskettes. PDW was developed in 1993.

Footnote: The Raytheon TDU-850 hardcopier is a ruggedized, high-quality, gray-scale hardcopying device utilized on the space shuttle, military tanks, submarines, and the like. As purchased it is neither 'PC' or 'Windows' compatible.

This program was written by Brett T. Parrish of Johnson Space Center. Further information is contained in a TSP [see page 1].
MSC-22444

BLANK PAGE

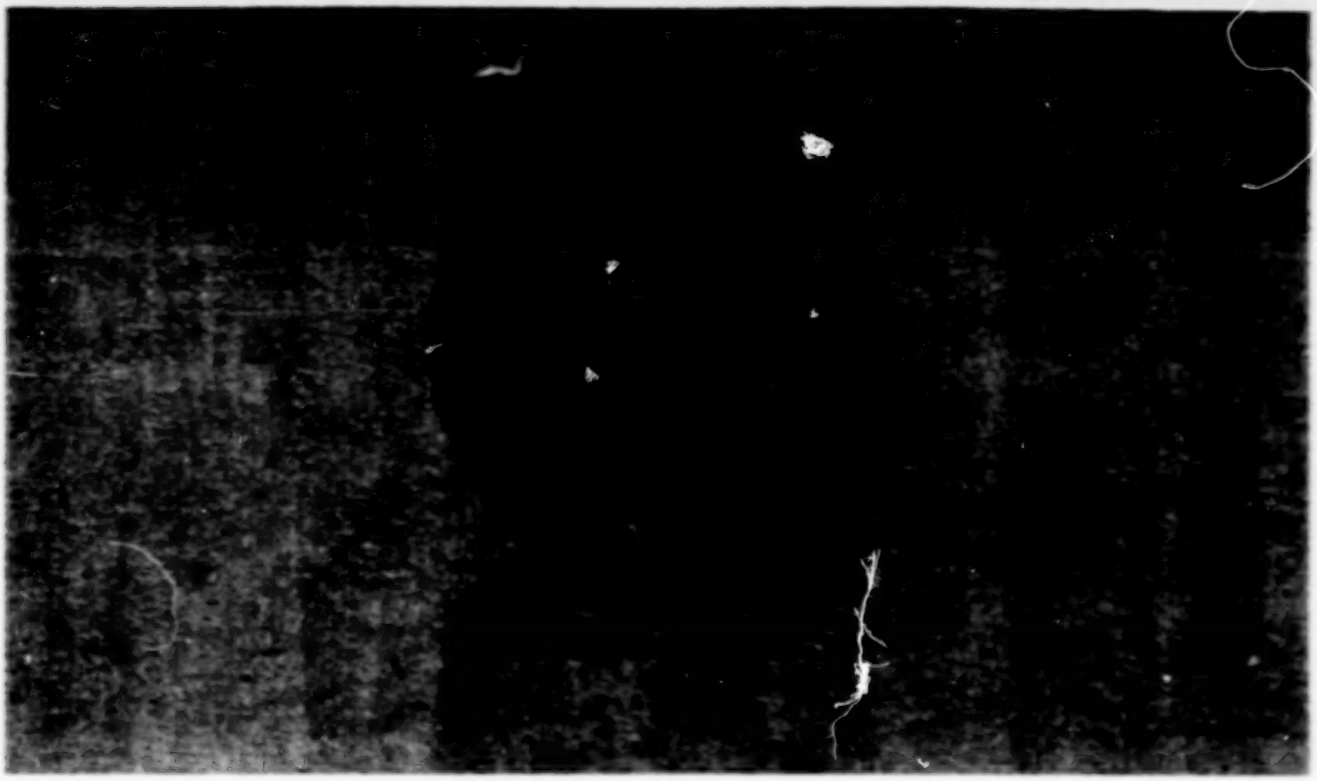

Hardware, Techniques, and Processes

57 Bearing-Mounting Concept Accommodates Thermal Expansion
57 Controlling Mirror Tilt With a Bimorph Actuator
58 Adjustable-Length Strut Withstands Large Cyclic Loads
59 Gravity Slides With Magnetic Braking
59 Parallel-Plate Acoustic Absorbers for Hot Environments
60 Burst-Disk Device Simulates Effect of Pyrotechnic Device
61 Flexseal Insulator Test Assembly
61 Tool Indicates Contact Angles in Bearing Raceways
61 High-Torque, Lightweight, Pneumatically Driven Wrench for Small Spaces
61 Device for Testing Compatibility of an O-Ring

Books and Reports

61 Attitude Control for the Cassini Spacecraft
62 Adaptive Finite-Element Computation in Fracture Mechanics
62 Analytical Model for Fluid Dynamics in a Microgravity Environment
62 Experiments on Vibration-Induced Loosening of Bolts
62 Study of Tracing of Airflow With Neutrally Buoyant Bubbles

Bearing-Mounting Concept Accommodates Thermal Expansion

Pins or splines allow radial expansion without slippage.

Lyndon B. Johnson Space Center, Houston, Texas

A design concept for mounting a rotary bearing accommodates differential thermal expansion between the bearing and any structure(s) to which the bearing is connected. Differential thermal expansion can be significant when, for example, a bearing is made of steel while the inner and outer races of the bearing are connected to housings made of aluminum, which expands at almost twice the rate of steel.

The present design concept prevents the buildup of thermal stresses by allowing thermal expansion to occur freely but accommodating the expansion in such a way as not to introduce looseness. In one version shown in the figure, the bearing races include integral flanges that fit loosely into the inner and outer housings. Each flange includes multiple radial slots just wide enough for a sliding fit with pins in the corresponding housing. Each slot is elongated in the radial direction to accommodate the differential thermal expansion between the bearing and the housing.

The contact between the pins and the edges of the slots ensures that each housing and the corresponding bearing race rotate together. This pin-in-slot configuration also maintains concentricity. In an alternative version, the pins and slots are replaced by mating radial splines, which function similarly.

This work was done by Robert Nespodzany and Toren S. Davis of Honeywell, Inc., for **Johnson Space Center**. *Further information is contained in a TSP [see page 1].*

Title to this invention has been waived under the provisions of the National Aeronautics and Space Act [42 U.S.C. 2457(f)], to Honeywell, Inc. Inquiries concerning licenses for its commercial development should be addressed to

Thomas Randous
Office of General Counsel
Honeywell, Inc.
Honeywell Plaza
P.O. Box 524
Minneapolis, MN 55440-0524

Refer to MSC-22414, volume and number of this NASA Tech Briefs *issue, and the page number.*

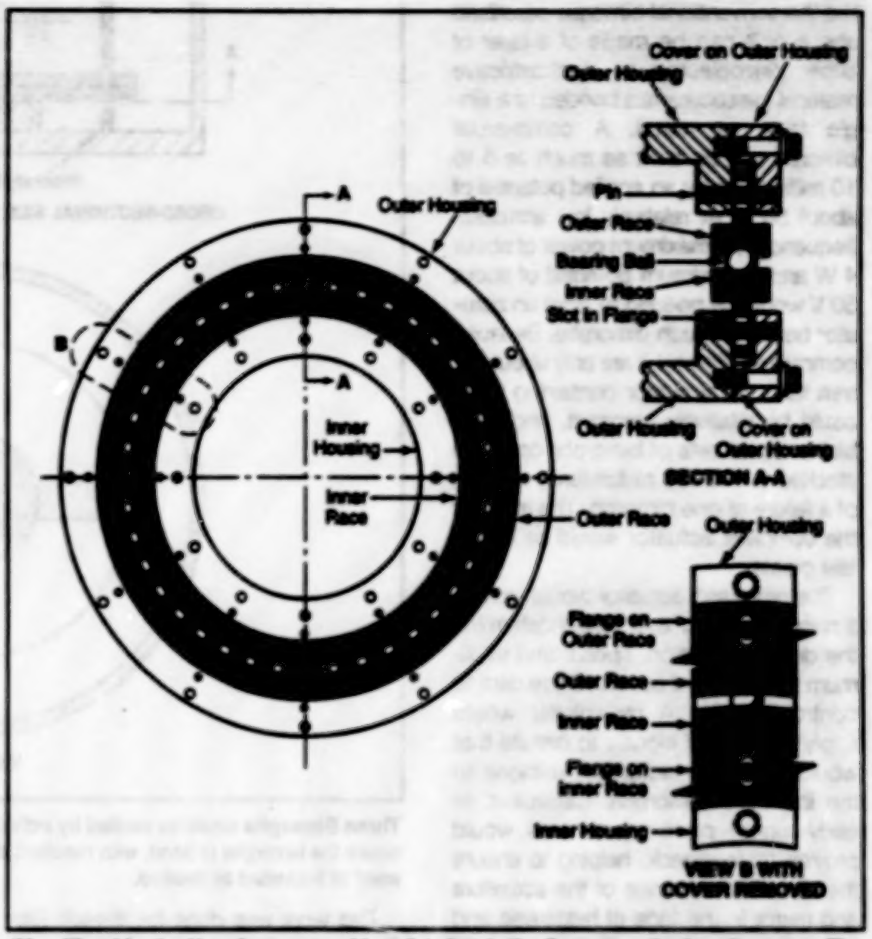

Pins Fixed in the Housings mate with radial slots in the flanges on the bearing races. The mating of pins and slots allows differential thermal expansion while maintaining concentricity.

Controlling Mirror Tilt With a Bimorph Actuator

Advantages would include light weight, small size, and low power.

NASA's Jet Propulsion Laboratory, Pasadena, California

A proposed mirror-tilting actuator would be based on bimorph cells. (A conventional bimorph cell is typically a unit in which two thin plates of piezoelectric material are cemented together so that when a voltage is applied, one plate expands and the other contracts, causing the unit to bend.) The actuator could be used to provide controllable tilt of a mirror in a copy machine or optical scanner, for example. In comparison with other mirror-tilting actuators based on stacks of piezoelectric and/or electrostrictive transducers, this one would be smaller and lighter, and in comparison with some of them, it would demand less voltage and power to produce equivalent tilts.

The figure illustrates the proposed actuator as installed behind a circular mirror. The actuator would include three bimorph cells at equal angular intervals. A separate voltage would be applied to each bimorph; thus, each bimorph could be bent independently of the other two, making it possible to tilt the mirror about either or both of the two perpendicular tilt axes to any angle within range. One end of an actuation pin would be anchored near the free tip of

each bimorph, which would push on the back of the mirror via the pin. The mirror end of each pin would be hemispherical.

Bimorphs are commercially available. A typical commercial bimorph can be like the conventional bimorph described above or it can be made of a layer of either piezoelectric or electrostrictive material (piezoceramic) bonded to a single layer of metal. A commercial bimorph can be bent as much as 6 to 10 milliradians by an applied potential of about 50 V. At relatively low actuation frequencies, a maximum power of about 4 W and a maximum potential of about 50 V would be needed to drive an actuator based on such bimorphs. Because commercial bimorphs are only about 0.5 mm thick, an actuator containing them could be relatively compact, and doublet or triplet sets of bimorphs could be stacked to provide redundancy in case of a failure of one bimorph. The mass of the complete actuator would be only a few grams.

The proposed actuator would include a microprocessor that would determine the desired direction, speed, and maximum tilt angle and convert these data to control signals. A multiplexer would apply the control signals to circuits that would apply the actuation voltages to the individual bimorphs. Capacitive or eddy-current proximity sensors would provide tilt feedback, helping to ensure the accurate response of the actuators and mirror in the face of hysteresis and other variables that could affect actuator performance.

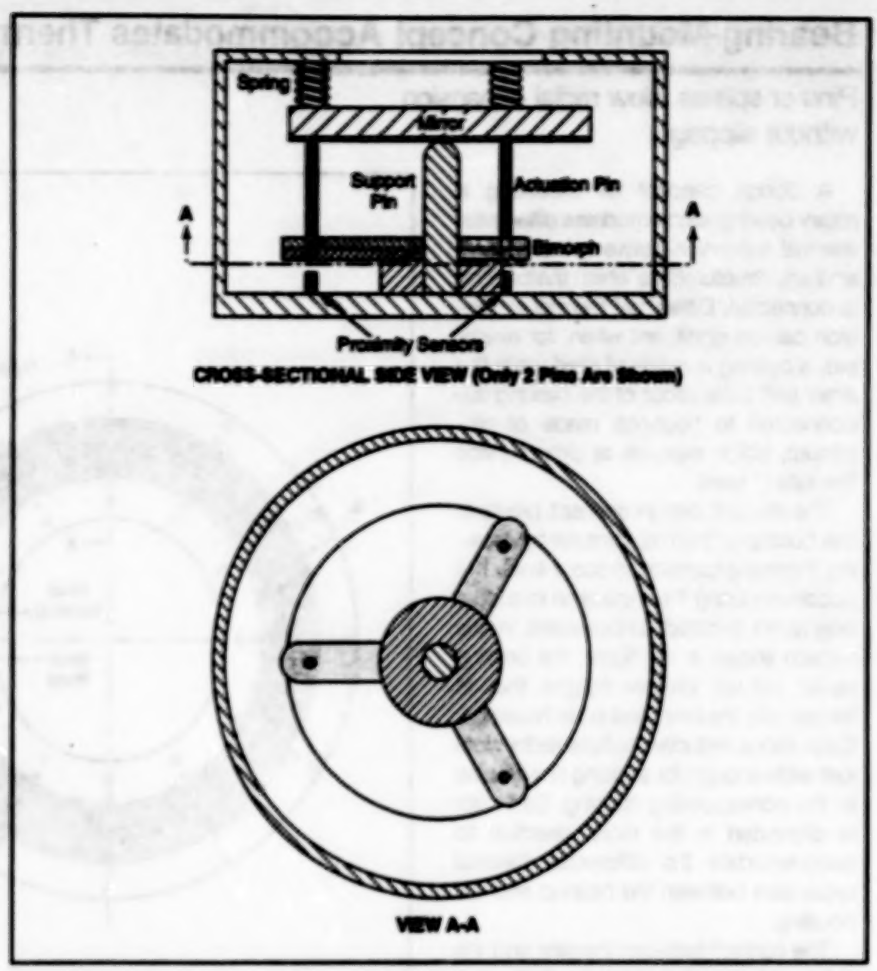

Three Bimorphs would be excited by individually or collectively applied voltages. This would cause the bimorphs to bend, with resultant tilting of the mirror, or translation of the mirror forward or backward as desired.

This work was done by Yoseph Bar-Cohen of Caltech for **NASA's Jet Propulsion Laboratory**. *Further information is contained in a TSP [see page 1].*
NPO-19303

Adjustable-Length Strut Withstands Large Cyclic Loads

Threaded flanges apply preloads larger than could be applied by simple jam nuts.

Lewis Research Center, Cleveland, Ohio

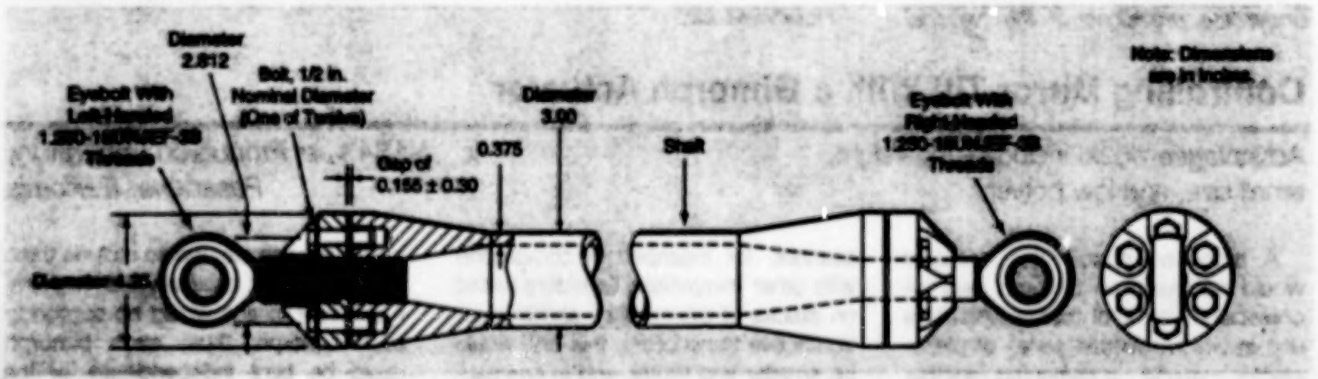

This Adjustable-Length Strut can be highly preloaded to enable it to handle high cyclic tensile and compressive loads.

An adjustable-length strut has been designed especially for installation in a structure in which it will be subjected to large cyclic loads. The strut partly resembles a large turnbuckle: it includes oppositely threaded eyebolts that engage correspondingly threaded holes at opposite ends of a shaft, and the shaft is turned to adjust the length. However, unlike in a turn-

buckle, the length setting is not fixed by use of simple jam nuts: instead, the length setting is fixed by use of more complex threaded-end flanges that partly resemble jam nuts but function somewhat differently.

In the particular situation for which this adjustable-length strut was devised, it is impractical to use jam nuts to apply the large preloads needed to offset the anticipated cyclic loads. However, the threaded end flanges can be made to apply the necessary preloads, by use of moderate assembly torques.

The length of the strut is adjustable in a range of ±1.25 in. (32 mm). Once the strut has been adjusted to the desired length, the threaded end flanges are turned to obtain a gap of 0.125 to 0.185 in. (3.2 to 4.7 mm). Then the six 1/2-in. (12.7-mm) bolts are inserted through clearance holes in each end flange to engage threaded holes in the end of the shaft. These bolts are tightened in a specified pattern, each to a final torque of 58±5 lb-ft (78±7 N-m). At this torque level, the preload is sufficient to withstand tensile and compressive loads as great as 4×10^4 lb (1.8×10^5 N).

This work was done by Fred P. Carner of Rockwell International Corp. for Lewis Research Center. Further information is contained in a TSP [see page 1].
LEW-15761

Gravity Slides With Magnetic Braking

These devices would enable safe emergency escape from tall buildings.

Marshall Space Flight Center, Alabama

Slides with magnetic braking have been proposed to enable safe emergency descent from tall buildings, fire-truck ladders, towers, and the like. The basic physical phenomenon exploited by these devices is one that has been utilized for decades in automotive speedometers, dampers in meters, and coin sorters in vending machines: Sideways motion between a permanent magnet and a nearby nonferromagnetic metallic object induces an electrical current (eddy current) in the object; the eddy current, in turn, gives rise to a magnetic repulsion between the permanent magnet and the nonferromagnetic object. This repulsion consists of a force that tends to push the magnets away from the slide, plus a drag force that opposes the motion and can thus be used for braking.

The figure illustrates an example of an emergency slide according to this concept. The slide would include a sled that would move along a stationary aluminum track tilted against the top of a building. The sled would hold a set of permanent magnets at a preset small distance [typically 1/32 to 1/16 in. (0.8 to 1.6 mm)] from the surface of the track. A passenger would stand on, sit on, or be strapped to a platform on the sled. A release device at the top of the slide would hold the sled in place until the passenger was prepared for descent.

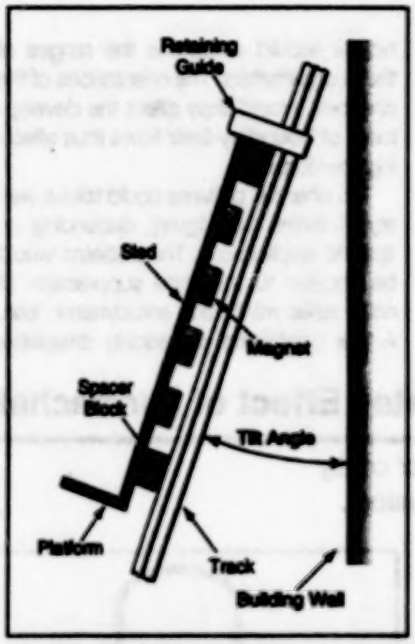

The Sled Would Descend Along the Track, its motion retarded by magnetic drag. The retaining guide would limit any lateral movement of the top of the platform away from the slide, and would keep the slide in place for inclination angles of 30° to 40°. At tilt angles of less than about 30°, additional retaining guides would be needed.

As the sled descended along the track, the magnets would induce electrical currents in the track. The currents and thus the drag force would increase with the speed of descent until equilibrium speed was reached; at this speed, the drag would equal the gravitational force pulling the sled down the track, and thus the speed would not increase beyond this value.

For a given passenger weight, the equilibrium speed would depend on several factors, including the properties of the magnets, the electrical conductivity of the slide, and the distance between the magnets and the track. For example, preliminary calculations and experiments with a scale model indicate that a slide could be designed to enable a passenger who weighs 250 lb (113 kg) to descend at a speed of about 8 ft/s (2.4 m/s). Corrosion of the track would not hinder operation of the slide as long as the electrical conductivity and thickness of the track were not altered significantly.

This work was done by Thomas F. Goodrick of Marshall Space Flight Center. Further information is contained in a TSP [see page 1].
MFS-31072

Parallel-Plate Acoustic Absorbers for Hot Environments

Stacking patterns and materials would be chosen to suppress noise.

Lewis Research Center, Cleveland, Ohio

Acoustic liners that incorporate parallel-plate absorbing elements have been proposed for use in suppressing broadband aerodynamic noise that originates in flows of hot gases in ducts. One potential application lies in suppressing the noise generated in the exhaust-jet mixer/ejectors in the propulsion system of the proposed High-Speed Civil Transport. In addition, such absorbers might be useful in any situation in which high temperature limits the use of such conventional resonant acoustic-liner materials as perforated face sheets bonded to honeycomb-core panels.

Because the parallel-plate liners would exploit viscous dissipation within narrow channels, there would be no need for face sheets. The main reason for using the parallel-plate configuration instead of other configurations is to inhibit the transfer of heat and thus

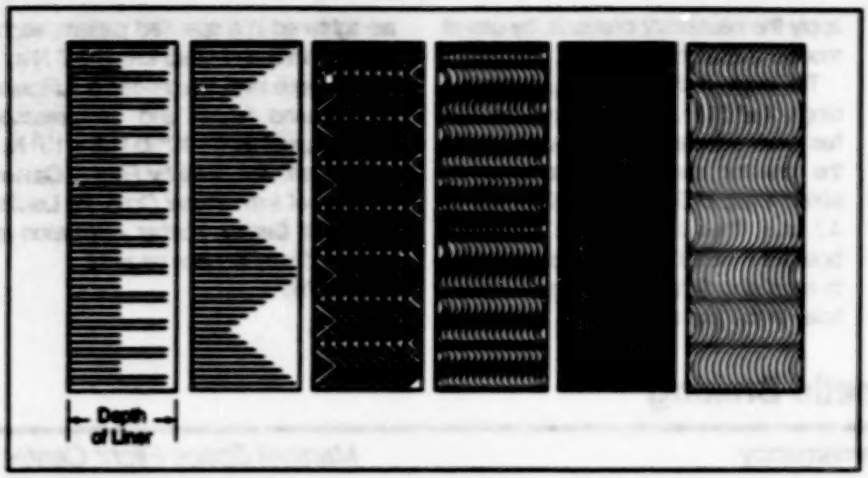

Shapes of Noise-Suppression Channels could range from sharply angled linear patterns to gently undulating waves.

inhibit the degradation of materials at high temperatures.

The absorption efficiency and frequency response would depend on a number of parameters, including (but not limited to) the widths and depths of the channels, the porosity (in terms of the fraction of total volume occupied by the channels), surface textures, and the total internal channel-surface area per unit volume of liner. Materials and fabrication techniques would determine the ranges of these parameters. The orientations of the channels would likely affect the development of boundary-layer flows thus affecting flow losses.

The channel patterns could take a variety of forms (see figure), depending on specific applications. The patterns would be chosen to maximize suppression of noise while minimizing aerodynamic loss. A liner containing acoustically dissipative channels could be constructed, for example, by stacking many cast plates in the required orientation(s) with respect to the wall of a duct. The plates could be straight or curved, smooth or rough, and dense or porous, depending on the application. The plates could be joined by any of a variety of methods, such as brazing, diffusion bonding, or using fasteners. The plate material would be selected to suit the noise to be suppressed as well as the velocity, temperature, and chemical species of the flowing gas. Some of the most desirable materials, although brittle, are readily cast into plates and thus are well suited to service in liners of this type.

This work was done by Joseph Doychak of **Lewis Research Center** *and Tony L. Parrott of Langley Research Center. Further information is contained in a TSP [see page 1].*

This invention has been patented by NASA (U.S. Patent No. 5,250,764). Inquiries concerning nonexclusive or exclusive license for its commercial development should be addressed to the Patent Counsel, Lewis Research Center [see page 1]. Refer to LEW-15430.

Burst-Disk Device Simulates Effect of Pyrotechnic Device

Expendable disks are substituted for costly pyrotechnic devices for testing actuators.

Lyndon B. Johnson Space Center, Houston, Texas

A burst-disk device produces a rush of pressurized gas similar to that produced by a pyrotechnic device. The burst-disk device was designed to reduce the cost of testing pyrotechnically driven emergency actuators (parachute-deploying mechanisms in the original application). The cost of replacing burst disks is much less than that of replacing pyrotechnic devices.

The device consists of a pressure chamber and associated plumbing (see figure). The chamber includes two burst disks; an upstage disk and a downstage disk, both designed to burst at a pressure of 3,569.50 psi (24.611 MPa). The space upstream of the upstage disk is connected via a wide pipe to a tank, which acts as a buffer or reservoir that supplies the rush of pressurized gas to the actuator when the device is operated. The space downstream of the downstage disk is connected via a pipe to the actuator that is to be driven by the rush of pressurized gas.

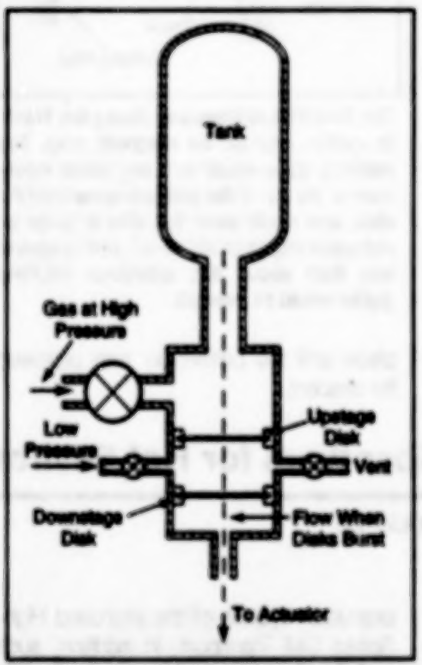

The Upstage and Downstage Disks Burst in rapid succession when the pressurized gas in the space between them is vented. The resulting sudden flow of pressurized gas drives the actuator.

Initially, the space between the disks is pressurized with the gas to 700 psi (4.8 MPa). Then the space upstream of the upstage disk is pressurized with the gas to 4,000 psi (27.6 MPa). Once the pressure has settled to a steady value, the differential pressure across the upstage disk is then 3,300 psi (22.8 MPa) — somewhat below the bursting pressure.

At the time for testing, the gas is vented slowly from the space between the disks, making the pressure across the upstage disk rise toward the upstream pressure of 4,000 psi (27.6 MPa). Eventually, this pressure exceeds the bursting pressure, causing the upstage disk to burst. The sudden rush of high-pressure gas immediately bursts the downstage disk and flows to the actuator.

This work was done by James P. Rogers and James H. Sexton of Rockwell International Corp. for **Johnson Space Center.** *Further information is contained in a TSP [see page 1].*
MSC-22407

Flexseal Insulator Test Assembly

A small-scale version of a solid-fuel rocket motor flexseal nozzle bearing assembly that can be instrumented and tested in a compression-testing fixture simulating conditions during rocket motor operation is described in a report. Flexseal bearing assembly is a structure used to attach a vectorable nozzle to a solid-fuel rocket motor case. This small-scale version includes a flexseal core and a flexseal insulator, each of which consists of three rubber pads between two shims and two steel endrings. The core and insulator shims are made of mild steel and tape wrapped with carbon-cloth phenolic, respectively. The core and insulator are assembled with a rubber buffer pad between them. By simultaneously compressing the assembly while orienting it at various angles, one produces strain fields in the assembly, similar to the strain fields expected in a full-scale version of the assembly. By measuring these strains and comparing them with theoretical predictions, one can calibrate structural models for the geometry and loading conditions of the fixture.

This work was done by Eric Buchanan of Thiokol Corp. for Marshall Space Flight Center. Further information is contained in a TSP [see page 1].
MFS-28911

Tool Indicates Contact Angles in Bearing Raceways

A tool has been devised for use in measuring contact angles between balls and races in previously operated ball bearings. The tool can be used on both inner and outer raceways of bearings that have cross-sectional widths between approximately 0.5 and 2.0 in. (12.7 and 50.8 mm). The tool consists of an integral protractor mounted in a vertical plane on a bracket equipped with leveling screws and a circular level indicator. The protractor includes a rotatable indicator needle and a set of disks of various sizes to fit various raceway curvatures. A disk with the radius of the raceway to be inspected is installed on the tool, and the tool is leveled on a flat surface. The tool is placed against the bearing raceway with the disk centered in the raceway. The indicator is rotated to the contact path marked on the raceway by the balls; this path indicates the contact angle to be measured, and the angle is simply read from the position of the indicator on the protractor scale. The measured angle can then be related to the load experienced by the bearing in service.

This work was done by Richard A. Aklan and Myles F. Buhner of Rockwell International Corp. for Marshall Space Flight Center. Further information is contained in a TSP [see page 1].
MFS-30012

High-Torque, Lightweight, Pneumatically Driven Wrench for Small Spaces

A pneumatically driven wrench can provide torque up to 3,000 lb-ft (=4 kN-m) in a small space. The head is designed to reach into a 2.6 × 2.75 × 6 in. (6.6 × 7.0 × 15.2 cm) pocket. The wrench weighs approximately 25 lbs (11.4 kg). The torque wrench includes a reversible pneumatic motor (an electric motor could be used instead) and a slip clutch. The wrench also includes a device that indicates the total angle through which the wrench has turned a bolt or nut. This feature can be used for a turn-of-the-nut tightening method.

This work was done by Thomas W. Miller of Kennedy Space Center. Further information is contained in a TSP [see page 1].
KSC-11731

Device for Testing Compatibility of an O-Ring

A fixture has been designed for use in exposing a compressed elastomeric O-ring or other ring seal to a test fluid. The fixture can be made of metal or plastic, with a threaded recess into which an O-ring can be placed. Opposite the threaded end is an opening through which a test fluid can be introduced and placed in contact with the O-ring. After exposure, the compression set and swell or shrinkage of the ring can be measured. The fixture can be set to compress the ring by a selected amount (usually, 25 percent), providing for reproducible compression.

This work was done by Dennis D. Davis of Lockheed Engineering and Sciences Co. for Johnson Space Center. Further information is contained in a TSP [see page 1].
MSC-22504

Books and Reports

Attitude Control for the Cassini Spacecraft

A report discusses design concepts for attitude control of the Cassini spacecraft, which is scheduled to be launched in 1997 and to arrive at Saturn in 2004. The mission requires accurate pointing and complex maneuvering of the spacecraft, which comprises a Saturn orbiter and a probe that will be detached from the orbiter and launched into the atmosphere of Titan (one of the moons of Saturn). The control architecture described in the report is hierarchical, modular, and object-oriented. The control design will provide thrust-vector control and precise high-stability pointing for scientific instruments; tracking of the probe after release at Titan; and radar mapping of the surface of Titan. Additional constraints for the control design have been imposed by sloshing liquid propellant (which constitutes 60 percent of the mass of the spacecraft at launch) and by low damping of vibrations of flexible spacecraft appendages. Results of computer simulations of attitude determination, pointing, and maneuver control are provided to demonstrate the capabilities of the design.

This work was done by Edward C. Wong, William G. Breckenridge, Robert Rasmussen, and Douglas E. Bernard of Caltech for NASA's Jet Propulsion Laboratory. To obtain a copy of the report, "An Attitude Control Design for the Cassini Spacecraft," see TSP's [page 1].
NPO-19674

Adaptive Finite-Element Computation in Fracture Mechanics

A report discusses recent progress in the use of solution-adaptive finite-element computational methods to solve two-dimensional problems in linear elastic fracture mechanics. A solution-adaptive method is described and used to compute stress-intensity factors of two-dimensional cracks with predetermined locations and loading conditions. The method is tested on demonstration problems and shown to yield results in reasonable agreement with those computed by an alternative theoretical method. The method is also shown to be extensible to three-dimensional problems.

This work was done by J. B. Min of **Marshall Space Flight Center**, *J. M. Bass of Computational Mechanics Co., and L. W. Spradley of ResearchSouth, Inc. To obtain a copy of the report, "Adaptive Finite Element Methods For Two-Dimensional Problems In Computational Fracture Mechanics," see TSP's [page 1].*

Inquiries concerning rights for the commercial use of this invention should be addressed to the Patent Counsel, Marshall Space Flight Center [see page 1]. Refer to MFS-26314.

Analytical Model for Fluid Dynamics in a Microgravity Environment

A report presents an analytical approximation methodology for providing coupled fluid-flow, heat, and mass-transfer equations in a microgravity environment. Experimental engineering estimates accurate to within a factor of 2 can be made quickly and easily, thus eliminating the need for time-consuming and costly numerical modeling. Any proposed experiment can be reviewed to see how it would perform in a microgravity environment. The fluid-flow, heat, and mass-transport rates can be used to optimize performance of an experiment within the microgravity environment. The model can be applied in a commercial setting for preliminary design of low-Grashoff/Rayleigh-number experiments. The effects of axial and transverse magnetic fields are also included, which apply to terrestrial processes if the Hartmann number is large.

This work was done by Robert J. Naumann of The University of Alabama in Huntsville for **Marshall Space Flight Center**. *To obtain a copy of the report, "Studies for USML-1: Glovebox Demonstrations," see TSP's [page 1].*

Inquiries concerning rights for the commercial use of this invention should be addressed to the Patent Counsel, Marshall Space Flight Center [see page 1]. Refer to MFS-26355.

Experiments on Vibration-Induced Loosening of Bolts

Design parameters that could affect loosening were evaluated for relative importance.

A report describes an experimental study of loosening of bolts in the presence of vibrations. Eleven design parameters that were considered likely to affect the tendency to loosen were evaluated for relative importance. These parameters were the bolt diameter, lubrication on the bolt, lubrication on mating materials, bolt-hole tolerance, preload, nut-locking device, grip length, thread pitch, class of fit, joint configuration, and mass of configuration. Bolts were tested in vibration for two values of each design parameter. The most significant parameters were found to be the type of nut-locking device, the joint configuration, bolt diameter, and the mass of the configuration; larger bolts resist loosening better than smaller bolts do, and transverse loading is much more detrimental to maintenance of bolt tightness than is axial loading.

This work was done by G. Ed Ramey and Robert C. Jenkins of Auburn University for **Marshall Space Flight Center**. *To obtain a copy of the report, "Experimental Analysis of Thread Movement in Bolted Connections Due to Vibrations," see TSP's [page 1].*

MFS-27325

Study of Tracing of Airflow With Neutrally Buoyant Bubbles

Such bubbles can be used to trace complex flows.

A report describes a study of the use of neutrally buoyant bubbles to make airflows visible. The equation of motion for a single bubble was derived and evaluated by use of a computational scheme to determine the factors that affect the trajectory of a bubble, particularly with respect to the degree to which bubble trajectories adhere to or deviate from flow-field streamlines. A two-dimensional-flow experiment was conducted, using an airfoil in a wind tunnel at 0° angle of attack along with a commercial bubble generator that made specially formulated soap bubbles containing helium. The bubble trajectories in the stagnation region of the airfoil were measured and compared with trajectories predicted by the computational scheme for bubbles of various sizes and densities. A bubble-tracing experiment was also conducted on the three-dimensional flow about a 30° swept semispan wing with simulated glaze ice, and the results of this experiment were compared with those of Navier-Stokes calculations of the flow and of a surface-oil-flow-visualization experiment. The conclusion drawn from the theoretical and computational parts of the study is that neutrally buoyant bubbles can trace even the most complex flow patterns. The conclusion reached from the experimental part of the study is that it is difficult to produce neutrally buoyant bubbles and, therefore, the use of bubbles to trace airflows should be limited to qualitative observations unless care is taken to ensure neutral buoyancy.

This work was done by Michael F. Kerho of the University of Illinois for **Lewis Research Center**. *To obtain a copy of the report, "A Study of the Accuracy of Neutrally Buoyant Bubbles Used as Flow Traces in Air," see TSP's [page 1].*

LEW-16085

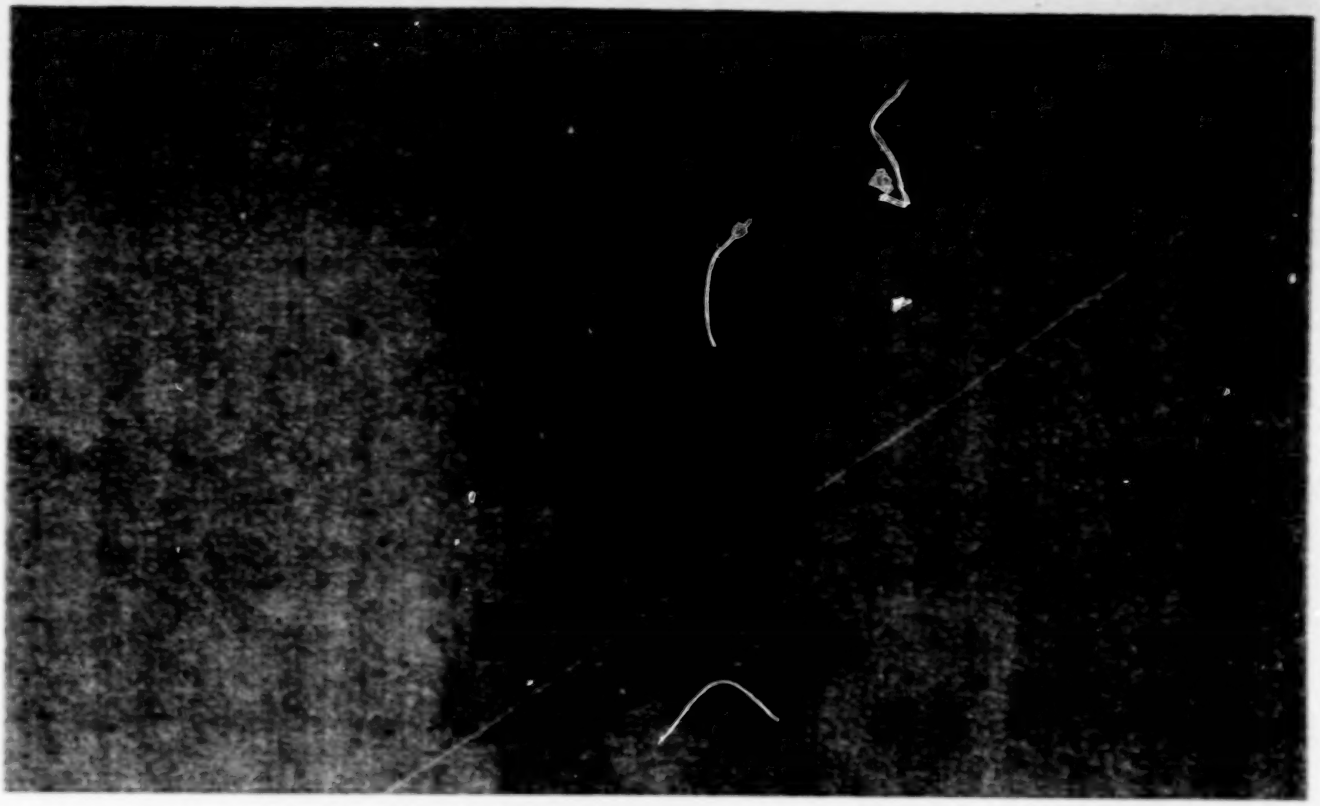

Hardware, Techniques, and Processes

65 Magnetic Heat Pump Containing Flow Diverters
66 "Beach-Ball" Robotic Rovers
66 Variable-Tilt Helicopter Rotor Mast
67 Apparatus Would Measure Temperatures of Ball Bearings

Books and Reports

67 Thermal Strap Increases Cryocooling Efficiency
68 Research in Diagnosing Bearing Defects From Vibrations
68 Control Algorithms for Kinematically Redundant Manipulators
68 Further Study of Face Gears for Helicopter Transmissions
68 Reversible Nut With Engagement Indication
68 Computed Hydrogen-Flow Splits in a Rocket Engine

BLANK PAGE

Magnetic Heat Pump Containing Flow Diverters

Flows that mix heated and cooled fluid would be suppressed.

John F. Kennedy Space Center, Florida

A proposed magnetic heat pump would contain flow diverters for suppression of undesired flows. If left unchecked, these undesired flows would mix substantial amounts of partially heated and partially cooled portions of a working fluid, effectively causing leakage of heat from the heated side to the cooled side. By reducing the leakage of heat, the flow diverters would increase the energy efficiency of the magnetic heat pump, which potentially offers an efficiency greater than that of a compressor-driven refrigerator.

In a magnetic heat pump of the type in question, a magnetic rotor would play a role analogous to that of the compressor in a compressor-driven heat pump. The outer surface of the rotor would include circumferential channels lined with, and separated by, walls and partitions containing a magnetic material. As shown in the figure, pumps would circulate the working fluid between heated-side and cooled-side heat exchangers. These pumped flows would be coupled into and out of the circumferential channels of the rotor via stationary ports in a housing in which the rotor turned.

The direction of rotation of the rotor would be opposite the intended direction of the pumped flows. At one location in its circumferential travel (between points 4 and 3 in the figure), the magnetic material would pass through a magnetic field, which would align magnetic moments of electrons in the magnetic material and thereby heat the electrons. The heat thus generated would be transferred to the rest of the magnetic material and then to the working fluid flowing toward the heated-side heat exchanger. The heated-side heat exchanger would transfer heat to the environment on that side.

When the magnetic material left the magnetic field at point 3, the freeing of the magnetic moments of the electrons would cool the magnetic material; because this magnetic cooling would occur immediately after the transfer of heat to the fluid during travel through the magnetic field, the magnetic material would emerge from the magnetic field cooler than it was before it entered the magnetic field. Continued rotation would carry the cooled magnetic material through the region between points 2 and 1, where it would cool the working fluid flowing toward the cooled-side heat exchanger. In the cooled-side heat exchanger, the working fluid would absorb heat from the environment on that side. From there, the fluid would flow into the rotor at point 3, then enter the portion of the rotor in the magnetic field, completing the magnetic heat-pump cycle.

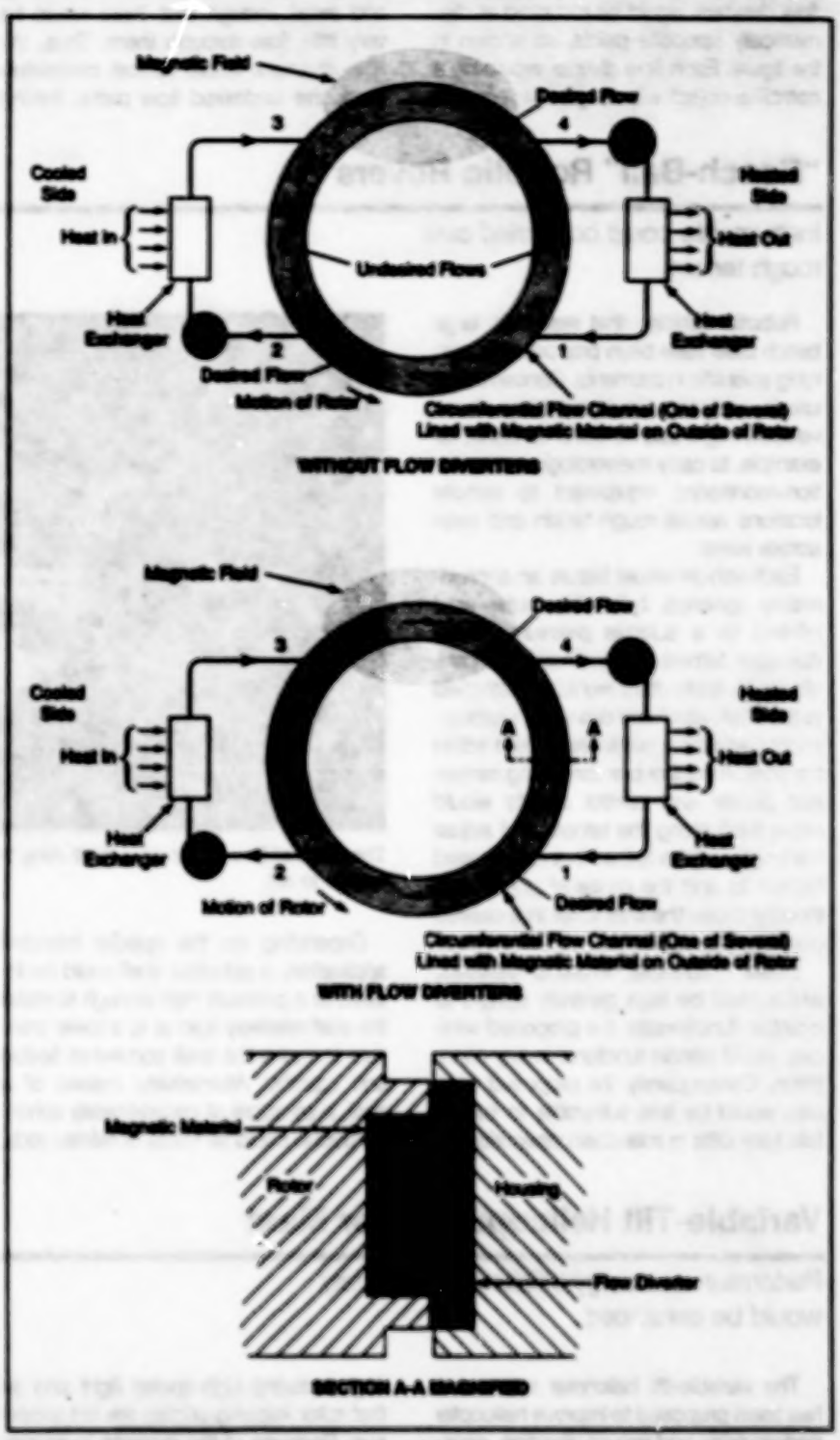

The Flow Diverters would concentrate most of the flow of the working fluid into the long outer loop, minimizing the undesired flow along the short paths from point 2 to point 3 and from point 1 to point 4, respectively.

In the absence of flow diverters, there would be spurious flows along two paths

BEST COPY AVAILABLE

through the rotor: from point 2 to point 3, bypassing the cooled-side heat exchanger; and from point 1 to point 4, as part of a short circuit through the heated-side heat exchanger. Accordingly, two flow diverters would be mounted at diametrically opposite points, as shown in the figure. Each flow diverter would be a combike object with tangs that would fit most of the cross sections of the circumferential channels in the rotor. The gaps between the flow diverters and the walls of the channels would be just large enough to allow the rotor to turn freely, and small enough that there would be very little flow through them. Thus, the flow diverters would almost completely block the undesired flow paths, forcing most of the fluid to follow the desired long path through both heat exchangers and the rotor.

This work was done by Frank S. Howard of Kennedy Space Center. Further information is contained in a TSP [see page 1].
KSC-11622

"Beech-Ball" Robotic Rovers

Instruments could be carried over rough terrain.

NASA's Jet Propulsion Laboratory, Pasadena, California

Robotic vehicles that resemble large beach balls have been proposed for carrying scientific instruments. Conceived for use in exploring the planet Mars, these vehicles might also be useful on Earth; for example, to carry meteorological or pollution-monitoring equipment to remote locations across rough terrain and even across water.

Each vehicle would feature an approximately spherical balloonlike outer shell inflated to a suitable pressure. Three diametral tethers approximately perpendicular to each other would be attached to the shell, effectively defining an approximate Cartesian coordinate system within the shell. A control box containing motors and power and control circuits would move itself along the tethers and adjust the lengths of the tethers in a coordinated fashion to shift the center of gravity and thereby cause the shell to roll in a desired direction (see figure).

Unlike traditional wheeled vehicles, which must be kept generally upright to maintain functionality, the proposed vehicles would remain functional in any orientation. Consequently, the proposed vehicles would be less vulnerable to loss in falls from cliffs or rolls down steep slopes.

The Control Box would move itself along the tethers to shift the center of gravity, causing the vehicle to roll.

Depending on the specific intended application, a spherical shell could be inflated to a pressure high enough to make the shell relatively rigid or to a lower pressure to make the shell somewhat flexible and squishy. Alternatively, instead of a shell, a structure of approximately spherical outline could be made of twisted rods; of course, this structure would not be suitable for traversing water or thick vegetation.

This work was done by David E. Smyth of Caltech for NASA's Jet Propulsion Laboratory. Further information is contained in a TSP [see page 1].
NPO-19272

Variable-Tilt Helicopter Rotor Mast

Performance, energy efficiency, and safety would be enhanced.

Langley Research Center, Hampton, Virginia

The variable-tilt helicopter rotor mast has been proposed to improve helicopter performance and reduce vibration, especially at the upper end of the forward-speed range of helicopters (above 140 knots (21.2 m/s)). Heretofore, the main rotor masts of most helicopters have been tilted forward at fixed angles, usually about 5°, so that the noses of the fuselages do not tilt downward at excessive angles during high-speed flight and so that rotor flapping angles are not excessive. Because of the increase in speeds attainable by newer helicopters, the extreme nose-down attitudes cause drag and download losses and, consequently, a need for more power.

The fixed forward tilt of the mast in a helicopter also necessitates a nose-high hover attitude, which is generally undesirable; for example, if the mast is tilted 5° forward, then the hover attitude for the pilot in the fuselage is 5° nose up. Thus, the increase in attainable speed makes it increasingly difficult to operate a fixed-tilt-mast helicopter at a satisfactory attitude over the entire range of velocities and other flight conditions; the selection of a fixed mast tilt becomes a design compromise between the angle needed in

BEST COPY AVAILABLE

forward cruise and the undesirable nose-up attitude in hover.

Designing a helicopter to incorporate a variable-tilt mast would make it possible to optimize the tilt for each flight condition; in particular, variable forward tilt to reduce the power needed by reducing aerodynamic drag and download and to reduce rotor vibratory loads via a decrease in the rotor flapping angle (the angle between the plane of the rotor-tip path and the axis of the mast). Variable lateral tilt of the main rotor mast could be used to balance the tail-rotor thrust and the aerodynamic side forces on the fuselage. Variable tilt would also contribute to safety by reducing the extreme nose-up angles that cause loss of visibility to pilots.

The tilt could be varied by use of a universal coupling in the main rotor mast and hydraulic or electric actuators connected to the mast between the main rotor and the coupling. Additional actuators could be used for redundancy or for additional variable tilt in other planes (e.g., lateral tilt). Tilt could be controlled manually, or else automatically with manual override. In automated control, sensors would detect the operational state of the helicopter and, in response to the sensor outputs, the actuators would be commanded to tilt the mast to the angle that yielded the best combination of fuselage attitude and flapping angle. Manual override of automated tilt control would be made available to enable the pilot to respond to system failures and other special conditions.

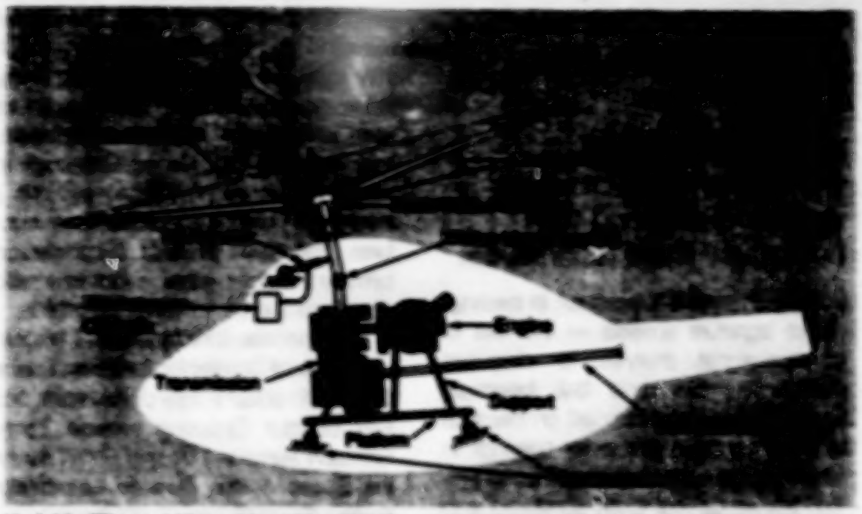

Variable Tilt could be achieved by use of a universal coupling in the main rotor mast or by tilting the entire engine-and-transmission platform.

According to an alternative variable-tilt concept, the main rotor mast would remain fixed and the entire engine-and-transmission platform would be tilted. In this case, the tail-rotor drive shaft would have to be designed to accept the tilt, inasmuch as the tail rotor is driven by the main transmission.

This work was done by Henry L. Kelley of the U. S. Army Aeroflight Dynamics Directorate at Langley Research Center. No further documentation is available.
LAR-13779

Apparatus Would Measure Temperatures of Ball Bearings

A rig for testing ball bearings under radial and axial loads and measuring their surface temperatures is undergoing development. The information to be obtained by this rig could be important because operating surface temperatures can affect the service lives of bearings. The rig includes extensible thermocouples: by means of bellows as longitudinal positioners, the thermocouples would be driven into contact with the bearing balls to sense their temperatures immediately after a test run. Unlike in the cases of some other bearing-testing rigs, it would not be necessary to disassemble the rig or to section the balls to obtain indirect indications of (discolorations) of maximum temperatures reached. The thermocouple measurements would also indicate temperatures better than do temperature-sensitive paints.

This work was done by John C. Gibson and Thomas H. Fredricks of Marshall Space Flight Center. Further information is contained in a TSP [see page 1].
MFS-31067

Books and Reports

Thermal Strap Increases Cryocooling Efficiency

Power needed for cooling can be reduced.

A report discusses a concept for decreasing the compressor power consumed by a spacecraft mechanical cryocooler that provides 0.5 W of refrigeration at a temperature of 61 K at the tip of a cold finger. The concept involves connecting a thermal strap between (1) a radiator or other heat sink at an intermediate temperature (e.g., 150 K) and (2) a stiffening ring that is located on the cold finger about one-third the way from the base to the tip and that attains a temperature of about 250 K during normal operation. Thermal conduction along the strap from the stiffening ring to the radiator diverts some of the parasitic heat load from the cold finger, reducing the parasitic heat that reaches the tip and thereby reducing the power needed to cool the tip. Because of fundamental thermodynamic considerations that affect cooling efficiency, the amount of power saved can greatly exceed the diverted thermal power. Depending upon the specific design, the electrical power consumed by the mechanical cryocooler could be reduced by as much as half.

This work was done by Ronald G. Ross, Jr., and Dean L. Johnson of Caltech, and Kenneth E. Green of Loral for NASA's Jet Propulsion Laboratory. To obtain a copy of the report, "Cryocooler Coldfinger Heat Interceptor," see TSP's [page 1].
NPO-19396

Research in Diagnosing Bearing Defects From Vibrations

Advanced nonlinear signal-analysis techniques were applied along with customary linear techniques.

A report describes research in bearing-defect signature analysis — the use of vibration-signal analysis to diagnose defects in roller and ball bearings. Experiments were performed on bearings in good condition and other bearings in which various parts were scratched to provide known defects to be correlated with vibration signals. The experiments were performed on a highly instrumented motor-driven rotor assembly at speeds up to 10,050 r/min (167.5 Hz), using accelerometers, velocity probes, and proximity sensors mounted at various locations on the assembly to measure vibrations. An acoustic-emission probe was also used to obtain sensitivity to vibrations at frequencies into the megahertz range, where signals are relatively uncontaminated by the structural, rotordynamic, and environmental noise that typically floods traditional sensors at lower frequencies. The various sensor outputs were digitized and characterized by both conventional linear signal-analysis techniques (e.g., power-spectral-density analysis) and advanced nonlinear signal-analysis techniques (e.g., bicoherence analysis). Traditional low-frequency (< 20 kHz) analysis and high-frequency envelope analysis of both accelerometer and acoustic-emission data were used to recover characteristic bearing-distress information buried deeply within the recorded signal data.

This work was done by T. Zolcik, E. Earhart, and T. Rorrudi of **Marshall Space Flight Center.** *To obtain a copy of the report, "Bearing Defect Signature Analysis Using Advanced Nonlinear Signal Analysis in a Controlled Environment," see TSP's (page 1).*
MFS-27326

Control Algorithms for Kinematically Redundant Manipulators

A report presents improved algorithms for controlling kinematically redundant robotic manipulators. Some other algorithms for control of redundant manipulators do not produce unique configurations for each end-effector position. In some cases, the configuration of a robot depends on the trajectory of the end effector, and on whether the robot is going forward or backward along the trajectory; this complicates operation and programming of the robot. The improved algorithms described in the report produce a unique configuration for each end-effector location. Furthermore, they generally produce configurations in which there is no interference between a robot boom and the payload or base structures. The report presents a comparison between various other robot-kinematic algorithms and the improved algorithms.

This work was done by David R. Wagner of McDonnell Douglas for **Johnson Space Center.** *To obtain a copy of the report, "An End Effector Opposing Inverse Transformation Function (ITF) and Rate Law for the Space Station Remote Manipulator System (SSRMS)," see TSP's (page 1).*
MSC-22313

Further Study of Face Gears for Helicopter Transmissions

Feasibility was demonstrated theoretically and experimentally.

A document describes theoretical, computational, and experimental studies of the feasibility of proposed lightweight, split-torque helicopter transmissions based on face gears. [The majority of the work described in the document was also described in a prior document that was the subject of "Face Gears for Helicopter Transmissions" (LEW-15840), *NASA Tech Briefs*, Vol. 18, No. 9 (September, 1994), page 130.] The studies concentrated largely on a specific conceptual split-torque face-gear transmission. Topics include finite-element analysis of a conceptual transmission (including effects of elasticity), the influence of eccentricity of gears, the basic design and geometry of face gears, analysis of contact between gear teeth, limiting inner and outer radii, and experimental tests of face gears. With respect to transmission errors, the conceptual transmission was found to be relatively insensitive to misalignment of gears, but gear-tooth contact was found to be affected by misalignment. A method of localizing the bearing contact to enable operation with misalignment was explored. The proper choice of shaft stiffness was found to enable favorable load sharing in the conceptual split-torque transmission. Two methods of generating face-gear teeth by grinding were investigated. Experiments demonstrated the feasibility of face gears in high-speed, high-load applications like those of helicopter transmissions.

This work was done by F. L. Litvin and J.-C. Wang of the University of Illinois at Chicago; R. B. Bossler, Jr., of Lucas Western, Inc.; Y.-J. D. Chen and G. Heath of McDonnell Douglas Helicopter Co.; and D. G. Lewicki of the Vehicle Propulsion Directorate of the U. S. Army Research Laboratory for **Lewis Research Center.** *To obtain a copy of the report, "Face-Gear Drives: Design, Analysis, and Testing for Helicopter Transmission Applications," see TSP's (page 1).*
LEW-16193

Reversible Nut With Engagement Indication

A document describes a nut that allows a fastener to be inserted or removed from either side by simply sliding the fastener in or out. Detents on each face of the nut, when pushed in, ensure positive engagement of the threads. This is followed by conventional clockwise turning to lock and counterclockwise turning to unlock the nut. The detents, when viewed, will show whether the nut is in a positive lock.

This work was done by Jay M. Wright of **Johnson Space Center.** *Further information is contained in a TSP (see page 1).*

This invention has been patented by NASA (U.S. Patent No. 5,118,237). Inquiries concerning nonexclusive or exclusive license for its commercial development should be addressed to the Patent Counsel, Johnson Space Center (see page 1). Refer to MSC-21799.

Computed Hydrogen-Flow Splits in a Rocket Engine

A report presents a study of flows of hydrogen (as both a coolant and a fuel) along various paths in the fuel injector of a rocket engine. The study included computational simulations of the flows. The computer program used in the study simultaneously solves for the flows along the various flow paths and determines the coolant pressure and hot-gas pressures in the injector. Injectors of various geometries can be modeled. The computer model implements equations of one-dimensional, steady, incompressible flow, with a standard correlation for the friction factor as a function of the Reynolds Number and surface roughness.

This work was done by W. Dennis Ramine of Rockwell International Corp. for **Marshall Space Flight Center.** *To obtain a copy of the report, "Computer Model For Determining SSME Main Injector Coolant Flow Splits," see TSP's (page 1).*
MFS-30024

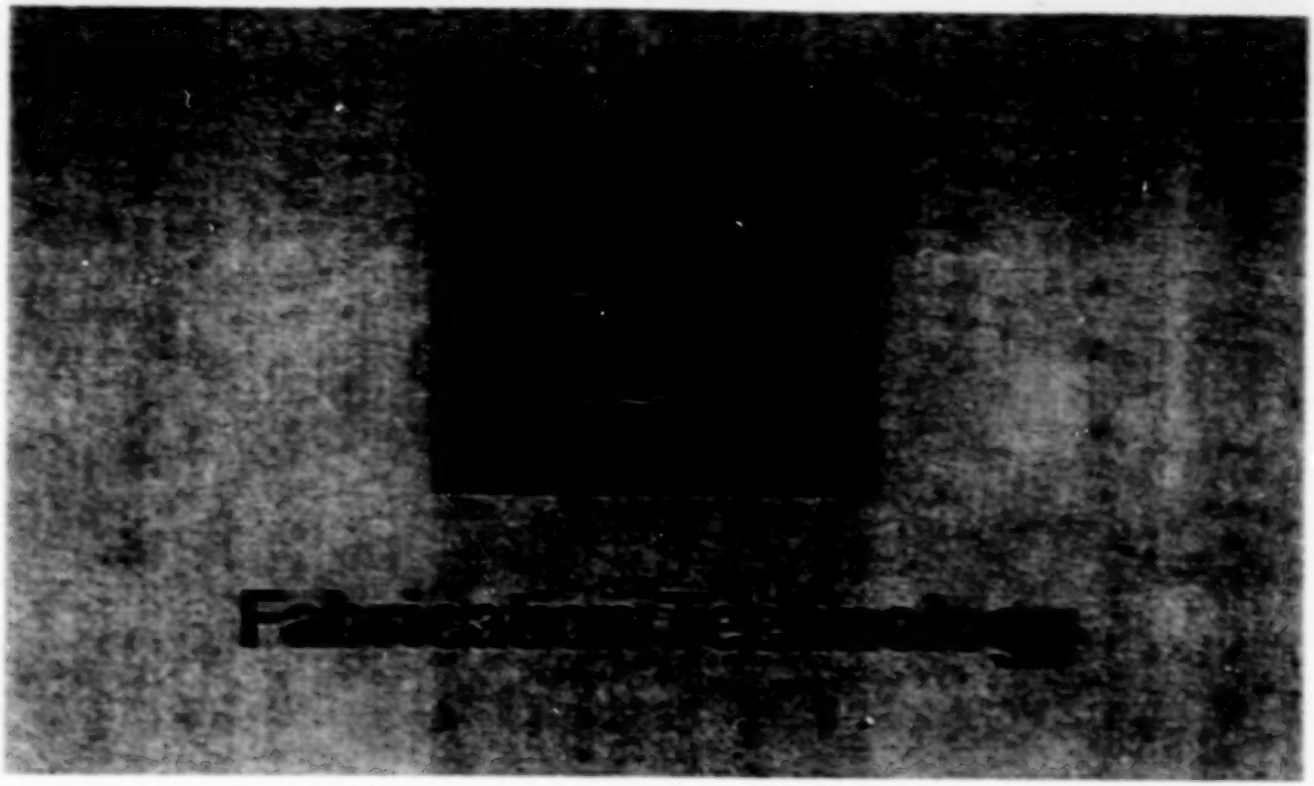

Hardware, Techniques, and Processes

71 Texturing Copper To Reduce Secondary Emission of Electrons
72 Automated Laser Cutting in Three Dimensions
73 Flexible Borescope for Inspecting Ducts

Books and Reports

73 Parameters for Welding Aluminum/Lithium Alloys
73 Lightweight Composite Intertank Structure
74 Foil Patches Seal Small Vacuum Leaks

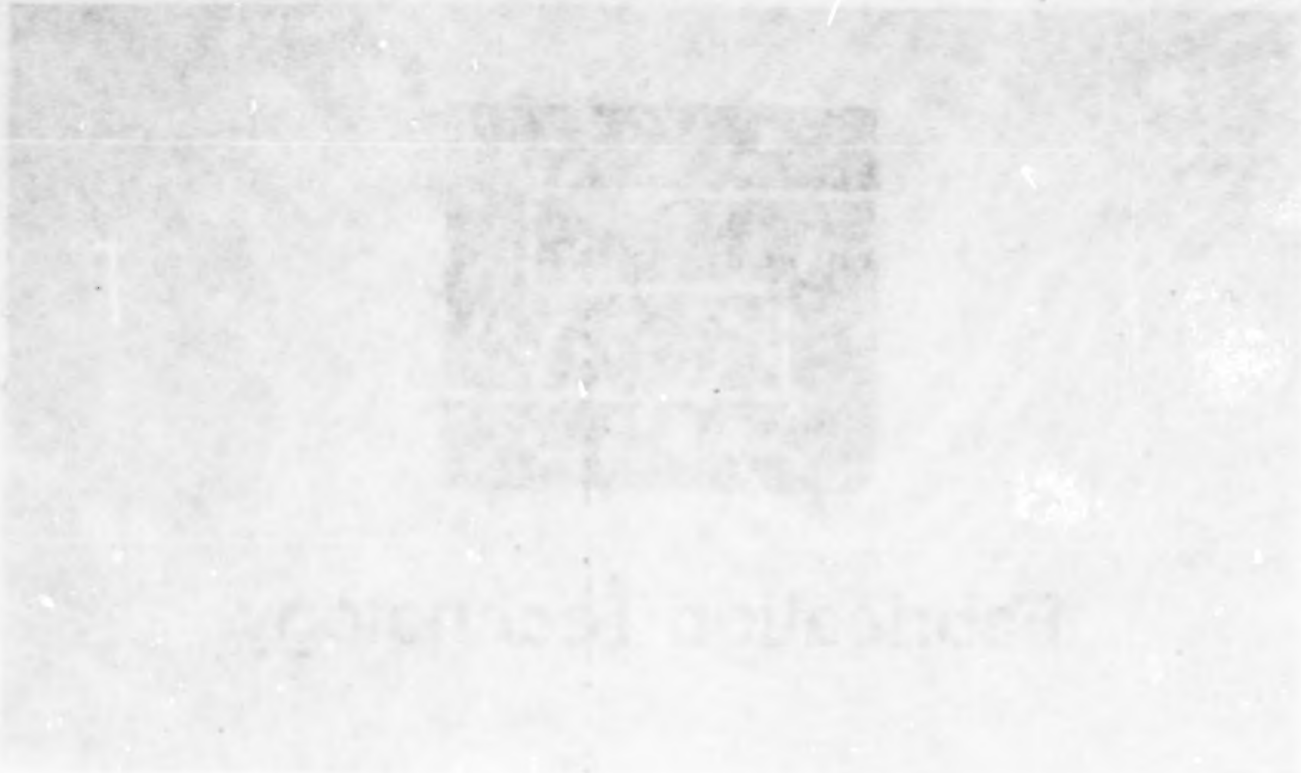

BLANK PAGE

Texturing Copper To Reduce Secondary Emission of Electrons

Ion-beam texturing produces clean surfaces with reduced secondary electron emission.

Lewis Research Center, Cleveland, Ohio

An ion-beam process produces clean, deeply textured surfaces on copper substrates. In the presence of incident electron beams, the ion-textured surfaces exhibit reduced (in comparison with untreated copper surfaces) emission of secondary electrons. Ion-beam-textured copper would be especially useful for making collector electrodes for traveling-wave-tube and klystron microwave amplifiers, in which secondary emission of electrons is undesirable because it reduces efficiency.

After ion-beam texturing, a copper surface consists of a dense, uniform array of pointed spires about 10 μm high, spaced about 5 μm apart (see Figure 1). The secondary-electron emission of the textured surface is 40 to 60 percent less than that of untreated copper. Most of the electrons in an impinging beam strike the bases or sloping walls of the spires; secondary electrons emitted from these regions are repeatedly intercepted by nearby spire walls with partial retention upon each interception, so that the net emission is greatly reduced.

Figure 1. This Scanning Electron Micrograph, taken at an angle of 30° from perpendicular to the nominal surface of a copper substrate, shows the forest of spires formed by ion-beam texturing.

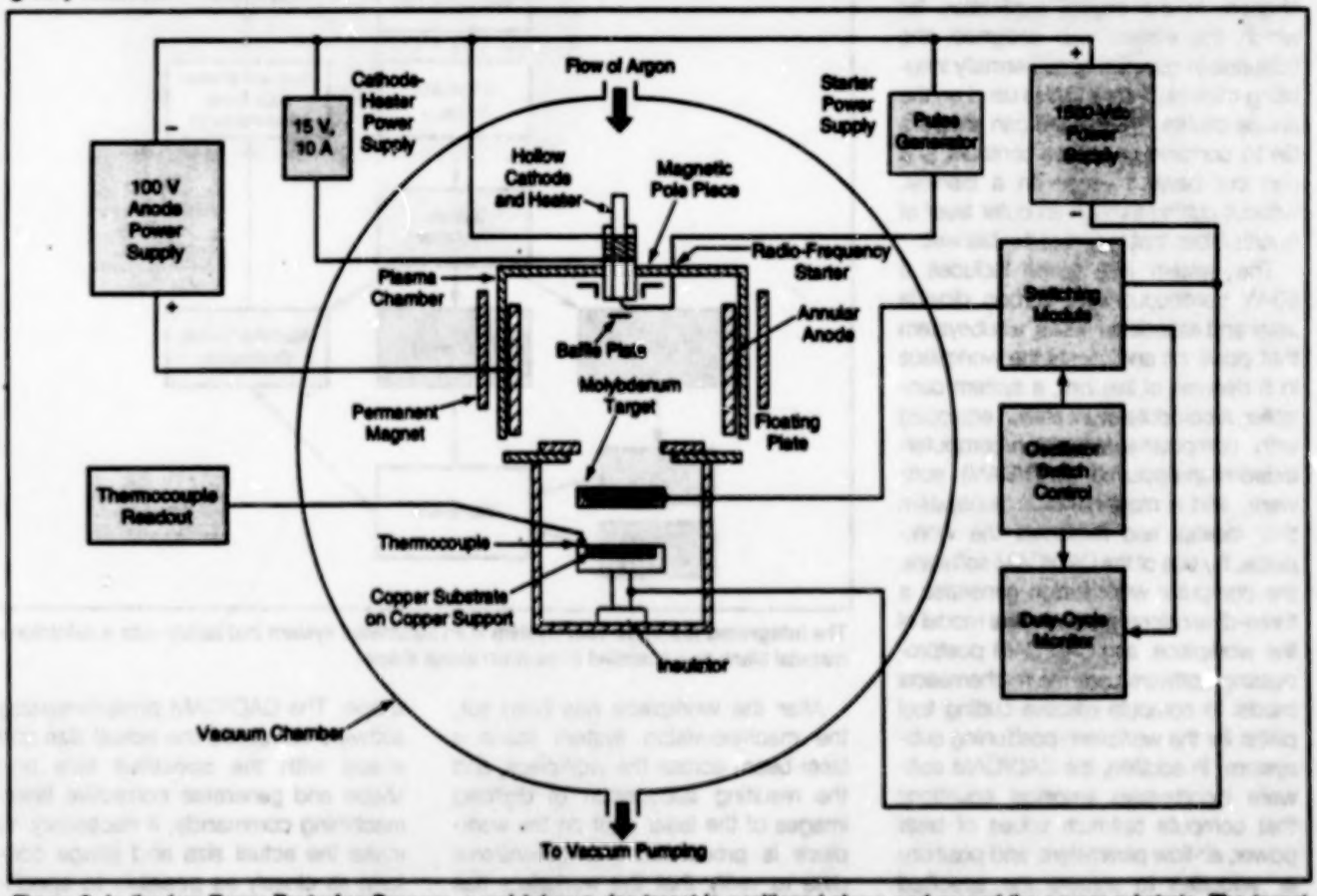

Figure 2. In the Ion-Beam Texturing Process, a molybdenum ring target is positioned above and around the copper substrate. The target potential is repeatedly switched on and off.

BEST COPY AVAILABLE

The ion-beam texturing process is a triode sputtering process in which a copper substrate and a molybdenum target are simultaneously exposed to an argon plasma in a low-pressure environment. The molybdenum target is a ring that is placed between a cathode and the substrate and is centered on the vertical axis that runs from the cathode to the substrate (see Figure 2). The axial (vertical) distance from the target to the substrate is approximately equal to the radius of the substrate; this distance is chosen, on the basis of experience, because it results in a uniformly textured surface.

In the presence of the argon plasma, an accelerating potential of 1,500 Vdc is set up between the cathode and the substrate. The current that flows from the cathode to the substrate is maintained at a level that yields a current density of about 5 mA/cm^2 on the substrate surface to be treated. The accelerating potential is also applied to the target, but in pulsed form; it is switched on and off at a frequency of 20 Hz by use of a switching module. [The switching module is described in "High-Voltage MOSFET Switching Circuit" (LEW-15986) page 12.] During the periods when the accelerating potential is not applied to the target, the entire current passes through the substrate, but when the target potential is switched on, the current is divided between the target and the substrate. The process is continued for 1 hour.

Unlike in previous methods of texturing copper with ion beams, this method provides control (via the frequency and duration of pulses of accelerating potential) over the amount and the rate of arrival of texture-inducing molybdenum at the surface of the copper. Unlike in some older methods, molybdenum residue (which can constitute a contaminant under some circumstances) is not present in significant amounts in treated copper substrates.

This work was done by Kenneth A. Jensen, Arthur N. Curren, and Robert F. Roman of Lewis Research Center. Further information is contained in a TSP [see page 1].

Inquiries concerning rights for the commercial use of this invention should be addressed to the Patent Counsel, Lewis Research Center [see page 1]. Refer to LEW-15898.

Automated Laser Cutting in Three Dimensions

The velocity, position, and angle of the cut are varied under computer control.

John F. Kennedy Space Center, Florida

A computer-controlled machine-tool system uses a laser beam assisted by a directed flow of air to cut refractory materials into complex three-dimensional shapes. In the original application for which the system was designed, the materials in question were thermally insulating thick blankets and tiles used on the space shuttle. The system can shape a tile to concave or convex contours and can cut beveled edges on a blanket, without cutting through an outer layer of quartz fabric that is part of the blanket.

The system (see figure) includes a 50-W continuous-wave carbon dioxide laser and associated optics, a subsystem that positions and orients the workpiece in 5 degrees of freedom, a system controller, a computer work station equipped with computer-aided-design/computer-aided-manufacturing (CAD/CAM) software, and a machine-vision subsystem that locates and measures the workpiece. By use of the CAD/CAM software, the computer work station generates a three-dimensional mathematical model of the workpiece, and CAD/CAM postprocessing software uses the mathematical model to compute effective cutting tool paths for the workpiece-positioning subsystem. In addition, the CAD/CAM software incorporates empirical equations that compute optimum values of laser power, air-flow parameters, and positioner velocities to achieve the specified depth and quality of cut.

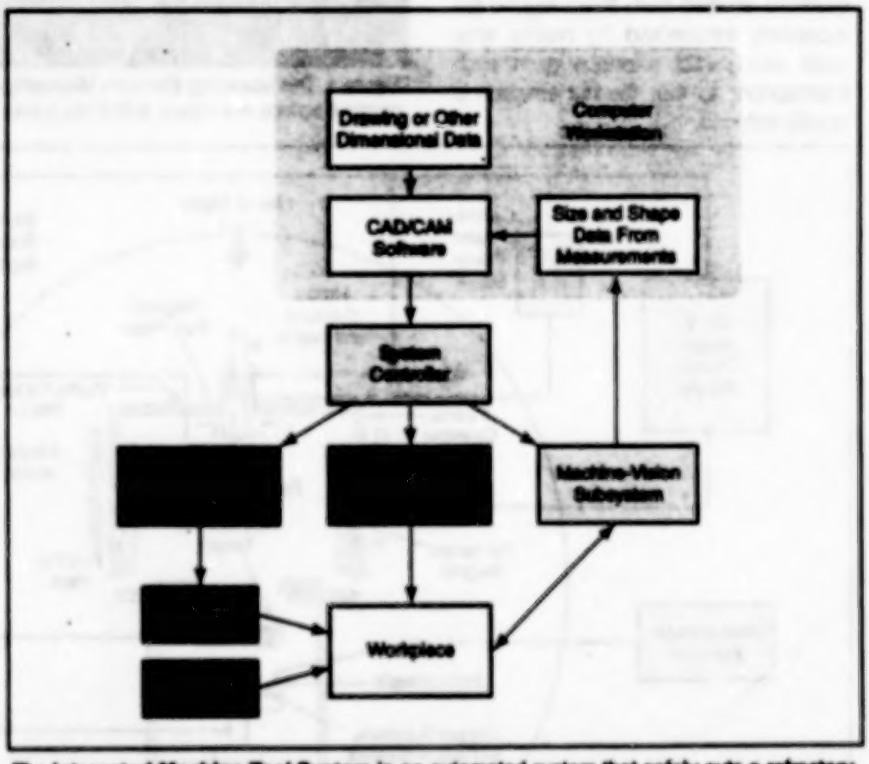

The Integrated Machine-Tool System is an automated system that safely cuts a refractory-material blank to a specified three-dimensional shape.

After the workpiece has been cut, the machine-vision system scans a laser beam across the workpiece, and the resulting succession of digitized images of the laser spot on the workpiece is processed into dimensional data to verify that the workpiece has been cut to the required size and shape. The CAD/CAM postprocessing software compares the actual size and shape with the specified size and shape and generates corrective laser-machining commands, if necessary, to make the actual size and shape conform as closely as possible to specifications.

BEST COPY AVAILABLE

72

The flow of air is directed at the workpiece by custom-made nozzles and performs three main functions: (1) The flow confines the plasma generated by the laser beam, concentrating its heat on the workpiece for maximum effect. (2) The flowing air reacts exothermally with some of the hot material dislodged from the surface, helping to vaporize the material and thus to ensure a clean operation. (3) The flowing air cools the parts of the workpiece immediately surrounding the plasma, so that the crystalline structure of the workpiece is not adversely affected by the heat; for example, in the case of a silica tile, the cooling air prevents undesired vitrification of the surrounding material.

For safety, the system can be entirely enclosed to prevent the escape of laser energy. No dust is generated during the cutting operation — all material is vaporized; larger solid chips dislodged from the workpiece can easily be removed later.

This work was done by Lisa T. Bird and Mark A. Ivanovich of Lockheed Space Operations and Terry R. Angell, Patricia J. Bishop, Weimin Dai, Robert D. Dobbs, Mingli He, Antonio Minardi, and Bret A. Shelton of the University of Central Florida for Kennedy Space Center. Further information is contained in a TSP [see page 1].

Inquiries concerning rights for the commercial use of this invention should be addressed to the Patent Counsel, Kennedy Space Center [see page 1]. Refer to KSC-11663/4/5.

Flexible Borescope for Inspecting Ducts

A borescope and associated equipment have been developed specifically for use in optical inspection of the inside of flexible joints in a rocket-engine fuel duct. The apparatus includes an assembly, characterized as a "mouse/canoe," at the sensing end of a 10-ft (3-m) borescope cable. The borescope tip rides in the mouse/canoe. The mouse/canoe is made laterally compressible, to facilitate movement past constrictions and to provide a fixed distance from the inspection point that permits its accurate description in a duct being inspected. The cable is covered by an outer sheath, which provides rigidity and controls legs that are connected to the back of the mouse/canoe. The legs help to orient the mouse/canoe between the flexible joint tripod legs within the duct. A metal nose and wire whiskers attached to the front of the mouse/canoe aid in the insertion.

This work was done by Keith Shinozaki, Mike P. Armstrong, and Ron Urquidi of Rockwell International Corp. for Marshall Space Flight Center. Further information is contained in a TSP [see page 1].
MFS-30003

Books and Reports

Parameters for Welding Aluminum/Lithium Alloys

Inert-gas shielding and other considerations are discussed.

A report discusses the parameters that must be controlled to properly weld aluminum/lithium alloys. Welds in these alloys are highly susceptible to oxidation and to formation of lines of hydrogen bubbles. To prevent these undesired effects, it is necessary to keep oxygen and water vapor away from the weld site on a workpiece by providing both back-side and front-side inert-gas shielding during the welding process. The report describes experiments that were conducted to determine the gas-shielding parameters that yield acceptable welds. These parameters include mixtures of inert gases, distances between workpieces and fixtures that supply the shielding gases, and the sizes and shapes of the fixtures. Successful welds were made on full-size aluminum/lithium-alloy hardware for the external tank of the space shuttle.

This work was done by Robert L. Gallegher of Martin Marietta for **Marshall Space Flight Center.** *To obtain a copy of the report, "Gas Backside Shielding Parameters and Methods for the Welding of Aluminum Lithium Alloys," see TSP's [page 1].*

Title to this invention has been waived under the provisions of the National Aeronautics and Space Act [42 U.S.C. 2457(f)] to Martin Marietta Corp. Inquiries concerning licenses for its commercial development should be addressed to

Martin Marietta Corp.
P. O. Box 29304
New Orleans, LA 70189

Refer to MFS-28894, volume and number of this NASA Tech Briefs *issue, and the page number.*

Lightweight Composite Intertank Structure

Weight and cost would be less as compared to existing, high-performance aluminum structures.

A report presents the results of a study for a proposed lightweight composite material alternative to the present semimonocoque aluminum intertank structure (the mechanical interface between the fuel and oxidizer tanks) for advanced launch vehicles. The proposed structure would be an integrated assembly of sandwich panels made of laminated epoxy-matrix/carbon-fiber skins, and aluminum honeycomb core. The proposed composite structure is designed, and has demonstrated compression load capacity 31 percent greater than a comparable aluminum STS ET intertank structure. The composite geometry weighs 29 percent less, and is estimated to cost less by an amount which depends upon the number of units produced. The study was conducted to assess the relative merits of the specific designs, and to demonstrate the feasibility of making large, low-cost composite material structures for advanced launch vehicles using automated lamination, and nonautoclave curing techniques. The study serves as an example of the "concurrent engineering" approach, in which design, analysis, and manufacturing are treated as an integrated process.

This work was done by Greg V. Mahle of Martin Marietta Astronautics for **Marshall Space Flight Center.** *To obtain a copy of the report, "Lightweight Composite Intertank Structure," see TSP's [page 1].*
MFS-31073

Foil Patches Seal Small Vacuum Leaks

A report discloses a technique to patch holes in nickel-alloy rocket-engine nozzle parts prior to vacuum brazing. The technique involves lightly spot-welding a nickel foil 0.002 in. (0.05 mm) thick over the hole to be patched, then spot-welding a corrosion-resistant steel foil of the same thickness over the nickel foil. Once the patches are subject to the pressure and temperature of the vacuum brazing, the nickel foil diffuses to bond with the nickel-alloy nozzle, thereby making a vacuum-tight seal.

This work was done by Kirk W. Spiegel and David W. Reed of Rockwell International Corp. for Marshall Space Flight Center. To obtain a copy of the report, "Foil Patch Repair of SSME Nozzle Jackets," see TSP's [page 1].

Inquiries concerning rights for the commercial use of this invention should be addressed to the Patent Counsel, Marshall Space Flight Center [see page 1]. Refer to MFS-30047.

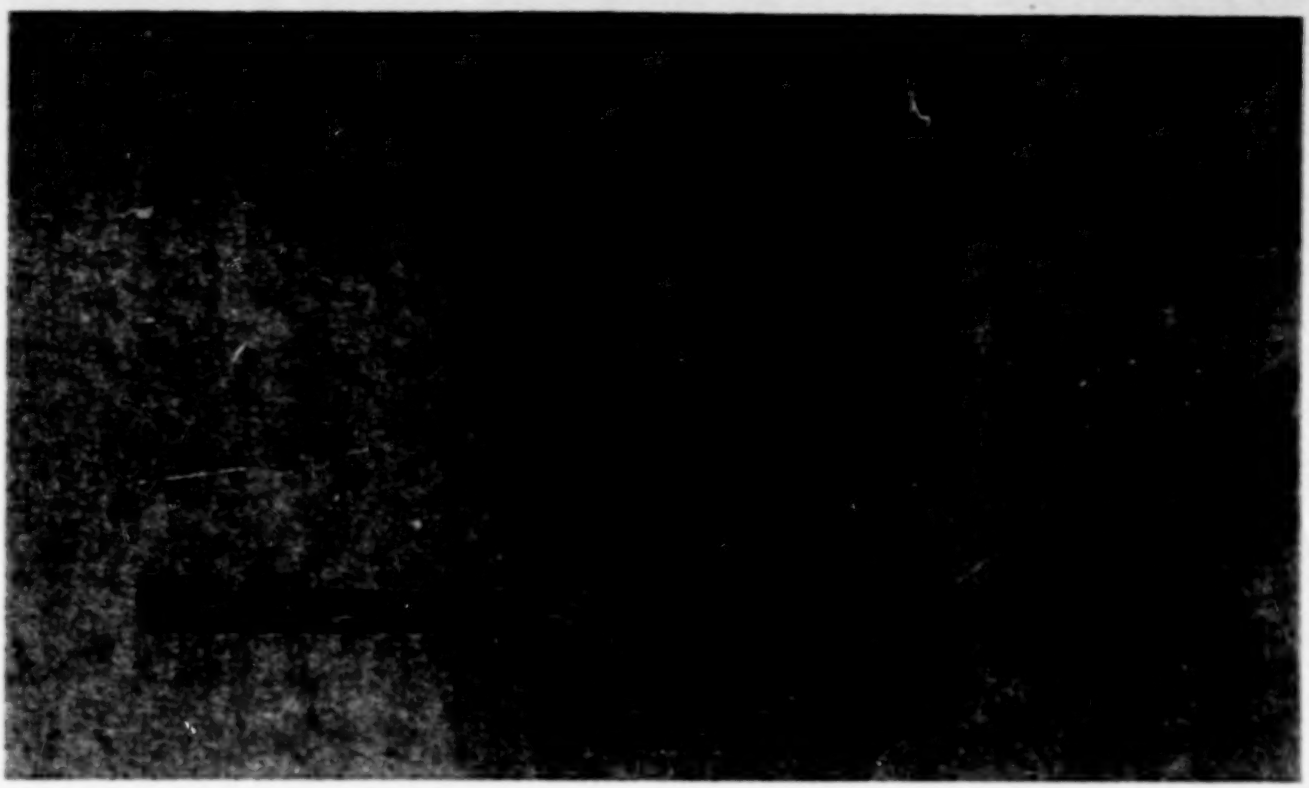

Hardware, Techniques, and Processes

77 Algorithm Helps Monitor Engine Operation
78 Flexible Revision of Data-Processing Communications
78 Software for Managing the Use of Land

Books and Reports

79 Fault-Tolerant Control for a Robotic Inspection System

BLANK PAGE

Algorithm Helps Monitor Engine Operation

Symptoms of impending failure are detected and processed into shutdown signals.

Marshall Space Flight Center, Alabama

The Real-Time Failure Control (RTFC) algorithm is part of an automated monitoring-and-shutdown system that is being developed to ensure safety and prevent major damage to equipment during ground tests of the main engine of the space shuttle. The monitoring-and-shutdown system includes redundant sensors, controller voting logic circuits, automatic safe-limit logic circuits, and conditional-decision logic circuits, all monitored by human technicians. The basic principles of the monitoring-and-shutdown system may also be applicable to stationary powerplants and other complex machinery systems.

Previous experience showed that selected critical operating parameters can reach their safety limits significant amounts of time after faulty conditions begin to develop. Consequently, shutdown based on reaching these limits can occur too late to prevent serious damage, which could include cascades of failures. The RTFC algorithm was incorporated into the monitoring-and-shutdown system to provide earlier indications of faulty conditions, so that shutdown can be effected in time to prevent further damage.

The RTFC algorithm monitors 24 operating parameters (e.g., pressures, temperatures, and speeds) to detect faults during nominally steady operation and during some transient operating conditions. The algorithm (see figure) provides fault detection in three phases. To avoid perturbation by starting transients, the initiation of the algorithm is delayed until 5 seconds after starting the engine. In the first phase, each of the 24 incoming measurements is immediately compared with the precomputed safety limits of the corresponding operating parameter. These limits are set at the expected mean of the parameter $\pm N_1\sigma_1$, where σ_1 is the expected engine-to-engine standard deviation of the parameter and N_1 is the applicable safety factor (typically, $N_1 = 3$). If at least three parameters simultaneously are beyond their limits at any sampling interval, a shutdown signal is generated; otherwise, the algorithm goes on to the second phase.

At the beginning of the second phase, the first measured value of each parameter is designated as a mean value to be used during the first succeeding 2-second interval. A safety band of $\pm N_2\sigma_2$ (where N_2 is a safety factor and σ_2 is a run-to-run standard deviation) is placed around each mean. Thereafter, each incoming measurement is stored and averaged with the four most recent measurements. The five-term moving average value of each parameter is thus updated and checked against safety limits at each sampling interval. The safety limits at each interval are also adjusted to account for transients caused by venting and repressurization of tanks. If the safety limits of three parameters are violated simultaneously at any sampling interval, then a cutoff signal is generated. Moreover, during the first 2-second interval, the standard deviation (σ_2) of each of the 24 parameters is calculated in real time. At the end of the 2 seconds, they are fixed to be used for the duration of the current operating condition. If no safety limits are violated, then the algorithm proceeds to the third phase.

The third phase begins at the end of the first 2-second interval, when the last of the calculated average values of each parameter is released as its mean value for the remainder of the operation. Safety limits are set at $\pm N_2\sigma_2$ above and below this mean value. The limits of certain parameters are again adjusted at each time step to account for venting and repressurization transients. The averaging process continues, and these averages are checked against their corresponding limits for violations. If three or more anomalies are indicated simultaneously, then cutoff is initiated. If not, the algorithm continues operating until a scheduled power transient occurs or until the scheduled cutoff time is reached. At the beginning of a power transient, the algorithm is interrupted for 2 seconds. This process is repeated until the test is completed or a failure occurs.

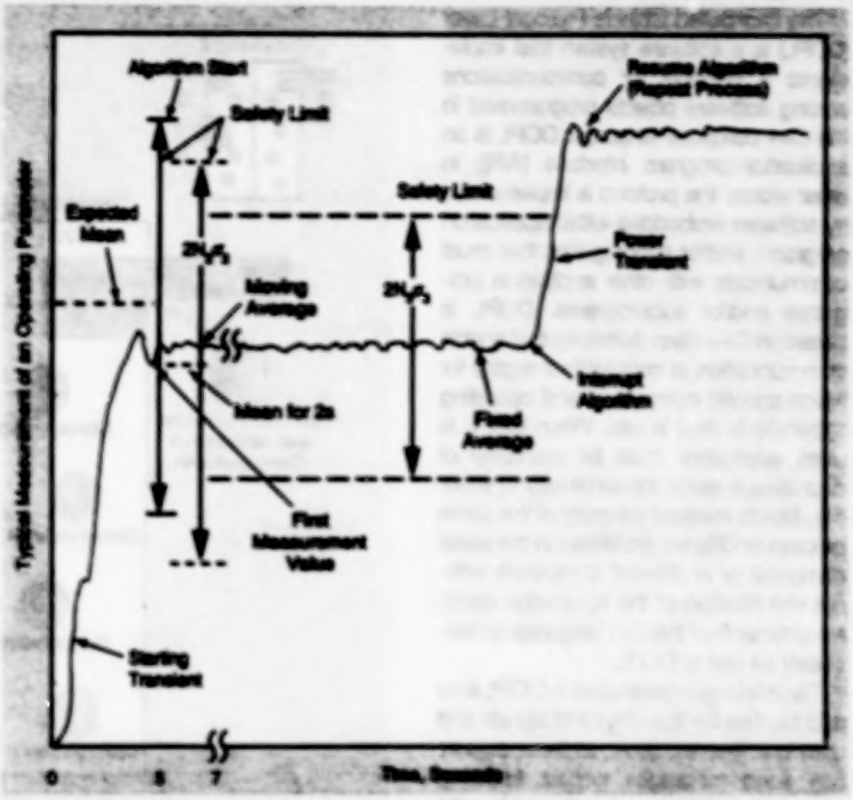

The RTFC Algorithm computes moving averages of parameter measurements and compares the averages with upper and lower safety limits, which delimit nominal operating ranges of the respective parameters. A fault that warrants safety shutdown is deemed to have occurred when three or more parameters lie outside their nominal operating ranges. The averaging process smoothes out some of the sensor noise.

This work was done by Sherry J. Eckerling, Hagop V. Panossian, Victoria R. Kemp, Mike H. Taniguchi, and Richard L. Nelson of Rockwell International Corporation for Marshall Space Flight Center. Further information is contained in a TSP [see page 1].

MFS-29975

BEST COPY AVAILABLE

Flexible Revision of Data-Processing Communications

Single or multiple processes and processors can be accommodated.

NASA's Jet Propulsion Laboratory, Pasadena, California

The Distributed Objects Protocol Layer (DOPL) is a software system that implements a protocol for communications among software objects programmed in the C++ computer language. DOPL is an application-program interface (API); in other words, the protocol is implemented by software embedded within application programs and/or subprograms that must communicate with other application programs and/or subprograms. DOPL is based on C++ class definitions that enable communication of data without regard for which specific computer(s) and operating system(s) is (are) in use. When DOPL is used, application code for exchange of data always works the same way whether the objects involved are parts of the same process or different processes in the same computer or in different computers without modification of the application code. No extension of the C++ language is necessary for use of DOPL.

The basic approach used in DOPL is to add facilities for flow of control signals and data to software objects, so these objects can send messages without knowing where the destination objects reside, and without knowing what communication protocol will be used. DOPL implements a system of asynchronous communication analogous to an efficient postal system (see figure). It enables a single software object to take part in multiple concurrent dialogues. A C++ application program thus becomes a collection of objects analogous to correspondents that communicate with each other via the mail.

The main benefit of the use of DOPL is facilitation of change between sequential processing on one computer and simultaneous processing on multiple computers. For example, an application program can be developed in the form of a single executable unit to ease debugging. Then the debugged application program can be divided into parts that can be executed separately or remotely to enhance performance. DOPL also facilitates the opposite transition from multiple to single processing.

As in other methods of implementing parallel processing, the use of DOPL could entail some increase in communication overhead. Furthermore, to incorporate DOPL, C++ programmers must make some basic changes in their approach to the design of software. In the short term, these changes could decrease programmer productivity. However, in the long term, they should increase productivity in that DOPL might facilitate the reuse of software.

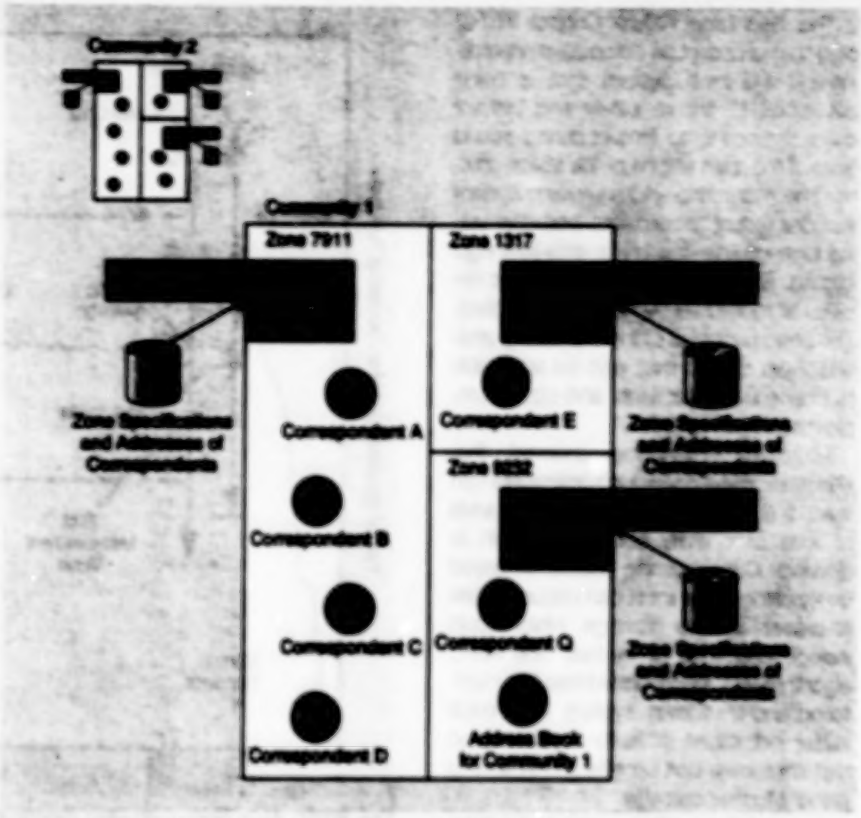

The Paradigm for DOPL is a postal system. Carrying the postal analogy further, communicating objects (correspondents) can be located within the same zone or different zones, which include the software analogues of mailrooms and are identified by zone numbers analogous to the postal codes used in some countries (e.g., ZIP codes in the United States).

This work was done by Scott C. Burleigh of Caltech for NASA's Jet Propulsion Laboratory. Further information is contained in a TSP [see page 1].
NPO-19099

Software for Managing the Use of Land

This software aids planning to satisfy multiple requirements, including environmental regulations.

John F. Kennedy Space Center, Florida

The Mapping Analysis and Planning System (MAPS) is a menu-driven interactive software system that provides information to aid in land-use planning. The MAPS assists the user in taking account of multiple requirements, including environmental regulations, that can affect the types and locations of facilities and structures.

The MAPS incorporates commercial software packages, including GIS; image-processing; video-capture-and-editing; statistical-data-analysis; three-dimensional graphical, numerical-modeling; and hypertext software; plus software for development of expert systems and neural networks. The software shell for a knowledge-based expert system is being developed to add expert, site-specific knowledge to the fusion-of-data and query processes. The MAPS is undergo-

BEST COPY AVAILABLE

ing development for use in planning locations for facilities at Kennedy Space Center (KSC); it may also be adaptable to municipal, commercial, and industrial land-use planning.

Solutions to environmental problems often involve complex, interdisciplinary subjects. Decisions must be made with regard to the requirements of such fields as engineering, hydrology, geology, ecology, geography, political science, public health, environmental planning, demography, and sociology. Therefore, the MAPS combines information from a variety of data bases, including digital imagery, GIS thematic layers, master planning files, and legal information derived from the World Wide Web.

Problems that can be addressed with the help of the MAPS include design and location of facilities, monitoring the environment, mitigation of habitat impacts, assessment and documentation of effects on the environment, and many others. The combination of GIS and expert-systems software is expected to result in a software tool that will support and enhance the process of reasoning and judgment regarding compliance with environmental regulations, rather than only automating the process through prescribed computation. This approach will allow managers and engineers access to expert knowledge, covering the highly diversified set of topics associated with a proactive environmental management strategy, easily and directly from their computer terminals.

In its current use at KSC, the MAPS assists in implementing the KSC environmental checklist — a precursor to deciding the locations of facilities at KSC. Depending on a user's responses to questions on the checklist, the MAPS can flag ancillary requirements, offer more detailed information on a topic, or prompt the user for additional data. For example, in the case of a fuel-storage facility, the user would answer "yes" to a question regarding the storage of hazardous material. The user would then be prompted to state the type and amount of hazardous material. The MAPS would then inform the user of any permits or official actions such as public meetings that may be required in connection with utilization and storage of the particular hazardous material.

This work was done by Burton R. Summerfield of Kennedy Space Center and C. Ross Hinkle, Carlton R. Hall, and Mark J. Provenche of The Bionetics Corp. Further information is contained in a TSP [see page 1].

Inquiries concerning rights for the commercial use of this invention should be addressed to the Patent Counsel, Kennedy Space Center [see page 1]. Refer to KSC-11719.

Books and Reports

Fault-Tolerant Control for a Robotic Inspection System

A distributed system would tolerate operational errors and hardware and software faults.

A report describes the first phase of a continuing program of research on a fault-tolerant control subsystem of a telerobotic visual-inspection system. The ultimate goal of the program is to develop a robotic system for remotely controlled visual inspection of structures in outer space. The innovation of this research is a comprehensive strategy that integrates system-level tolerance of hardware and software faults with task-level handling of uncertainties and unexpected events. The operational characteristics that are sought in this research include (1) tolerance of two or more faults that occur serially at any level of command, control, sensing, or actuation, (2) minimized potential for damage to humans, the workcells, and the robot, and (3) continuous operation with a minimum of uncommanded motion in the presence of failures. The research included an in-depth analysis of the modes of failure of a laboratory telerobotic inspection system at NASA's Jet Propulsion Laboratory. The results of the analysis were used to refine the design of the control system, which is a distributed system that not only tolerates hardware and software faults but also includes a knowledge-based diagnosis-and-recovery subsystem that tolerates operational errors. Central to the diagnosis-and-recovery subsystem is an intelligent (in the sense of artificial intelligence) planner, which is implemented in software and has been integrated into the laboratory system to demonstrate the feasibility of implementing planning and recovery functions in such outer-space applications as automated inspection of surfaces.

This work was done by Kam Sing Tso of SoHaR, Inc., for NASA's Jet Propulsion Laboratory. To obtain a copy of the report, "A Fault Tolerant Intelligent Robotic Control System," see TSP's [page 1].
NPO-30012

National Aeronautics and
Space Administration

END

DATE FILMED

03/14/96